ANTIFOULING SILICONE COATINGS PREPARED WITH PEO-SILANE AMPHIPHILES

A Dissertation

by

MELISSA LEANNE HAWKINS

Submitted to the Office of Graduate and Professional Studies of
Texas A&M University
in partial fulfillment of the requirements for the degree of

DOCTOR OF PHILOSOPHY

Chair of Committee,	Melissa Grunlan
Committee Members,	Elizabeth Cosgriff-Hernandez
	Arum Han
	Mike McShane
Head of Department,	Gerard Coté

December 2014

Major Subject: Biomedical Engineering

ABSTRACT

The protein resistance, subsequent thromboresistance, and marine anti-biofouling ability of poly(ethylene oxide) (PEO) was enhanced by the addition of a flexible, hydrophobic siloxane tether which imparts configurational mobility and amphiphilicity to the PEO. Conventional PEO-silanes (i.e. no tether) lack these beneficial properties and thus are limited in their ability to reduce biological adhesion onto bulk-crosslinked, silicone medical devices (e.g. hemodialysis catheters) or onto silicone marine coatings. To achieve antifouling behavior, PEO-modified silicones require the ability to undergo extensive water-driven surface restructuring so as to form a hydrophilic, PEO-enriched layer. A siloxane tether, due to its flexibility and similar hydrophobic nature as a silicone matrix, may potently enhance PEO migration to the silicone-water interface.

New PEO-silane amphiphiles were prepared by variations to the siloxane tether length and PEO end-group chemistry to enhance water-driven surface-restructuring and PEO hydration, respectively. General formulas for the PEO-silane amphiphiles include α-$(EtO)_3Si$-$(CH_2)_2$-oligodimethylsiloxane$_m$-*block*-poly(ethylene oxide)$_8$-OCH_3 for those with variable siloxane tether length (m = 0, 4, 13, 17, 24, and 30) and α-$(EtO)_3Si$-$(CH_2)_2$-oligodimethylsiloxane$_{13}$-*block*-poly(ethylene oxide)$_{11}$-sulfobetaine for those with a zwitterion PEO end-group.

PEO-silane amphiphiles were used to bulk-modify silicones towards the goal of reducing protein adsorption and biofouling. First, a PEO-silane amphiphile bearing a siloxane tether of length m = 13 was incorporated into medical-grade silicone with

variable amounts. It was determined that only a small amount (≤ 5wt%) was necessary for high protein resistance. PEO-silane amphiphiles of variable siloxane tether length (*m* = 0–30) and a conventional PEO-silane control (i.e. no tether) were bulk-crosslinked into silicones and surface-grafted onto silicon wafers. Although the surface-grafted PEO-silane amphiphiles were less protein resistant than the PEO-silane control, when incorporated into a bulk-modified silicone, the PEO-silane amphiphiles exhibited superior surface restructuring and, hence, protein resistance. An intermediate siloxane tether length was observed to maximize surface restructuring and subsequent protein and biofouling resistance. Lastly, the chemistry of PEO-silane amphiphiles was modified to include a zwitterion PEO end-group. These novel PEO-silane amphiphiles may be used for the bulk-modification of silicones to achieve high levels of PEO hydration while maintaining the ability of the PEO to restructure to the surface via a siloxane tether.

DEDICATION

To My Husband

You are my best friend and the love of my life. Thank you for being the inspiration and motivation that carries me through all of my endeavors.

ACKNOWLEDGEMENTS

I would like to thank my graduate advisor, Professor Melissa Grunlan, for her generous commitment to provide guidance, support, and encouragement throughout my graduate studies, and for sharing her vast knowledge of polymeric biomaterials. I am extremely grateful for every opportunity that she has given me to advance my career in biomaterials research, and for sharing in both my challenges and accomplishments.

I am thankful for the support of my committee members, Professors Elizabeth Cosgriff-Hernandez, Mike McShane, and Arum Han, and for their commitment to assist me throughout the course of this research.

I thank my lab mates for making my graduate school career at Texas A&M University an enjoyable, life-changing experience. Thanks also to the Texas A&M University Graduate Diversity Fellowship for financial support throughout the majority of my doctoral studies.

Finally, I want to thank my family for their incredible love, praise, encouragement, and inspiration in my graduate studies and in every aspect of my life.

TABLE OF CONTENTS

Page

LIST OF FIGURES

Page

Page

Page

LIST OF TABLES

CHAPTER I

INTRODUCTION AND LITERATURE REVIEW

1.1 Background

1.1.1 Surface-Induced Thrombosis

Thrombosis is a natural function of the body which prevents significant blood loss from sites of injury. However, this mechanism can also occur when blood makes contact with the surface of a foreign material in a process known as surface-induced thrombosis (**Figure 1.1**). Upon implantation of a blood-contacting medical device, plasma proteins rapidly adsorb onto the artificial material surface through various interactions. Proteins in their native structure have low conformational entropy as a result of protein folding. However, the adsorption of proteins onto surfaces leads to unfolding of the proteins and thus a favorable increase in entropy [1]. This adsorption process is facilitated in part by hydrophobic interactions. Contact with hydrophobic surfaces causes proteins to undergo a conformational change such that the hydrophobic residues are exposed and adhere to the surface [1]. Moreover, the Vroman effect causes proteins to adsorb in a specific order such that high concentration, low molecular weight proteins such as albumin adsorb first and are successively replaced by higher molecular weight proteins such as fibrinogen [2,3]. Subsequently, platelets interact with the adsorbed proteins, specifically fibrinogen and von Willebrand factor [4], and adhere and become activated through receptors in the plasma membrane [5,6]. Additionally, thrombin formation leads to the polymerization of fibrinogen to fibrin which, combined

with adhered platelets, results in clot formation on the biomaterial surface [6]. Ultimately, surface-induced thrombosis may compromise device efficacy and safety [7-10] and can result in embolism if the clot were to break off from the surface and travel through the bloodstream.

A variety of medical devices including hemodialysis catheters, cardiac pacing leads, catheter balloons, coated metal stents, extracorporeal device tubing, and various surgical devices naturally make contact with blood for their designated use [11-13]. A majority of such devices are commonly composed of silicone due to its favorable properties which include thermal and oxidative stability, gas permeability, flexibility, and ease of processing [11,12]. Silicones may be formed by crosslinking with radicals, by condensation (e.g. acetoxy cure), or by addition (e.g. platinum cure) and can be readily reinforced with amorphous, fumed silica to increase modulus, strength, and hardness [11]. Although silicones exhibit unique and advantageous properties, their extreme hydrophobicity results in poor resistance to blood proteins and hence surface-induced thrombosis [7,8,14-16].

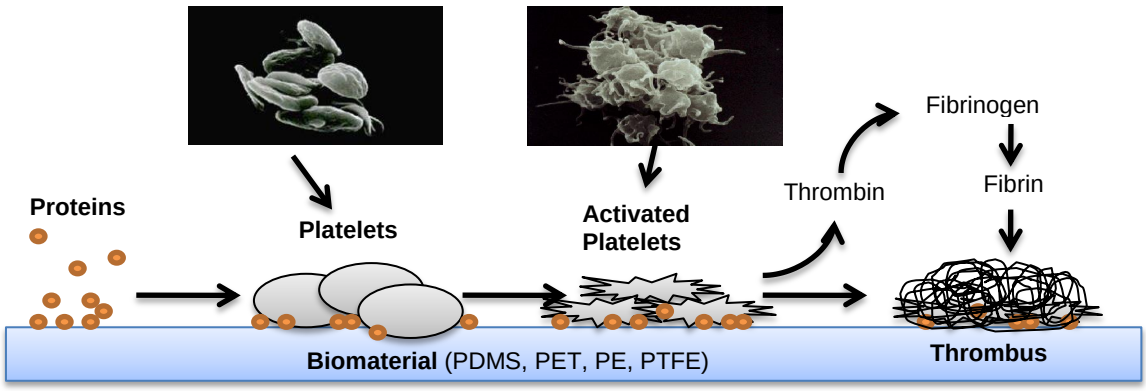

Figure 1.1. Surface-induced thrombosis.

1.1.2 Current Methods of Reducing Surface-Induced Thrombosis

Heparinization is currently the gold standard of treatment for controlling surface-induced thrombosis, along with other pharmacological agents such as aspirin [17,18]. Heparin's anticoagulant property stems from its ability to bind to antithrombin, a serine protease inhibitor, causing it to inactivate thrombin and thus prevent clot formation [19]. It is extensively used due to its availability and favorable properties such as rapid onset of action [18]. However, heparin therapies are associated with high costs, limited efficacy, and potentially severe side effects such as bleeding, allergies, and heparin-induced thrombocytopenia [18,20,21]. Heparin coatings exhibit similar problems and have reduced efficacy due to leaching, non-uniform distribution, and reduced anti-coagulant activity when compared to unbound heparin [22,23].

Poly(ethylene oxide) [PEO or poly(ethylene glycol) (PEG)] is a neutral, hydrophilic polymer commonly used in medical device coatings for reducing surface-induced thrombosis due to its particularly high protein resistance [14,15,24,25]. This behavior is due to its hydrophilicity and hydration [26] as well as its configurational mobility which leads to a large excluded volume, steric repulsion, blockage of underlying adsorption sites, and an entropic penalty if protein adsorption were to occur (**Figure 1.2**) [14,15,25,27,28]. To enhance the protein resistance of biomaterials, PEO has been immobilized onto material surfaces by self-assembly [29,30], physisorption [31,32], formation of surface physical interpenetrating networks (SPINs) [33-35], or covalent grafting [36-43]. Grafted chains can provide long-term chemical stability of functionalized surfaces without altering the bulk properties of the substrate material [44-

46]. Thus, covalent grafting of PEO onto activated surfaces is considered to be the most effective method to prepare surface-modified materials [25]. In regards to the modification of silicone, both trimethoxysilylpropyl and triethoxysilylpropyl PEO monomethyl ether have been grafted onto silanol-covered silicone surfaces [40-42]. Additionally, allyl PEO monomethyl ether (CH_2=$CHCH_2$–(OCH_2CH_2)$_n$–OCH_3) has been surface-grafted onto silane (Si–H)-enriched silicone surfaces [43]. PEO has also been crosslinked throughout the bulk of silicone materials via the condensation cure of triethoxysilylpropyl PEO monomethyl ether with α,ω-bis(Si–OH)PDMS and tetraethoxysilane ($Si(OEt)_4$) [47,48].

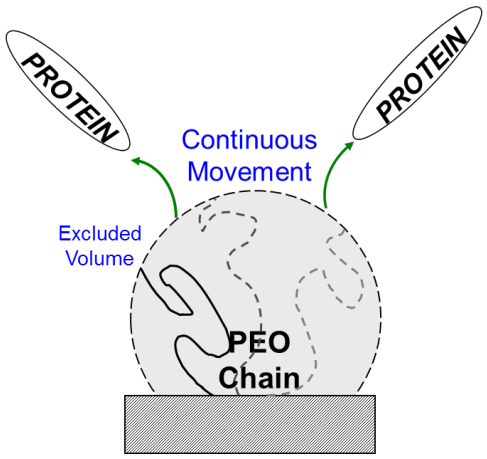

Figure 1.2. Protein resistance is attributed in part to its configurational mobility, leading to a large exclusion volume and steric repulsion of proteins.

Zwitterionic polymers are neutral polymers with a positive and negative electrical charge at different locations within the molecule. Whereas PEO and other non-ionic materials achieve hydration via hydrogen-bonding, zwitterions achieve stronger

hydration via electrostatic interactions [49,50]. Water is believed to be an important factor in surface resistance to protein adsorption due to the resulting repulsive steric forces that prevent proteins from adsorbing to hydrated surfaces [51-54]. Thus, zwitterions are considered excellent candidates for non-fouling materials due to their ability to bind a substantial amount of water molecules. Types of zwitterionic polymers include poly(phosphobetaine), poly(sulfobetaine), and poly(carboxybetaine) (**Figure 1.3**) and have been shown to exhibit excellent non-fouling properties [55-58]. Phosphobetaine-based polymers are biomimetic due to the presence of phosphorylcholine headgroups which are a major component of the outer membrane of erythrocytes and thus aid in the suppression of thrombogenesis [55,57,59]. However, phosphobetaine monomers such as 2-methacryloyloxyethyl phosphorylcholine can be difficult to synthesize, and the phosphoester group has a tendency to be hydrolyzed [60]. Poly(sulfobetaine) and poly(carboxybetaine) are the most popular choices for antifouling applications due to their relative ease of fabrication [60] and chemical stability [55], but are otherwise similar to phosphobetaine. All three types of zwitterions exhibit similar antifouling properties and have been shown to adsorb very low levels of protein (<0.3 ng/cm^2 fibrinogen adsorption) [60-62]. Zwitterionic polymers have been covalently attached to PEO with varying repeat unit number (n = 0-4) to produce phosphorylcholine-oligoethylene glycol-alkane thiols which were subsequently used to form self-assembled monolayers (SAMs) [58]. Protein resistance was enhanced by as much as 62% when compared to the corresponding oligoethylene glycol-alkane thiols. In limited reports, silicone surfaces have been modified with carboxybetaine and

sulfobetaine to reduce protein adsorption and platelet adhesion [63-65] as well as to form coatings with enhanced stability against the migration of grafted chains below a silicone surface [66].

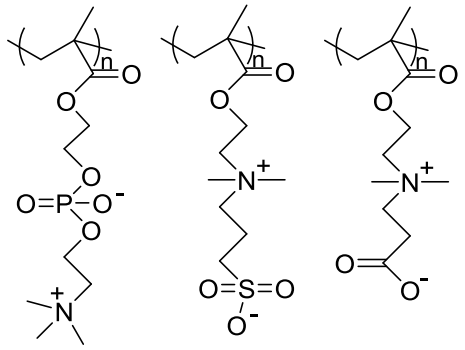

Figure 1.3. Zwitterionic polymers. From left to right: phosphobetaine, sulfobetaine, and carboxybetaine.

1.1.3 Marine Biofouling

Marine biofouling consists of the adhesion of marine organisms such as diatom slimes, algae and barnacles (i.e. biofilms) to ship hulls or other marine structures. Consequently, biofilm formation increases surface roughness and hydrodynamic drag as the ship travels through the water and thus fuel consumption rises [67]. Marine biofouling is therefore problematic due to the substantial economic consequences associated with increased fuel consumption, hull cleaning, and repainting [67]. This issue is particularly prominent for static marine structures or for ships in port or traveling at less than two knots [68].

The biofouling process typically begins with the adsorption of a conditioning film consisting of ions, proteins, and other organic macromolecules (e.g. glycoproteins and polysaccharides) [69,70], followed by the adhesion of bacteria, diatoms, and other micro and macroorganisms [71,72]. Diatoms are unicellular algae that are a major component of biofilms [73]. They secrete extracellular polymeric substances to attach to surfaces and quickly multiply to form diatom slimes [68]. Diatom slimes are particularly challenging due to their robust ability to adhere to hydrophobic marine surfaces [74,75].

1.1.4 Current Methods of Reducing Marine Biofouling

The traditional method of resisting biofouling is through the use of toxic, ablative antifouling paints including those comprised of copper, organotin, and organic biocides [76]. However, their accumulation in marine waters has a negative impact on non-target marine life and has led to a call for restrictions on the use of organotin and biocide-based paints by the International Maritime Organization [77].

Foul-release (FR) coatings represent a non-toxic alternative to ablative antifouling paints [78]. By weakening the attachment of biofouling organisms, FR coatings facilitate the facile removal of biofilms upon application of a hydrodynamic force (e.g. ship movement or cleaning) [79,80]. Two types of materials are utilized for commercial FR coatings, namely fluoropolymers and silicones. Fluoropolymers exhibit low surface energy and sufficient chemical stability [81]. However, they are relatively high in modulus which encourages biofilm formation [82], are comparatively expensive [83], and are also an environmental persistent [84,85]. Silicones, particularly crosslinked

poly(dimethyl siloxane), are commonly used for commercial FR coatings [78] due to their low surface energy, roughness, glass transition temperature, and modulus which minimize adhesion and enhance the release of marine biofoulers [78,86,87]. Conversely, the hydrophobicity of silicones leads to poor resistance to biofouling, particularly to diatom slimes [88]. Furthermore, the FR performance of commercial silicone coatings requires vessel speeds approaching 30 knots [89] whereas a moderate ship speed is 10-15 knots [90].

To overcome the limitations of silicone FR coatings, amphiphilic antifouling (AF) coatings have appeared as an approach to diminish the initial attachment of fouling organisms including diatoms. Amphiphilic coatings combine hydrophobic and hydrophilic polymers to form chemically complex surfaces [91-94]. Several examples of amphiphilic coatings comprise those based on combinations of PEO with a hydrophobic component such as polystyrene [95,96] or fluoropolymers [97,98]. However, these amphiphilic AF coatings are composed solely of a co- or multi-polymer whereas an amphiphilic additive would be a more desirable approach for a simple one-step modification of silicones.

1.2 Approach

1.2.1 Overview

Herein, we have developed various PEO-silane amphiphiles that may be introduced into silicones in order to reduce protein adsorption and platelet adhesion as well as to reduce marine biofouling. The structure of conventional triethoxysilane PEO

was modified to achieve this. First, a hydrophobic, flexible siloxane tether of variable length was introduced to impart amphiphilicity as well as mobility, including water-driven restructuring to the silicone surface-water interface. Second, a zwitterionic PEO end-group was introduced to increase the antifouling efficacy.

1.2.2 PEO Modification with a Hydrophobic, Flexible Siloxane Tether

The protein resistance of silicones bulk-modified with conventional PEO-silanes may be limited by the chemical structure of PEO. Specifically, the PEO-silane spacer or "tether" separating the PEO segment and reactive end group (e.g. triethoxy) is a short alkane spacer (e.g. propyl) (**Figure 1.4**) [40,43]. This spacer may limit PEO's configurational mobility, including migration through the silicone matrix to the surface-water interface where biofouling occurs. In a previous report by Grunlan, PEO-silane amphiphiles (m = 0, 4 and 13) were prepared and used to bulk-modify silicones resulting in enhanced protein resistance which improved as the siloxane tether length increased [99]. In this work, we have similarly prepared PEO-silane amphiphiles in which the siloxane tether length (m) was increased to 17, 24, and 30 repeat units.

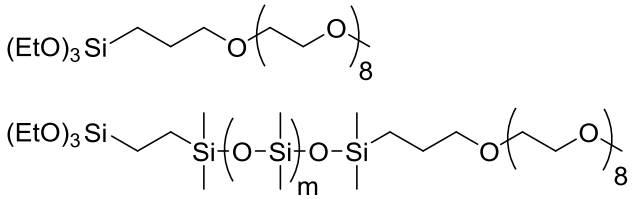

Figure 1.4. Structure of a conventional PEO-silane (top) versus a PEO-silane amphiphile containing a siloxane tether where m = 0, 4, 13, 17, 24, and 30 (bottom).

1.2.3 Water-Driven Surface-Restructuring of PEO-Silane Amphiphiles

The notable protein resistance of PEO has largely been assessed of chains surface-grafted onto a physically stable, model substrate such as gold, silicon wafer, or glass [29,30,37,38,100-103] (**Figure 1.5a**). For such grafted chains, exposure to the aqueous biofouling environment does not require their migration since chains remain at the surface. However, when PEO chains (e.g. PEO-silanes) are incorporated into silicone matrices and other polymeric materials, *in vivo* results are often disappointing [41,104,105]. The lack of protein resistance for PEO-modified silicones may stem from the inability of PEO chains to migrate from the bulk to the surface-water interface to impart a PEO-enriched surface with high hydrophilicity and molecular mobility [106] (**Figure 1.5b**). In this work, the ability of PEO-silane amphiphiles (m = 0, 4, 13, 17, 24 and 3) to enhance the hydrophilicity of bulk-modified silicones was compared to that of conventional PEO-silane controls (i.e. no siloxane tether). Furthermore, each of these was surface-grafted onto physically stable silicon wafer and the protein resistance compared to each other as well as versus the bulk-modified silicones. In this way, the validity of assessing the antifouling behavior of PEO-silane amphiphiles as well as PEO-silane controls could be determined.

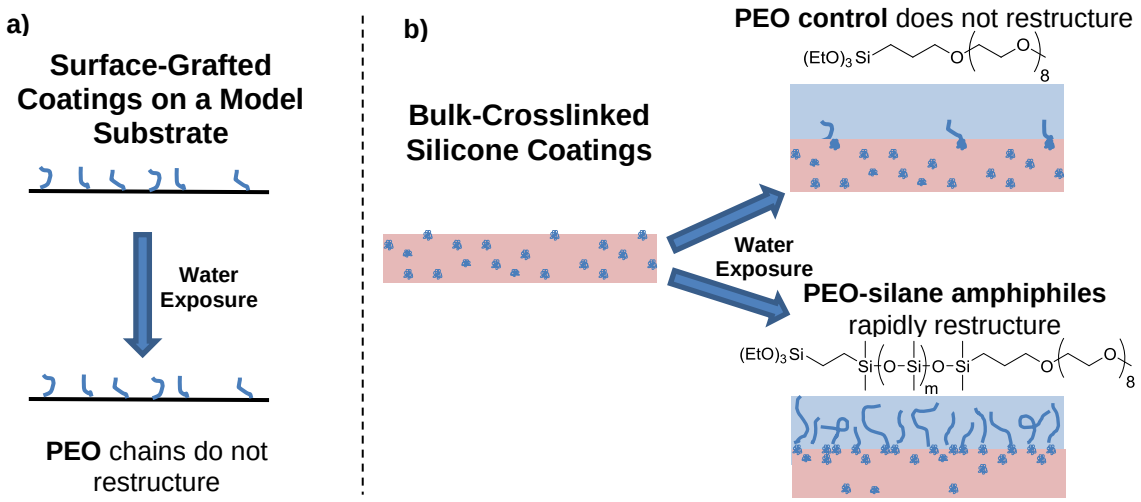

Figure 1.5. The effect of coating substrate and siloxane tether on the restructuring ability of PEO. a) Surface-grafted PEO on a model substrate does not restructure upon exposure to water. b) PEO-modified bulk-crosslinked silicone coatings undergo substantial restructuring upon exposure to water only with the addition of a siloxane tether (i.e. PEO-silane amphiphile).

1.2.4 Incorporation of Zwitterions

The protein resistance behavior of PEO is partly attributed to its hydrophilicity and hydration [26]. Zwitterions, however, achieve a stronger hydration when compared to PEO. Thus, the substitution of the methoxy group (-OCH_3) on the PEO-silane amphiphile with a zwitterionic end-group is expected to enhance PEO hydration (**Figure 1.6**). To this end, a zwitterionic PEO-silane amphiphile as well as zwitterion and PEO controls were synthesized and may be used to prepare surface-grafted and bulk-crosslinked coatings.

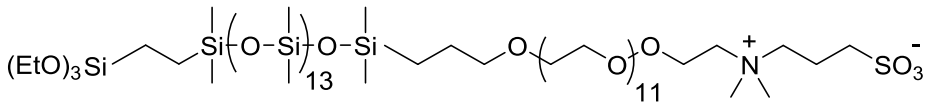

Figure 1.6. Structure of zwitterionic PEO-silane amphiphile.

1.3 Innovation

The need for heparin-free thromboresistant coatings as well as nontoxic antifouling coatings remains critical. While PEO continues to be the gold standard for passive antifouling coatings, opportunities exist to improve its capacity to prevent *in vivo* surface-induced thrombosis as well as marine biofouling via modifications to its structure. Given the prevalent use of silicones in blood-contacting medical devices and for foul-release marine coatings, new PEO-derivatives should permit the ready bulk- and surface-modification of silicones.

Because the protein resistance of PEO is attributed to its hydrophilicity and hydration as well as its configurational mobility, modification to its structure has the potential to enhance protein resistance. In this work, antifouling silicone coatings were prepared via bulk-modification with PEO-silane amphiphiles. Several key structural features were considered in the design of PEO-silane amphiphiles. First, similar to conventional PEO-silanes, the PEO-silane amphiphiles bear a triethoxy-silane [$(EtO)_3$-Si-] end group. Thus, it permits the bulk-modification of silicones via condensation reaction with silanol (Si-OH)-terminated PDMS and crosslinkers. In addition, the triethoxy-silane group also permits covalent surface attachment to hydroxylated surfaces such as oxidized silicone prepared via simple oxidation treatments (e.g. plasma). Second,

a flexible, hydrophobic siloxane tether was used to separate the PEO segment from the triethoxy-silane group. This is in contrast to conventional PEO-silanes in which the PEO segment is separated from the reactive end group via a short alkane spacer (e.g. propyl) [40,43]. The siloxane tether is highly flexible due to the wide bond angle (~145°) and low barrier to linearization (~0.3 kcal mol^{-1}) of Si–O–Si in dimethylsiloxanes [107,108]. The dynamic flexibility of the dimethylsiloxane backbone results in polymers with extremely low glass transition temperatures (T_gs) (e.g. PDMS, T_g = -125 °C). Thus, the siloxane tether was anticipated to enhance the molecular mobility of the PEO segment, including migration through the silicone matrix to the surface-water interface. Moreover, the hydrophobic siloxane tether imparts amphiphilicity, a feature associated with enhanced antifouling [109,110]. In addition, the hydrophobic tether may enhance the solubility of the PEO in the silicone matrix to further enhance its migration to the surface-water interface. As a third and final structural modification, a zwitterion end-group was introduced to the PEO segment to further increase antifouling efficiency by enhancing PEO hydration.

This approach is innovative in several ways. First, it is heparin-free thereby eliminating the potential harmful side effects associated with even bound heparin. Second, the strategy to prepare modified silicone coatings is simple, yet versatile, and is in stark contrast to other more complex coatings, particularly those that are heparin-based. Specifically, with these PEO-silane amphiphiles, modification of silicones can be done via simple blending (“bulk modification”) or direct surface-grafting (“surface modification”). Third, the PEO-silane amphiphile molecular design permits a unique

strategy to impart protein resistance: combined molecular mobility and amphiphilicity as well as enhanced hydration. Compared to other PEO coating designs that may limit PEO configurational mobility, the addition of a flexible siloxane tether will enhance configurational mobility, a fundamental protein resistant property of PEO (**Figure 1.4**). The hydrophobicity of the siloxane tether also imparts amphiphilic character to the PEO-silane amphiphile which is also associated with reduced protein adhesion [111,112]. Finally, in an attempt to enhance the hydration of the PEO-silane amphiphiles, a zwitterionic PEO end group was substituted for the methoxy group ($-OCH_3$) (**Figure 1.6**).

CHAPTER II

THE PROTEIN RESISTANCE OF SILICONES PREPARED WITH A PEO-SILANE AMPHIPHILE[*]

2.1 Overview

Silicone coatings with improved resistance to plasma proteins were prepared by incorporating a PEO-silane amphiphile: α-$(EtO)_3Si$-$(CH_2)_2$-oligodimethylsiloxane$_{13}$-*block*-poly(ethylene oxide)$_8$-OCH_3. The oligodimethylsiloxane tether imparts amphiphilicity and molecular mobility to the chain thereby enhancing protein resistance. Using a medical grade, silica-filled acetoxy-cure silicone, the PEO-silane amphiphile was introduced at varying levels (0, 1, 5, 10, 15 and 20 wt%) and films prepared via solvent-casting. Increased PEO-silane amphiphile content led to increased surface hydrophilicity and improved resistance to bovine serum albumin (BSA) and human fibrinogen (HF). When maintained in air, the surfaces of the coatings did not display hydrophobic recovery.

---

[*] Hawkins, M.L.; Grunlan, M.A. The protein resistance of silicones prepared with a PEO-silane amphiphile. J Mater Chem 2012, 22, 19540-19546.
http://pubs.rsc.org/en/content/articlelanding/2012/jm/c2jm32322b – Reproduced by permission of The Royal Society of Chemistry

2.2 Introduction

Silicones such as crosslinked polydimethylsiloxane (PDMS) are commonly used in biomedical applications [11-13]. Their utility stems from a unique set of properties that includes thermal and oxidative stability, gas permeability, flexibility and ease of processing [11,12]. In addition, silicones are readily reinforced with amorphous, fumed silica powder to systematically increase modulus, strength and hardness [11]. These properties have led to the widespread use of reinforced silicones for a variety of blood-contacting medical devices, including hemodialysis catheters, cardiac pacing leads, catheter balloons, coated metal stents, extracorporeal device tubing and various surgical devices [11-13]. Unfortunately, due to their extreme hydrophobicity, silicones exhibit poor resistance to blood proteins [7,8,14-16]. Adsorbed proteins initiate platelet adhesion and activation of coagulation pathways leading to thrombosis thereby compromising device efficacy and safety [7-10]. In efforts to diminish protein adsorption, silicones have been hydrophilized by various physical, chemical and combined approaches [8,113-116].

Poly(ethylene oxide) (PEO; or poly(ethylene glycol) (PEG)) is a neutral, hydrophilic polymer which displays high protein resistance [14,15,24,25]. This behavior is attributed to its hydrophilicity and hydration [26] as well as its configurational mobility which leads to a large excluded volume, steric repulsion, blockage of underlying adsorption sites, and an entropic penalty associated with protein adsorption [14,15,25,27,28]. In efforts to improve the protein resistance of silicones, PEO has been introduced via surface-grafting [39-43] and bulk crosslinking [47,48,99,117] strategies.

PEO-silanes containing the appropriate reactive end groups are often utilized [118]. PEO alkoxysilanes readily react with silanol (Si–OH) groups located on the terminal ends of PDMS chains or surfaces of oxidized silicone. For instance, PEO was introduced into silicones via the condensation crosslinking of triethoxysilylpropyl PEO monomethyl ether [$(RO)_3Si(CH_2)_3$–$(OCH_2CH_2)_n$–OCH_3) with α,ω-bis(Si–OH)PDMS [47,48]. Both trimethoxysilylpropyl and triethoxysilylpropyl PEO monomethyl ether have been grafted onto silanol-covered silicone surfaces [40-42]. In addition, allyl PEO monomethyl ether (CH_2=$CHCH_2$–$(OCH_2CH_2)_n$–OCH_3) has been surface-grafted onto silane (Si–H)-enriched silicone surfaces [43].

The protein resistance of PEO-modified silicones using the aforementioned strategies is limited by the chemical structure of conventional PEO-silanes as well as the hydrophobic recovery of PEO-modified silicones. The structure of the PEO-silane will significantly influence its efficiency to repel proteins. A key structural feature is the nature of the PEO-silane spacer or "tether" separating the PEO segment and reactive end group. As noted above, conventional PEO alkoxysilanes contain a short alkane spacer (e.g. propyl) which may limit PEO configurational mobility [40-43,47,48]. Silicones are well-known to undergo extensive surface reconstruction when exposed to air versus aqueous environments [119]. Likewise, hydrophilic polymer chains incorporated into silicones restructure below the surface when maintained in air [106]. This effect has been observed for silicones modified with conventional PEO-silanes in which surface hydrophilicity decreases with exposure time in air [40]. Thus, upon exposure to aqueous

protein-containing environments, such surfaces are unable to optimally inhibit protein adsorption.

We recently reported new PEO-silanes prepared with a siloxane tether [α-$(EtO)_3Si(CH_2)_2$-oligodimethylsiloxane$_n$-*block*-$(OCH_2CH_2)_8$-OCH_3; n = 0, 4 and 13] [39,99]. The siloxane tether is highly flexible due to the wide bond angle (~145°) and low barrier to linearization (~0.3 kcal/mol) of Si–O–Si in dimethylsiloxanes [120,121]. The dynamic flexibility of the dimethylsiloxane backbone results in polymers with extremely low glass transition temperatures (T_gs) (e.g. PDMS, T_g = -125 °C). In addition to enhanced configurational mobility, the hydrophobicity of the siloxane tether imparts amphiphilic character to the PEO-silane amphiphile. Amphiphilicity is known to inhibit the adsorption of proteins [109,110]. Thus, PEO-silane amphiphiles surface-grafted onto silicon wafers exhibited enhanced protein resistance as the siloxane tether length was increased (i.e. n = 13) [39]. Also, when combined in a stoichiometric molar ratio with α,ω-bis(Si–OH)PDMS (M_n = 3000 g/mol; 2:3), the resulting bulk-crosslinked coatings similarly repelled proteins most effectively when formed with the PEO-silane containing the longest siloxane tether (i.e. n = 13) [99]. For these crosslinked coatings, contact angle analysis revealed that PEO chains restructured to both the air- and water-interface to a greater extent as the siloxane tether length increased.

In this study, the PEO-silane amphiphile bearing the longest siloxane tether (n = 13) was introduced into a medical grade, silica-reinforced silicone at varying levels (1 – 20 wt%) (**Figure 2.1**). The acetoxy cure RTV silicone is based on the acid-catalyzed condensation of a α,ω-bis(Si–OH)PDMS base and methyl-triacetoxysilane and

ethyltriacetoxysilane crosslinkers. PEO-modified silicone films were formed via solvent-casting (**Figure 2.2**). The thermal, mechanical and surface properties as well as protein adsorption behavior of the films were characterized.

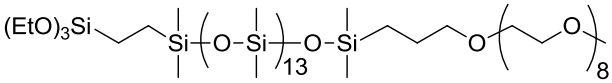

Figure 2.1. Structure of PEO-silane amphiphile.

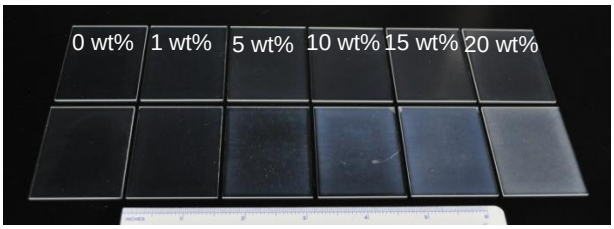

Figure 2.2. PEO-modified silicone before (top row) and after (bottom row) soaking in water (6 days). "wt%" corresponds to wt% PEO-silane amphiphile introduced.

2.3 Materials and Methods

2.3.1 Materials

Sodium bicarbonate and ACS-grade solvents were obtained from Sigma-Aldrich. Phosphate buffered saline (PBS, without calcium and magnesium, pH = 7.4) and glass microscope slides (75 x 50 mm; cut to a final size of 37.5 x 50 mm) were obtained from Fisher Scientific. Medical-grade silicone (MED-1137) was obtained from NuSil Technology (Carpinteria, CA). Per manufacturer specifications, MED-1137 is comprised of α,ω-bis(Si–OH)PDMS, silica (11-21%), methyltriacetoxysilane (<5%), ethyltriacetoxysilane (<5%), and trace amounts of acetic acid. The Alexa Fluor 555-dye

conjugate of bovine serum albumin (AF-555 BSA; MW = 66 kDa; lyophilized powder; > 96% BSA) and the Alexa Fluor 546-dye conjugate of human fibrinogen (AF-546 HF; MW = 340 kDa; lyophilized powder; 95% clottable protein) were purchased from Invitrogen (Carlsbad, CA). Silicone isolator wells for protein adsorption studies were prepared from silicone sheets (2 mm thick; McMaster Carr) with a die punch (18 mm diameter). The PEO-silane amphiphile (n = 13) was synthesized as previously reported [99].

2.3.2 Film Preparation

Microscope slides were sequentially washed with acetone, dichloromethane, and acetone and dried in a 100 ºC oven for at least 2 hr prior to use.

In a scintillation vial, MED-1137 was combined with hexane (1:3, wt:wt) and the PEO-silane amphiphile at varying amounts based on silicone weight (0, 1, 5, 10, 15 and 20 wt%). The sealed vial was placed on a shaker table for 4 hr to achieve a homogeneous solution.

Solutions were solvent-cast onto levelled glass microscope slides (1.5 mL per slide) and a polystyrene Petri dish cover placed on top of each. In this way, solvent evaporation was slowed which prevented the formation of gas bubbles in the resulting films. In this way, films were allowed to cure for seven days at room temperature (RT) and immediately used for designated tests. Free-standing films for thermal gravimetric analysis (TGA), dynamic mechanical thermal analysis (DMTA), and tensile testing were obtained by removing the films from slides with a clean single-edge razor blade. Coated

microscope slides were used for water-extractable content, water absorption, contact angle and protein adsorption measurements.

2.3.3 Thermal Gravimetric Analysis (TGA)

TGA was performed on the neat PEO-silane amphiphile and PEO-modified films (~10 mg) in Pt pans with a TA Instruments Q50 under N_2 or air at a flow rate of 60 cm^3/min. The sample weight was recorded while the temperature was increased 4 ºC/min from 25 to 800 ºC.

2.3.4 Glass Transition Temperature (T_g)

The T_g of each film was determined from the peak maximum of the measured loss modulus (G") as a function of temperature on a TA Instruments Q800 dynamic mechanical analyzer (DMA). Specimens (length x width = 37.5 x 5.5 mm^2) were cut from free-standing films using a single-edge razor cutting tool. Electronic calipers were used to measure film thickness (~0.12 mm) prior to testing. The DMA was operated using a tension clamp assembly at a gauge length of 6 mm, a frequency of 5 Hz, a displacement of 4 μm, and a pre-load force of 0.01 N. After equilibration at -140 ºC for 3 min, the temperature was increased 4 ºC/min to 25 ºC. Measurements were completed in triplicate.

2.3.5 Tensile Tests

Tensile properties of the films were performed at RT on a tensile tester (Instron 3345). Rectangular specimens (~37.5 mm x ~5.5 mm x ~0.12 mm) were tested with a gauge length of 5.5 mm and at a crosshead speed of 500 mm/min. From the resulting stress versus strain curves, tensile modulus (E), tensile strength (TS), and percent elongation at break (%ε) were determined. E was taken as the slope from 20-100% strain. Measurements were completed in triplicate.

2.3.6 Water-Extractable Content

Coated slides were weighed (W_i) and then continually soaked in DI water at 37 °C for 2 weeks. The films were subsequently dried at RT in a vacuum oven (30 in. Hg, 24 h) and weighed (W_f). The weight of the uncoated glass slide was subtracted from W_i and W_f before calculating the water-extractable content. Water-extractable content is defined as: water-extractable content = $[(W_i - W_f)/W_i] \times 100$. Measurements were completed in triplicate.

2.3.7 Absorbed Water Content

Coated slides were weighed (W_i) and then continually soaked in DI water at RT for 6 days. After removal from water, the surface was gently dried with a stream of air and immediately weighed (W_s). The weight of the uncoated glass slide was subtracted from W_i and W_s before calculating the water content. The absorbed water content is defined as: absorbed water content = $[(W_s - W_i)/W_i] \times 100$.

2.3.8 Contact Angle Measurements

Static contact angles (θ_{static}) of distilled/deionized water droplets at the film-air interface were measured at RT with a CAM200 (KSV Instruments) goniometer equipped with an autodispenser, video camera, and drop-shape analysis software. Following cure, coated microscope slides were immediately subjected to contact angle analysis and/or subsequent conditioning in water or air (described below). A sessile drop of water (5 μL) was measured 15 sec, 1 min, and 2 min after deposition onto the film surface. The reported values are an average of three measurements taken on different areas of the same film sample. For each film composition, two coated microscope slides were analyzed. One slide served to measure the contact angles of a film surface during conditioning in water ("water-equilibrated"; for a period of 6 days) and the other during conditioning in air ("air-equilibrated"; for a period of 60 days). For air-equilibrated films, sessile water droplets were removed under a stream of air such that the film could continue to equilibrate in air until the next measurement. For water-equilibrated films, the surface water was removed under a stream of air just prior to contact angle analysis and subsequently re-submerged in water until the next measurement.

2.3.9 Protein Adsorption

The adhesion of Alexa Fluor dye conjugates of bovine serum albumin (AF-555 BSA) and human fibrinogen (AF-546 HF) onto film surfaces was studied with fluorescence microscopy. A silicone isolator (18 mm well diameter, 2 mm well depth) was affixed to each coated microscope slide. For each film composition, four coated

microscope slides were analyzed. Two slides served to test a film surface exposed to air prior to the deposition of AF-555 BSA and AF-546 HF solutions whereas the other two served to likewise test a film surface that was first exposed to PBS for 24 h.

For "air-equilibrated" films, the exposed surface of the film inside each isolator well was filled with 0.7 mL of AF-555 BSA solution (0.1 mg/mL in PBS) [39,99,117] or AF-546 HF solution (0.1 mg/mL) [39,117]. (Note: Per manufacturer specifications, the AF-546 HF was first dissolved in 0.1 M $NaHCO_3$ to obtain 1.5 mg/mL solution and was further diluted in PBS to obtain a final concentration of 0.1 mg/mL.) After equilibrating in the dark at RT for 3 h, the solution was removed and 0.7 mL of fresh PBS was then added to each well and removed after 5 min. This process was repeated a total of three times. The samples were then dried under a stream of N_2 and immediately imaged.

For "PBS-equilibrated" films, the exposed surface of the film inside each isolator well was filled with 0.7 mL of PBS and removed after 24 hr. Exposure to AF-555 BSA or AF-546 solutions (3 hr) was immediately executed using the same protocol as above.

A Zeiss Axiovert 200 optical microscope equipped with an A-plan 5x objective, Axiocam (HRC Rev. 2), and filter cube (excitation filter of 546 ± 12 nm [band pass] and emission filter 575-640 nm [band pass]) was used to obtain fluorescent images on three randomly selected regions of the surface within each isolator well. The fluorescent light source was permitted to warm up for 10 min prior to image capture. Linear operation of the camera was ensured and constant exposure time used during the image collection to permit quantitative analyses of the observed fluorescent signals. The fluorescence microscopy images were analyzed using ImageJ, which yielded the mean of the

fluorescence intensity for a given image. The fluorescence intensity of each non-exposed region was subtracted from the corresponding protein-exposed region to ensure correction for any fluorescence signal from the material itself. The background-corrected fluorescence intensities for each film were then used to quantify AF-555 BSA or AF-546 HF levels adsorbed by comparison against a calibration curve constructed from the measured fluorescence intensities of AF-555 BSA or AF-546 HF standard samples, respectively. The obtained value was converted to $\mu g/cm^2$ by dividing by the area inside the isolator well. Standard samples were prepared by adding 0.7 mL of AF-555 BSA or AF-546 HF solutions of known concentrations (0, 0.001, 0.0025, 0.005, 0.0075 and 0.01 mg/mL AF-555 BSA or AF-546 HF diluted in the same manner as described above) to individual wells in a 24-well plate. For all film surfaces, the reported protein adsorption value is an average of three measurements taken from different areas of the same sample.

2.4 Results and Discussion

2.4.1 Preparation of Films

A medical grade, silica-reinforced acetoxy cure RTV silicone was modified with different levels of a PEO-silane amphiphile (0, 1, 5, 10, 15 and 20 wt%) (**Figure 2.1**). Films were prepared by solvent-casting with hexane onto glass slides. The resulting PEO-modified silicones remained transparent (**Figure 2.2**).

2.4.2 TGA

The exceptional thermal stability of polysiloxanes is further enhanced upon crosslinking [122]. Thus, the thermal stabilities of PEO-modified silicones were used as an indicator of successful formation of crosslinked networks (**Figure 2.3**). The degradation profiles of these films were compared to that of unmodified silicone film controls (i.e. 0 wt% PEO-silane amphiphile) as well as that of the neat PEO-silane amphiphile. As expected, all films began to degrade at lower temperatures in air versus in N_2. In air, degradation of polysiloxanes are known to produce silica residue [122]. Thus, in air, ~60-65% silica was produced for all films. Compared to the unmodified silicone control, the thermal stabilities of the PEO-modified silicones did not vary substantially. In addition, no significant weight loss from these films was observed at

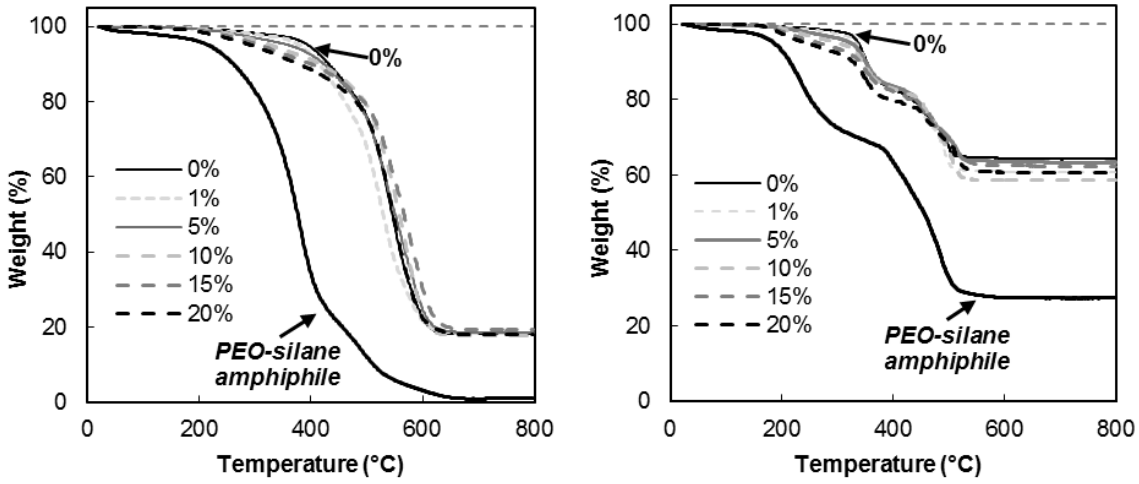

Figure 2.3. TGA of films in N_2 (left) and in air (right).

lower temperatures characteristic of neat PEO-silane amphiphile degradation. Thus, the PEO-silane amphiphile was successfully crosslinked into the modified silicone films.

2.4.3 T_g

The T_gs of the PEO-modified silicones were measured by dynamic mechanical thermal analysis (DMTA) (**Table 2.1**). The T_g of each film was determined from the peak of the G" [123]. An unmodified silicone film (i.e. 0 wt% PEO-silane amphiphile) served as a control. A depression in the film T_g (i.e. plasticization) relative to the control would be observed if the PEO-silane amphiphile did not effectively crosslink during formation of the silicone network. However, all films exhibited similar T_g values between -112 and -110 °C and were not significantly different versus the unmodified silicone (T_g = -111 ºC).

Table 2.1. T_g and mechanical properties.

wt% PEO-silane	T_g (ºC)	E (MPa)	TS (MPa)	%Strain
0%	-111 ± 0.1	0.33 ± 0.04	6.37 ± 0.4	1165 ± 47
1%	-110 ± 0.7	0.33 ± 0.01	5.25 ± 0.6	1093 ± 25
5%	-112 ± 0.6	0.35 ± 0.01	5.63 ± 0.2	1212 ± 200
10%	-111 ± 0.2	0.29 ± 0.02	4.09 ± 0.4	1128 ± 125
15%	-111 ± 0.2	0.18 ± 0.01	3.64 ± 0.2	1490 ± 166
20%	-110 ± 0.2	0.19 ± 0.01	2.47 ± 0.2	1169 ± 59

2.4.4 Tensile Testing

The tensile mechanical properties of the PEO-modified silicones are summarized in **Table 2.1**. Following crosslinking, the PEO amphiphile segments in all films exist as "dangling free ends". Because of the low crosslink density of the films, the beta transition temperature (T_β) was not observed in DMTA [124]. However, the presence of an increasing number of PEO dangling ends with wt% of PEO-silane amphiphile produced an expected decrease in E and TS. In addition, as PEO-silane amphiphile concentration was raised, there was a concomitant decrease in the total amount of reinforcing silica in the resulting film. The average %ε of all films was around 1200%. While an increase in %ε with increasing amounts of PEO-silane amphiphile was expected, the films apparently became too weak to withstand higher strains.

2.4.5 Water-Extractable Content

Given their targeted use in an aqueous environment, PEO-modified silicone films were continually soaked in DI water at 37 °C for 2 weeks. For all films, weight loss did not exceed 0.05%. This indicates that PEO-silane amphiphile or other components do not readily leach from the films.

2.4.6 Absorbed Water Content

With increased levels of PEO-silane amphiphile, surface and bulk hydrophilicity were increased and subsequently led to water uptake (**Table 2.2**). Water content increased to ~6.5 wt% for films containing 15 and 20 wt% PEO-silane amphiphile.

Following water exposure, the films became progressively more opaque as PEO-silane amphiphile content was increased (**Figure 2.2**). The presence of increasing amounts of water in the films causes them to become more opaque due to their incompatibility. Upon drying in a vacuum oven, the films returned to their original transparent appearance.

Table 2.2. Contact angle measurements.

wt% PEO-silane	wt% adsorbed water	*t* = 0 ("air-equilibrated")			*t* = 6 days ("water-equilibrated")		
		15 s	1 min	2 min	15 s	1 min	2 min
0%	0.15	113.7 ± 0.2	113.1 ± 0.3	112.3 ± 0.8	103.8 ± 3.0	102.6 ± 3.4	101.8 ± 2.9
1%	0.53	113.8 ± 1.2	104.4 ± 1.5	95.0 ± 1.4	106.0 ± 1.8	104.9 ± 0.7	101.6 ± 0.2
5%	2.07	91.6 ± 0.7	59.9 ± 1.3	49.1 ± 1.1	105.3 ± 0.7	68.1 ± 1.1	53.3 ± 0.9
10%	3.65	61.7 ± 1.1	43.9 ± 0.2	33.4 ± 0.1	89.6 ± 2.0	54.7 ± 1.4	45.8 ± 1.1
15%	6.57	50.1 ± 0.4	30.6 ± 0.3	26.2 ± 0.2	71.2 ± 18.8	44.8 ± 7.1	38.9 ± 4.2
20%	6.4	44.1 ± 0.1	30.8 ± 0.1	27.2 ± 0.2	58.8 ± 9.4	41.2 ± 1.4	37.5 ± 0.8

2.4.7 Contact Angle Analysis

Contact angle measurements of water droplets on freshly cured films before (t = 0 days; air-equilibrated) and after subsequent conditioning in water (t = 6 days; water-equilibrated) are reported in **Table 2.2**. By measuring θ_{static} over a period of 2 minutes following droplet deposition, we were able to effectively monitor surface reorganization at the water-film interface. The longer time period of this analysis versus conventional dynamic contact angle analysis (~7 sec) better captures surface reconstruction [39,117]. As expected, the unmodified silicone film exhibited high values of θ_{static} (~113 º) that did not significantly change over the 2 minute contact angle measurement nor was there a substantial change in before and after water equilibration. In contrast, for PEO-modified

silicone films, θ_{static} (15 sec) substantially decreased (i.e. hydrophilicity increased) as the PEO-silane amphiphile content increased. In addition, for a given film, the θ_{static} systematically decreased from 15 sec to 2 min. This indicates that the PEO-silane amphiphile chains are readily mobilized to the water-film interface. After 6 days, water-equilibrated films displayed θ_{static} values which were unexpectedly higher relative to the corresponding air-equilibrated film (t = 0 days). This observation became more pronounced as the PEO-silane amphiphile content was increased. As previously noted, films absorbed increasing amounts of water as PEO-silane amphiphile content was increased (**Table 2.2**, **Figure 2.2**). Thus, given the presence of water in the bulk, PEO-silane amphiphile chains are less thermodynamically driven to the water-droplet-film interface. Still, for a given water-equilibrated film, θ_{static} still systematically decreased from 15 sec to 2 min after droplet deposition. Thus, in the time it took to remove the films from water, air dry the surfaces and immediately begin analysis, some chains began to reorganize below the surface, but they began to rearrange to the surface after exposure to the water-droplet. θ_{static} (2 min) of films was also recorded throughout the 6 day period of water equilibration (**Figure 2.4a**).

We likewise characterized film surfaces following prolonged periods of exposure to air (**Figure 2.4b**). When conditioned in air over extended periods, hydrophilic polymer chains (including conventional PEO-silanes) [40] incorporated into silicones restructure below the surface leading to reduced surface hydrophilicity [106]. For PEO-modified silicones, during 60 days of conditioning in air, θ_{static} (2 min) values were

generally quite stable. Moreover, these films did not display marked hydrophobic recovery, particularly those containing with 5-20 wt% PEO-silane amphiphile.

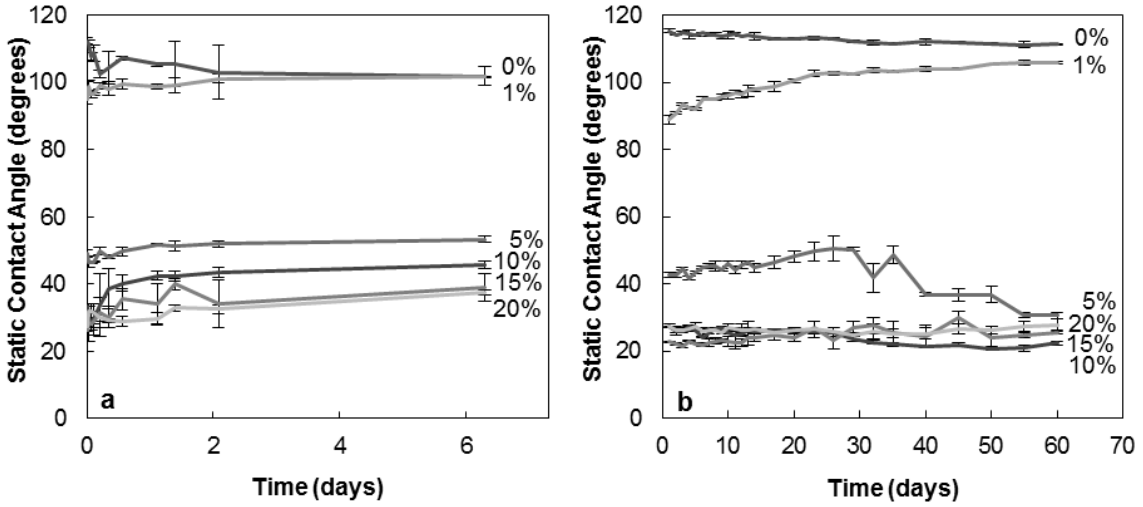

Figure 2.4. θ_{static} (2 min) of films (a) before (t = 0) and during 6 days of exposure to DI water and (b) during exposure to air for 60 days. "wt%" = wt% of PEO-silane amphiphile.

2.4.8 Protein Adsorption

Albumin is the most abundant plasma protein (60%) and fibrinogen (4%), also a plasma protein, converts thrombin to insoluble fibrin during clot formation [125]. Thus, the amounts of BSA and HF proteins adsorbed onto films were analyzed to determine plasma protein resistance (**Figure 2.5**). Protein adsorption of BSA and HF conjugated with a fluorescent dye was measured via fluorescence microscopy [39,97,99,117,126-128]. The detection limit of this method was ≤ 0.003 μg protein adsorbed/cm^2. For films adsorbing less than this amount, the values in **Figure 2.5** were reported to be "zero". For

each film composition, protein adsorption was measured before (air-equilibrated) and after (PBS-equilibrated) equilibration in PBS (24 hr).

As a result of its extreme hydrophobicity [7,8], the unmodified silicone control adsorbed the highest levels of BSA and HF as expected. The observed levels of protein adsorption are similar to those previously reported in the literature [43,129,130]. For all films, including the control, higher amounts of HF were adsorbed versus BSA due to the greater hydrophobicity and rod-like structure of HF [125,131,132].

Incorporation of the PEO-silane amphiphile into the silicone produced a dramatic decrease in adsorption of BSA and HF proteins. This is attributed to the associated reduction in surface hydrophobicity (**Table 2.2**). When conditioned in air, films exhibited protein adsorption below the detectable limit when based on 5-20 wt% (BSA, **Figure 2.5a**) and 10-20 wt% (HF, **Figure 2.5b**) PEO-silane amphiphile. Thus, although increased wt% of PEO-silane amphiphile progressively increases surface hydrophilicity (**Table 2.2**), maximum reduction in protein adsorption is realized before reaching 20 wt%.

For all PEO-silane modified silicones having a detectable amount of adsorbed protein when equilibrated in air, equilibrating the films in PBS (24 hr) produced a relative reduction in protein adsorption. The contact angles of films conditioned for 24 hr in water is noted in **Figure 2.4a**. As previously noted, hydrophilicity decreased somewhat due to the water uptake into the film and reduced concentration of PEO-silane amphiphile chains at the surface. The reduction in protein adsorption of PBS-

equilibrated films may be due to the improved hydration of the PEO chains on the surface.

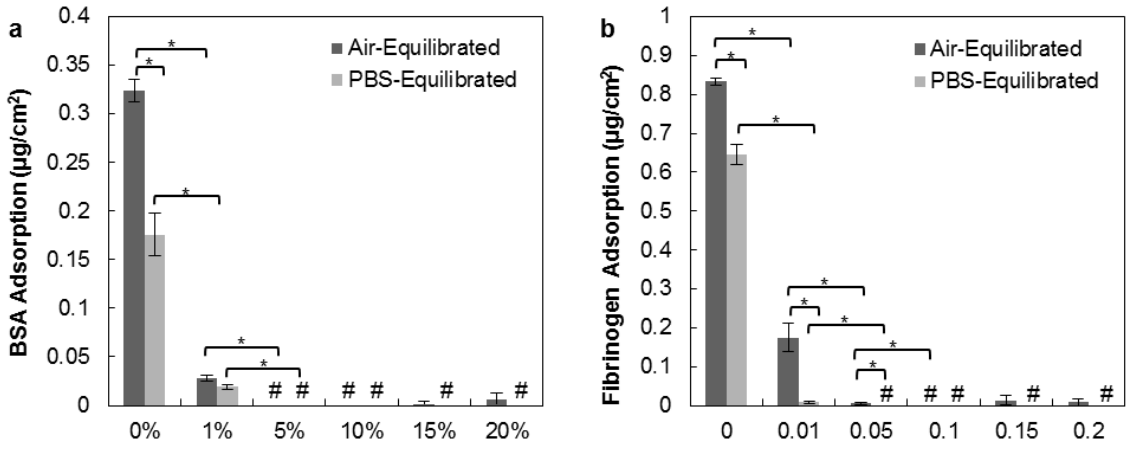

Figure 2.5. Adsorption of (a) BSA and (b) HF. Error bars represent the standard deviation between fluorescence measurements of 3 randomly selected regions. Statistical significance was determined by one-way analysis of variance (Holm–Sidak method where $p = 0.05$) and is denoted by *. Values below the detection limit are indicated by # and recorded as "0" µg cm^{-2}.

2.5 Conclusions

A PEO-silane amphiphile bearing a hydrophobic, flexible siloxane tether (n = 13) was introduced into a medical grade, silica-reinforced silicone at varying levels (1 – 20 wt%). TGA and DMTA confirmed that the PEO-silane modified silicones were effectively crosslinked. As expected, E and TS of the films were decreased with high levels of PEO-silane amphiphile. As the amount of PEO-silane amphiphile was increased, surfaces became more hydrophilic. Following water-equilibration, film surfaces were somewhat more hydrophobic versus the corresponding air-equilibrated

films. This was attributed to water uptake by the films and the subsequent reduction of PEO amphiphile chains located at the surface. Notably, surfaces maintained in air over a 60 day period did not exhibit notable hydrophobic recovery. As a result of their surface properties, these PEO-modified silicones exhibited exceptional protein resistance to BSA and HF, particularly when prepared with ≥ 5 wt% of PEO-silane amphiphile. This was observed for films both before and after conditioning in water. Such behavior is significant, as blood-contacting silicone-based coatings and devices are stored for extended periods of time (in air) before implantation. Thus, such PEO-modified silicones would be excellent candidates for these applications.

2.5.1 Acknowledgements

Funding from the Texas Engineering and Experiment Station (TEES) is gratefully acknowledged. M.L.H. thanks the Texas A&M University Diversity Fellowship Program for support.

CHAPTER III

PITFALLS OF PEO MODIFICATION OF SILICONES: PEO-SILANE AMPHIPHILES' SUPERIOR ABILITY TO REDUCE PROTEIN ADSORPTION

3.1 Overview

Versus with conventional PEO-silanes (i.e. no siloxane tether), silicones with improved water-driven surface hydrophilicity and resistance to protein adsorption were prepared by bulk-modification with PEO-silane amphiphiles: α-$(EtO)_3Si$-$(CH_2)_2$-oligodimethylsiloxane$_m$-*block*-poly(ethylene oxide)$_8$-OCH_3 having varying lengths of the siloxane tether (m = 0, 4, 13, 17, 24, and 30). As a control, a conventional PEO_8-silane was prepared. To examine protein resistance in the absence and presence of water-driven surface restructuring, respectively, the amphiphiles and control were surface-grafted onto silicon wafers and used to bulk-modify a medical-grade silicone. While surface-grafted PEO_8-silane control exhibited superior protein resistance, it failed to restructure to the surface-water interface of a bulk-modified silicone and thus led to poor protein resistance. In contrast, the PEO-silane amphiphiles, while less protein resistant when surface-grafted onto silicon wafers, rapidly and substantially restructured in the bulk-modified silicone thereby exhibiting superior hydrophilicity and protein resistance. An intermediate siloxane tether length was observed to maximize surface restructuring as well as subsequent protein resistance.

3.2 Introduction

Silica-reinforced silicones such as polydimethylsiloxane (PDMS) are widely used in biomedical applications [11,12,133] due to their unique properties including thermal and oxidative stability, gas permeability, flexibility, and ease of processing [11,12]. Silicone-based medical devices include hemodialysis catheters, cardiac pacing leads, catheter balloons, coated metal stents, extracorporeal device tubing, and various surgical devices [11,12,133]. Unfortunately, due to their hydrophobic nature, silicones lack resistance to protein adsorption [14-16,134,135]. Thus, upon implantation of silicone medical devices, plasma proteins are rapidly and substantially adsorbed, leading to subsequent platelet adhesion, activation of coagulation pathways, and eventual thrombosis [9,134-137]. To improve the efficacy and safety of silicone-based devices, reduction of protein adsorption is essential. In efforts to diminish protein adsorption, silicones have been hydrophilized by various physical, chemical, and combined approaches [116,135,138-140].

Poly(ethylene oxide) (PEO; or poly(ethylene glycol) (PEG)) is noted for its exceptional protein resistance [14,15,141,142]. This behavior is attributed to its hydrophilicity and hydration [143] as well as its configurational mobility which leads to a large excluded volume, steric repulsion, blockage of underlying adsorption sites, and an entropic penalty associated with protein adsorption [14,15,28,142,144]. PEO's biocompatibility [145] and recently noted *in vivo* oxidative stability [146] contributes to its widespread use in biomaterials. However, the protein resistance of PEO has largely been demonstrated for chains surface-grafted onto physically stable, model substrates

such as gold [102,147,148], silicon wafers [101,149,150], and glass [100,103]. Such "model PEO surfaces" maintain the PEO chains at the surface whether exposed to air or to an aqueous environment [100-103,147,148,151,152]. This is in contrast to modified silicones in which PEO chains may undergo surface-reorganization following exposure to different environments [153]. Thus, since protein adsorption occurs in an aqueous environment, it is critical that PEO chains migrate to the surface-water interface to create a PEO-enriched silicone surface. Surface-restructuring of silicones has largely been studied in terms of hydrophobic recovery (i.e. loss of hydrophilicity upon exposure to air) as observed for plasma treated silicones [154]. This recovery is attributed to their low surface energy [155,156] and high chain flexibility [120,121]. PEO-modified silicones likewise display hydrophobic recovery. For instance, silicones prepared by bulk crosslinking with triethoxysilylpropyl PEO monomethyl ether [$(EtO)_3Si(CH_2)_3$-$(OCH_2CH_2)_m$-OCH_3] [48,157] as well as allyl PEO monomethyl ether [CH_2=$CHCH_2$-$(OCH_2CH_2)_m$-OCH_3] [158] hydrophobically recover. This is also observed for surface-grafted PEO chains such as those prepared with allyl PEO monomethyl ether [43,158]. Notably lacking is the systematic evaluation of water-driven hydrophilicity of PEO-modified silicones which is of critical importance to protein resistance. Recent reports highlight the poor efficacy of PEO-modified and other polymer matrices to prevent thrombosis [104,105,159] which may indicate poor mobilization of the PEO to the surface-water interface [153].

To enhance PEO's ability to undergo water-driven surface reorganization in silicones, the chemical structure of a PEO-silane was altered to include a hydrophobic,

flexible siloxane "tether" separating the PEO segment and crosslinkable end group (**Figure 3.1**). This is in contrast to conventional PEO alkoxysilanes that contain a short alkane spacer (e.g. propyl) [42,43,48,157,159,160]. Previously, we reported three different PEO-silane amphiphiles prepared with short siloxane tethers [α-$(EtO)_3Si(CH_2)_2$-oligodimethylsiloxane$_m$-*block*-$(OCH_2CH_2)_8$-OCH_3; m = 0, 4, and 13] [39,99]. The high mobility of the siloxane tether is a result of its highly flexible nature, attributed to the wide bond angle (~145°) and low barrier to linearization (~0.3 kcal/mol) of Si–O–Si [120,121]. The dynamic flexibility of the backbone accounts for the extremely low glass transition temperature (T_g) of PDMS (T_g = -125 °C). In addition to enhanced configurational mobility, the hydrophobic siloxane tether renders the PEO-silane amphiphilic, a property associated with enhanced protein resistance [161,162]. The flexibility and similarly hydrophobic nature of the siloxane tether was anticipated to enhance reorganization of PEO to the surface-water interface and reduce protein adsorption. Our previous studies showed that, in addition to enhanced protein resistance versus a conventional PEO-silane, protein adsorption decreased with increased siloxane tether length (i.e. m = 13 < 4 < 0) [99,163].

Herein, to better understand the influence and to maximize the influence of the siloxane tether, PEO-silane amphiphile were also prepared with longer siloxane tether lengths [m = 0 (**m=0**), M_n = 749 g/mol; 4 (**m=4**), M_n = 1044 g/mol; 13 (**m=13**), M_n = 1710 g/mol; 17 (**m=17**), M_n = 2006 g/mol; 24 (**m=24**), M_n = 2524 g/mol; and 30 (**m=30**), M_n = 2968 g/mol] (**Figure 3.1**). PEO-silane amphiphiles were both surface-grafting onto a model substrate and used for bulk-modification of silicone. Grafting onto silicon

wafers permitted the evaluation of protein resistance in the absence of surface restructuring effects. PEO-silane amphiphiles were also incorporated into a medical grade, silica-reinforced silicone via bulk modification. Water-driven surface-restructuring of PEO-modified silicones was quantified using temporal static contact angle analysis of water droplets and protein resistance measured. A conventional PEO-silane (i.e. no siloxane tether) $(EtO)_3Si–(CH_2)_3–$poly(ethylene oxide)$_8–OCH_3$ was utilized as a "PEO control".

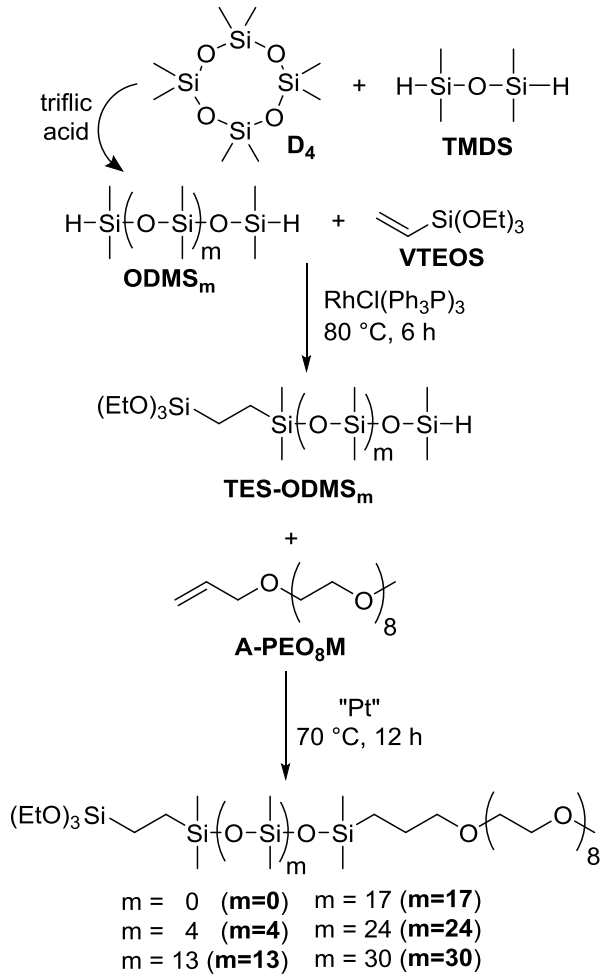

Figure 3.1. Synthesis of PEO-silane amphiphiles **m=0** – **m=30**.

3.3 Materials and Methods

3.3.1 Materials

Triflic acid, $RhCl(Ph_3P)_3$ (Wilkinson's catalyst), solvents, sulfuric acid (H_2SO_4), hexamethyldisilazane (HMDS), and fibrinogen from human plasma (HF; M_w = 340 kDa; lyophilized powder; ≥90% clottable protein) were obtained from Sigma-Aldrich (St. Louis, MO). Solvents were dried over 4Å molecular sieves prior to use in hydrosilylation reactions. Octamethylcyclotetrasiloxane (**D_4**; MW = 296 g/mol), Pt–divinyltetramethyldisiloxane complex (Karstedt's catalyst), vinyltriethoxysilane (**VTEOS**; MW = 190 g/mol), α,ω-bis-(Si–OH)oligodimethylsiloxanes {**$ODMS_0$** or tetramethyldisiloxane (**TMDS**) [M_n = 118 g/mol per manufacturer's specifications; M_n = 134 g/mol per ^{1}H NMR end group analysis; ^{1}H NMR (δ, ppm): 0.17 – 0.21 (m, 12H, SiCH_3) and 4.66 – 4.72 (m, 2H, Si*H*)]; **$ODMS_4$** [M_n = 400-500 g/mol per manufacturer's specifications; M_n = 430 g/mol per ^{1}H NMR end group analysis; ^{1}H NMR (δ, ppm): 0.07 – 0.09 (m, 24H, SiCH_3), 0.18 – 0.19 (d, J = 2.7 Hz, 12H, SiCH_3) and 4.67 – 4.73 (m, 2H, Si*H*); **$ODMS_{13}$** [M_n = 1000-1100 g/mol per manufacturer's specifications; M_n = 1096 g/mol per ^{1}H NMR end group analysis; ^{1}H NMR (δ, ppm): 0.05 – 0.10 (m, 78H, SiCH_3), 0.185 (d, J = 2.7 Hz, 12H, SiCH_3) and 4.67 – 4.73 (m, 2H, Si*H*)]}, and monovinyl-terminated PDMS (**CH_2=CH–PDMS-*n*-Bu**) [M_n = 62,700 g/mol, essentially 100% monovinyl-terminated with the nonfunctional end *n*-butyl-terminated per manufacturer's specifications] were obtained from Gelest. PEO allyl methyl ether (Polyglycol AM-450; **A-PEO_8M**) [M_n = 292 – 644 g/mol per manufacturer's specifications; M_n = 424 g/mol per ^{1}H NMR end group analysis; ^{1}H NMR (δ, ppm): 3.35 (s, 3H, OCH_3), 3.51 – 3.66 (m,

32H, OCH_2CH_2), 4.00 (d, J = 5.4 Hz, 2H, CH_2=CHCH_2O), 5.13 – 5.28 (m, 2H, CH_2=CHCH_2O), 5.82 – 5.96 (m, 1H, CH_2=CHCH_2O)] was obtained from Clariant and was dried overnight under high vacuum prior to use. Silicon wafers (111) were obtained from University Wafers, Inc. (Boston, MA). Silica-coated QCM-D sensors (QSX-303) were obtained from Q-Sense. Hydrogen peroxide (H_2O_2), glass microscope slides (3" x 1"), and phosphate buffered saline (PBS, without calcium and magnesium, pH = 7.4) were obtained from Fisher Scientific. Medical-grade silicone (MED-1137) was obtained from NuSil Technology (Carpinteria, CA). Per manufacturer specifications, MED-1137 is comprised of α,ω-bis(Si–OH)PDMS, silica (11-21%), methyltriacetoxysilane (<5%), ethyltriacetoxysilane (<5%), and trace amounts of acetic acid. The Alexa Fluor 546-dye conjugate of human fibrinogen (AF-546 HF; M_w = 340 kDa; lyophilized powder; 95% clottable protein) was purchased from Invitrogen (Carlsbad, CA). Silicone isolator wells for protein adsorption studies were prepared from silicone sheets (2 mm thick; McMaster Carr) with a die punch (18 mm diameter). The PEO-silane amphiphiles (m = 0 (**m=0**), 4 (**m=4**), and 13 (**m=13**)) and the **PEO control** were synthesized as previously reported [99].

3.3.1 Polymer Characterization

3.3.1.1 NMR

^{1}H spectra were obtained on a Mercury 300 MHz spectrometer operating in the Fourier transform mode. Five percent (w/v) $CDCl_3$ (dried over 4 Å molecular sieves)

solutions were used to obtain spectra. Residual $CDCl_3$ was used as an internal standard set to 7.26 ppm.

3.3.1.2 IR Spectroscopy

IR spectra of neat liquids on NaCl plates were recorded using a Bruker TENSOR 27 Fourier transform infrared spectrometer.

3.3.1.3 Gel Permeation Chromatography (GPC)

GPC analysis was performed on a Tosoh Corporation (Tokyo, Japan) model HLC-8320 EcoSEC system with a two-column set of TOSOH Bioscience TSKgel columns (Super HM-M 6.0 mm ID x 15 cm columns) and a guard column (Super H-H 4 μm). The system was equilibrated at 40 °C in chloroform, which served as the polymer solvent and eluent (flow rate set to 0.6 mL/min). The differential refractometer was calibrated with Polymer Laboratories, Inc. polystyrene standards (580 to 370,000 Da).

3.3.1.4 Synthetic Approach

All reactions were run under a nitrogen (N_2) atmosphere with a Teflon-covered stir bar to agitate the reaction mixture.

$ODMS_m$ (**$ODMS_{17}$**, **$ODMS_{24}$**, and **$ODMS_{30}$**) was prepared by a triflic acid-catalyzed ring-opening reaction of **D_4** with **TMDS** (**Figure 3.1**) [164]. **D_4** and **TMDS** (4:1, 5:1, and 6:1 molar ratios) were combined with triflic acid in a 100 mL round-bottom (rb) flask equipped with a rubber septum at RT. After 2.5 h, HMDS was added to

the reaction to neutralize the acid. The reaction was then filtered to remove salts, and volatiles removed under reduced pressure.

α-Triethoxysilylethyl-ω-silane-oligodimethylsiloxane$_m$ (**TES-ODMS$_{17}$**, **TES-ODMS$_{24}$**, and **TES-ODMS$_{30}$**) and triethoxysilylethyl-oligodimethylsiloxane$_n$-*block*-poly(ethylene oxide)$_8$ (**m=17**, **m=24**, and **m=30**) were likewise prepared using a previously reported strategy [99]. Briefly, **TES-ODMS$_{17}$**, **TES-ODMS$_{24}$**, and **TES-ODMS$_{30}$** were synthesized by the Rh-catalyzed regioselective hydrosilylation of equimolar amounts of **VTEOS** with **ODMS$_{17}$**, **ODMS$_{24}$**, and **ODMS$_{30}$**, respectively (**Figure 3.1**). An equimolar ratio of **ODMS$_m$** and **VTEOS** were combined with Wilkinson's catalyst and toluene and then heated to 80 °C. After 12 h, toluene was removed under reduced pressure, the product was purified by flash column chromatography on silica gel with hexanes/ethyl acetate (2:1 v/v), and volatiles were removed under reduced pressure. PEO-silane amphiphiles **m=17**, **m=24**, and **m=30** were synthesized by the Pt-catalyzed hydrosilylation of **A-PEO$_8$M** with **TES-ODMS$_{17}$**, **TES-ODMS$_{24}$**, and **TES-ODMS$_{30}$**, respectively (**Figure 3.1**). **TES-ODMS$_m$** and **A-PEO$_8$M** (1:1 molar ratio) were combined with Karstedt's catalyst and toluene and then heated to 70 °C. After 12 h, the progress of the reaction was confirmed by the disappearance of the Si–H (~2125 cm^{-1}) absorbance via IR spectroscopy. The catalyst was removed by refluxing the reaction mixture with activated charcoal for 2 h at 80 °C. After filtration, the volatiles were removed under reduced pressure so that **m=17**, **m=24**, and **m=30** were isolated as colorless liquids.

3.3.1.5 Synthesis of **ODMS$_{17}$**

D$_4$ (20.03 g, 0.068 mol), **TMDS** (2.28 g, 0.017 mol), and triflic acid (40 μL) were reacted as above and quenched with the final addition of HMDS (94 μL). In this way, **ODMS$_{17}$** (13.3 g, 60% yield) was obtained. ^{1}H NMR (δ, ppm): 0.03–0.12 (m, 102H, SiC*H*$_3$), 0.19 (m, 12H, SiC*H*$_3$), 4.70 (m, 2H, Si*H*).

3.3.1.6 Synthesis of **ODMS$_{24}$**

D$_4$ (20.07 g, 0.07 mol), **TMDS** (1.85 g, 0.014 mol), and triflic acid (40 μL) were reacted as above and quenched with the final addition of HMDS (94 μL). In this way, **ODMS$_{24}$** (18.2 g, 83% yield) was obtained. ^{1}H NMR (δ, ppm): 0.05–0.11 (m, 144H, SiC*H*$_3$), 0.19 (m, 12H, SiC*H*$_3$), 4.70 (m, 2H, Si*H*).

3.3.1.7 Synthesis of **ODMS$_{30}$**

D$_4$ (20.05 g, 0.07 mol), **TMDS** (1.53 g, 0.011 mol), and triflic acid (40 μL) were reacted as above and quenched with the final addition of HMDS (94 μL). In this way, **ODMS$_{30}$** (16.5 g, 76% yield) was obtained. ^{1}H NMR (δ, ppm): 0.03–0.11 (m, 180H, SiC*H*$_3$), 0.19 (m, 12H, SiC*H*$_3$), 4.70 (m, 2H, Si*H*).

3.3.1.8 Synthesis of **TES-ODMS$_{17}$**

ODMS$_{17}$ (7.12 g, 5.1 mmol), **VTEOS** (0.98 g, 5.1 mmol), and Wilkinson's catalyst (10 mg) in toluene (50 mL) were reacted as above. In this way, **TES-ODMS$_{17}$** (7.8 g, 96% yield) was obtained. ^{1}H NMR (δ, ppm): 0.02–0.20 (m, 114H, SiC*H*$_3$), 0.56

(m, 3H, SiCH_2CH_2), 1.09 (m, 1H, SiCH_2CH_2), 1.23 (m, 9H, SiOCH$_2$CH_3), 3.82 (m, 6H, SiOCH_2CH$_3$), 4.71 (m, 1H, Si*H*).

3.3.1.9 Synthesis of **TES-ODMS$_{24}$**

ODMS$_{24}$ (13.0 g, 6.8 mmol), **VTEOS** (1.3 g, 6.8 mmol), and Wilkinson's catalyst (10 mg) in toluene (50 mL) were reacted as above. In this way, **TES-ODMS$_{24}$** (13.8 g, 97% yield) was obtained. ^{1}H NMR (δ, ppm): 0.001–0.22 (m, 156H, SiCH_3), 0.56 (m, 3H, SiCH_2CH_2), 1.09 (m, 1H, SiCH_2CH_2), 1.23 (m, 9H, SiOCH$_2$CH_3), 3.82 (m, 6H, SiOCH_2CH$_3$), 4.70 (m, 1H, Si*H*).

3.3.1.10 Synthesis of **TES-ODMS$_{30}$**

ODMS$_{30}$ (11.9 g, 5.1 mmol), **VTEOS** (0.97 g, 5.1 mmol), and Wilkinson's catalyst (10 mg) in toluene (50 mL) were reacted as above. In this way, **TES-ODMS$_{30}$** (12.7 g, 99% yield) was obtained. ^{1}H NMR (δ, ppm): 0.02–0.20 (m, 192H, SiCH_3), 0.56 (m, 3H, SiCH_2CH_2), 1.09 (m, 1H, SiCH_2CH_2), 1.23 (m, 9H, SiOCH$_2$CH_3), 3.82 (m, 6H, SiOCH_2CH$_3$), 4.70 (m, 1H, Si*H*).

3.3.1.11 Synthesis of **m=17**

TES-ODMS$_{17}$ (7.8 g, 0.005 mol), **A-PEO$_8$M** (2.1 g, 0.005 mol), and Karstedt's catalyst (50 μL) in toluene (100 mL) were reacted as above. In this way, **m=17** (7.7 g, 78% yield) was obtained. ^{1}H NMR (δ, ppm): 0.01–0.11 (m, 114H, SiCH_3), 0.47-0.54 (m, 2H, SiCH_2CH$_2$CH$_2$), 0.55 (m, 3H, SiCH_2CH_2), 1.08 (m, 1H, SiCH_2CH_2), 1.22 (m, 9H,

$SiOCH_2CH_3$), 1.59 (m, 2H, $SiCH_2CH_2CH_2$), 3.37 (s, 3H, OCH_3), 3.56 (m, 2H, $SiCH_2CH_2CH_2$), 3.64 (m, 32H, OCH_2CH_2), 3.81 (m, 6H, $SiOCH_2CH_3$). IR (ν): no Si–H band.

3.3.1.12 Synthesis of **m=24**

TES-ODMS$_{24}$ (13.4 g, 6.4 mmol), **A-PEO$_8$M** (2.7 g, 6.4 mmol), and Karstedt's catalyst (50 μL) in toluene (80 mL) were reacted as above. In this way, **m=24** (14.3 g, 89% yield) was obtained. ^{1}H NMR (δ, ppm): 0.02–0.11 (m, 156H, $SiCH_3$), 0.47-0.54 (m, 2H, $SiCH_2CH_2CH_2$), 0.55 (m, 3H, $SiCH_2CH_2$), 1.09 (m, 1H, $SiCH_2CH_2$), 1.22 (m, 9H, $SiOCH_2CH_3$), 1.60 (m, 2H, $SiCH_2CH_2CH_2$), 3.38 (s, 3H, OCH_3), 3.56 (m, 2H, $SiCH_2CH_2CH_2$), 3.64 (m, 32H, OCH_2CH_2), 3.82 (m, 6H, $SiOCH_2CH_3$). IR (ν): no Si–H band.

3.3.1.13 Synthesis of **m=30**

TES-ODMS$_{30}$ (12.32 g, 4.8 mmol), **A-PEO$_8$M** (2.05 g, 4.8 mmol), and Karstedt's catalyst (50 μL) in toluene (100 mL) were reacted as above. In this way, **m=30** (12.6 g, 88% yield) was obtained. ^{1}H NMR (δ, ppm): 0.02–0.11 (m, 192H, $SiCH_3$), 0.47-0.54 (m, 2H, $SiCH_2CH_2CH_2$), 0.55 (m, 3H, $SiCH_2CH_2$), 1.09 (m, 1H, $SiCH_2CH_2$), 1.22 (m, 9H, $SiOCH_2CH_3$), 1.61 (m, 2H, $SiCH_2CH_2CH_2$), 3.38 (s, 3H, OCH_3), 3.56 (m, 2H, $SiCH_2CH_2CH_2$), 3.64 (m, 32H, OCH_2CH_2), 3.82 (m, 6H, $SiOCH_2CH_3$). IR (ν): no Si–H band.

3.3.1.14 Synthesis of **mono-17**

TES-ODMS$_{17}$ (0.05 g, 0.03 mmol), **CH$_2$=CH–PDMS-*n*-Bu** (2.1 g, 0.03 mmol), and Karstedt's catalyst (50 μL) were combined in toluene in a round-bottom (rb) flask equipped with a rubber septum and heated to 70 °C for 12 h. The reaction was monitored by IR until the disappearance of Si–H was observed. The catalyst was removed by refluxing the reaction mixture with activated charcoal for 12 h. The reaction mixture was filtered and the volatiles were removed under reduced pressure. In this way, **mono-17** (1.66 g, 77% yield) was obtained. IR (ν): no Si–H band.

3.3.1.15 Synthesis of **mono-24**

TES-ODMS$_{24}$ (0.08 g, 0.038 mmol), **CH$_2$=CH–PDMS-*n*-Bu** (2.03 g, 0.034 mmol), and Karstedt's catalyst (50 μL) in toluene were reacted as above. In this way, **mono-24** (1.03 g, 49% yield) was obtained. IR (ν): no Si–H band.

3.3.1.16 Synthesis of **mono-30**

TES-ODMS$_{30}$ (0.10 g, 0.039 mmol), **CH$_2$=CH–PDMS-*n*-Bu** (2.32 g, 0.039 mmol), and Karstedt's catalyst (50 μL) in toluene were reacted as above. In this way, **mono-30** (1.48 g, 61% yield) was obtained. IR (ν): no Si–H band.

3.3.1.17 Synthesis of **non-17**

ODMS$_{17}$ (2.00 g, 1.4 mmol), **VTEOS** (0.54 g, 2.8 mmol), and Wilkinson's catalyst (10 mg) were combined in toluene in a rb flask equipped with a rubber septum

and heated to 80 °C for 12 h. Toluene was removed under reduced pressure, the product was purified by flash column chromatography, and volatiles were removed under reduced pressure. In this way, **non-17** (2.32 g, 91% yield) was obtained.

3.3.1.18 Synthesis of **non-24**

$ODMS_{24}$ (2.01 g, 0.001 mol), **VTEOS** (0.40 g, 0.002 mol), and Wilkinson's catalyst (10 mg) in toluene were reacted as above. In this way, **non-24** (2.16 g, 90% yield) was obtained.

3.3.1.19 Synthesis of **non-30**

$ODMS_{30}$ (1.98 g, 0.84 mmol), **VTEOS** (0.32 g, 1.7 mmol), and Wilkinson's catalyst (10 mg) in toluene were reacted as above. In this way, **non-30** (2.14 g, 93% yield) was obtained.

3.3.1.20 Synthesis of **di-17**

$ODMS_{17}$ (0.03 g, 0.022 mmol), **CH_2=CH–PDMS-*n*-Bu** (2.32 g, 0.039 mmol), and Karstedt's catalyst (50 μL) were combined in toluene in a round-bottom (rb) flask equipped with a rubber septum and heated to 70 °C for 12 h. The reaction was monitored by IR until the disappearance of Si–H was observed. The catalyst was removed by refluxing the reaction mixture with activated charcoal for 12 h. The reaction mixture was filtered and the volatiles were removed under reduced pressure. In this way, **di-17** (1.80 g, 77% yield) was obtained. IR (ν): no Si–H band.

3.3.1.21 Synthesis of **di-24**

$ODMS_{24}$ (0.037 g, 0.019 mmol), **CH_2=CH–PDMS-*n*-Bu** (2.13 g, 0.036 mmol), and Karstedt's catalyst (50 μL) in toluene were reacted as above. In this way, **di-24** (0.96 g, 44% yield) was obtained. IR (ν): no Si–H band.

3.3.1.22 Synthesis of **di-30**

$ODMS_{30}$ (0.04 g, 0.017 mmol), **CH_2=CH–PDMS-*n*-Bu** (2.03 g, 0.034 mmol), and Karstedt's catalyst (50 μL) in toluene were reacted as above. In this way, **di-30** (0.95 g, 46% yield) was obtained. IR (ν): no Si–H band.

3.3.2 Surface-Grafting PEO-Silane Amphiphiles onto Silicon Wafers

Silicon wafers (1" x 1") were ultrasonically cleaned in acetone (10 min) followed by rinsing with acetone, repeating with DI water and then drying in a 120 °C oven overnight. Next, wafers were placed in a 7:3 (v/v) concentrated H_2SO_4/30% H_2O_2 (Piranha) solution for 30 min (warning: Piranha must be handled with extreme caution), thoroughly washed with DI water and dried under a stream of air. The resulting oxidized wafers were then each placed in a sealed jar containing the grafting solution comprised of the designated PEO-silane amphiphile or the PEO-control in HPLC-grade toluene (0.048 M) and placed on a shaker table for 12 h. The grafted wafers were subsequently removed from the grafting solution, dried with a gentle stream of air, and annealed in a vacuum oven (36 mmHg) at 150 °C for 12 h. To remove unbound chains, the wafers were subjected to sequential soaking (1 h) and sonication (3 min) with ethanol, the

sequence repeated with DI water, and lastly dried under a stream of air. Grafted silicon wafers were analyzed by x-ray photoelectron spectroscopy (XPS), ellipsometry, and contact angle analysis. Grafted, silica-coated QCM-D sensors used for protein adsorption measurements were prepared as above following oxidation with a plasma cleaner (O_2, 2 min).

3.3.3 Preparation of Silicone Films

Microscope slides were sequentially washed with acetone, dichloromethane, and acetone and dried in a 100 ºC oven for at least 2 hr prior to use.

In a scintillation vial, MED-1137 was combined with hexane (1:3, wt:wt) and each PEO-silane amphiphile or the PEO control at 50 μmol per gram of MED-1137 for a total of 7 solutions. Likewise, an unmodified silicone control was prepared without the addition of a PEO-silane amphiphile. The sealed vials were placed on a shaker table for 4 hr to achieve homogeneous solutions.

Solutions were solvent-cast onto leveled glass microscope slides (1.5 mL per slide) and a polystyrene Petri dish cover placed on top of each. In this way, solvent evaporation was slowed which prevented the formation of air bubbles in the resulting coatings. Films were allowed to cure for seven days at room temperature (RT) and immediately used for designated tests. Free-standing films for thermal gravimetric analysis (TGA) were obtained by removing the films from slides with a clean single-edge razor blade. Coated microscope slides were analyzed for water absorption, contact angle, and protein adsorption.

3.3.4 X-Ray Photoelectron Spectroscopy (XPS)

Surface composition analysis of grafted silicon wafers was performed using a Kratos AXIS Ultra Imaging X-ray photoelectron spectrometer with a monochromatised Mg K_α source and operating at a base pressure of ~2% x 10^{-9} mbar. All analyses were performed over 7 x 3 mm. Survey spectra were obtained from 0 to 1100 eV to detect elements present at the surface of each silicon wafer. High-resolution (HR) analyses with pass energy of 40 eV were performed at a take-off angle of 90° to determine elemental atomic percent composition. HR scans (180 s sweeps) were performed at 526 to 536 eV for O 1s, 280 to 295 eV for C 1s, and 96 to 106 eV for Si 2p. The raw data was quantified and analyzed using XPS Peak Processing software.

3.3.5 Ellipsometry

Ellipsometry measurements on grafted silicon wafers were performed using an Alpha-SE ellipsometer (J.A. Woollam Co., Inc.) with an incident angle of 70° in the spectral range of 380-900 nm and in the high-precision mode (30 sec data acquisition time). Using a standard two-layer (silica-silicon) optical model included in the manufacturer's software, the average thickness of the silicon wafer oxide layer was determined at three different regions of five individual wafers. The obtained average oxide layer thickness of 2.01 nm is in agreement with literature values [165-167]. To measure the thickness of the grafted chains, the oxide layer thickness was utilized in a second optical model that included the third "Cauchy layer" (polymer-silica-silicon). The index of refraction (*n*) of the PEO-silane amphiphiles and the PEO-control was set

to that of crystalline PEO (n = 1.450) [39,168]. The reported thickness value (h) was based on three wafers, each measured at three different regions.

3.3.6 Thermal Gravimetric Analysis (TGA)

TGA was performed on the neat PEO-silane amphiphiles and the PEO control as well as on the PEO-modified silicone films (~10 mg) in Pt pans with a TA Instruments Q50 under N_2 or air at a flow rate of 60 cm^3/min. The sample weight was recorded while the temperature was increased 4 ºC/min from 25 to 800 ºC.

3.3.7 Absorbed Water Content

Coated slides were weighed (W_i) and then continually soaked in DI water at RT for 6 days. After removal from water, the surface was gently dried with a stream of air and immediately weighed (W_s). The weight of the uncoated glass slide was subtracted from W_i and W_s before calculating the water content. The absorbed water content is defined as: absorbed water content = $[(W_s - W_i)/W_i] \times 100$.

3.3.8 Contact Angle Measurements

Static (θ_{static}) contact angles of DI water at the surface-air interface were measured at RT with a CAM200 (KSV Instruments) goniometer equipped with an autodispenser, video camera, and drop-shape analysis software. θ_{static} of a sessile drop of water (5 μL) was measured at 0, 15, 60 and 120 sec after deposition onto the coating surface for silicone films and at 0 and 120 sec for surface-grafted wafers. The reported

θ_{static} values are an average of three measurements taken from three different areas of the same sample.

3.3.9 Protein Adsorption

The adsorption of human fibrinogen (HF) onto surface-grafted wafers was studied with QCM-D (Q-Sense E4). PBS was flowed over grafted sensors (150 μL/min) until stable baselines were observed (~1 hr), and then the frequency and dissipation were recorded for 5 min. A HF protein solution (0.1 mg/mL in PBS) was then flowed over the sensors (150 μL/min) for 20 min. Finally, PBS was flowed over the sensors (150 μL/min) for 5 min to remove any non-adherent protein. A sensor grafted with a siloxane tether (**TES-ODMS$_{13}$**; m = 13) was used as a hydrophobic siloxane control. The raw data was quantified and analyzed using Q-Sense software.

The adsorption of the Alexa Fluor dye conjugate of human fibrinogen (AF-546 HF) onto silicone films was studied with confocal laser scanning microscopy. A silicone isolator (18 mm well diameter, 2 mm well depth) was affixed to each coated microscope slide. The exposed surface of the film inside each isolator well was filled with 0.7 mL of AF-546 HF solution (0.1 ml/mL) [39,169]. (Note: Per manufacturer specifications, the AF-546 HF was first dissolved in 0.1 M $NaHCO_3$ to obtain a 1.5 mg/mL solution and was further diluted in PBS to obtain a final concentration of 0.1 mg/mL.) After equilibrating in the dark at RT for 3 h, the solution was removed and 0.7 mL of PBS was then added to each well and removed after 5 min. This rinsing process was repeated with PBS and then with DI water for a total of three rinses. The samples were then dried

under a stream of air and imaged. An unmodified silicone-coated slide served as a hydrophobic **silicone** control with well-known high protein adhesion [101,134,135].

3.3.10 Confocal Laser Scanning Microscopy (CLSM)

A FV1000 (Olympus) confocal laser scanning microscope was use for quantification of protein adsorption onto all films. Imaging conditions, both in excitation and collection, were identical for all samples: objective (SPLSAPO 10x objective, NA 0.40); laser excitation type and intensity (HeNe 543 nm source); field of view and resolution (256 x 256 pixels, 317 x 317 micron field of view); depth (40 slices at 1 micron per slice); slice averaging; collection (150 micron pinhole, 560 nm long-pass filter followed by a 560-660 nm band-pass filter, identical photomultiplier voltages/sensitivities). Data analysis was performed on the FV10-ASW v3.1 software suite (Olympus). Each protein exposed sample was imaged in three locations and aggregate intensities were computed. These were compared to three images obtained from samples that had similar treatment without protein exposure. Changes in intensity upon exposure to protein were then obtained and compared, with errors reported as the standard deviation of three measurements.

3.4 Results and Discussion

3.4.1 Synthesis of $\boldsymbol{ODMS_m}$

The triflic acid-catalyzed ring-opening reaction of variable molar ratios of $\mathbf{D_4}$ with **TMDS** produced $\mathbf{ODMS_{17}}$, $\mathbf{ODMS_{24}}$, and $\mathbf{ODMS_{30}}$ in good yields (≥60%) (**Figure 3.1**). The M_n $\mathbf{ODMS_{17}}$-$\mathbf{ODMS_{30}}$ were confirmed by ^{1}H NMR end-group analysis.

3.4.2 Synthesis of $\boldsymbol{TES\text{-}ODMS_m}$

The Rhodium-catalyzed regioselective hydrosilylation reaction of equimolar amounts of $\mathbf{ODMS_{17}}$, $\mathbf{ODMS_{24}}$, or $\mathbf{ODMS_{30}}$ with **VTEOS** effectively produced $\mathbf{TES\text{-}ODMS_{17}}$, $\mathbf{TES\text{-}ODMS_{24}}$, and $\mathbf{TES\text{-}ODMS_{30}}$, respectively, in good yields (≥96%). ^{1}H NMR spectra of $\mathbf{TES\text{-}ODMS_{17}}$, $\mathbf{TES\text{-}ODMS_{24}}$, and $\mathbf{TES\text{-}ODMS_{30}}$ showed a reduction in the Si–H peak integration value by one-half compared to the starting material.

3.4.3 Verification of the Composition of $\boldsymbol{TES\text{-}ODMS_m}$

For Rh-catalyzed regioselective hydrosilylation, it has been suggested that an increased distance between terminal Si–H groups may result in their decreased reactivity [121]. However, our previous work has demonstrated successful regioselective hydrosilylation of α,ω-bis(Si–H)oligodimethylsiloxanes ($\mathbf{ODMS_0}$, $\mathbf{ODMS_4}$, and $\mathbf{ODMS_{13}}$) [99]. Further, we sought to confirm the compositions of the products of regioselective hydrosilylation of $\mathbf{ODMS_{17}}$, $\mathbf{ODMS_{24}}$, and $\mathbf{ODMS_{30}}$ each with **VTEOS** by GPC as previously reported [99]. ^{1}H NMR cannot be the sole basis for evidence of

the pure monosubstitution of regioselective hydrosilylation since the spectra represent the average composition of each sample.

Subsequent to Rh-catalyzed hydrosilylation of **ODMS$_{17}$**, **ODMS$_{24}$**, and **ODMS$_{30}$** each with **VTEOS** (1:1 molar ratio), the products (**TES-ODMS$_{17}$**, **TES-ODMS$_{24}$**, and **TES-ODMS$_{30}$**) were each reacted with **CH$_2$=CH–PDMS-*n*-Bu** (M_w/M_n = 83,000/60,000 g/mol) by Pt-catalyzed hydrosilylation thereby producing **mono-17**, **mono-24**, and **mono-30**, respectively. If the initial Rh-catalyzed hydrosilylation reaction was regioselective, then the products would be pure **mono-17**, **mono-24**, or **mono-30**. However, non-regioselective Rh-catalyzed hydrosilylation would have resulted in a mixture of products which would subsequently react with **CH$_2$=CH–PDMS-*n*-Bu** to yield: **mono-17**, **mono-24**, and **mono-30**, the products of monosubstituted **TES-ODMS$_{17}$**, **TES-ODMS$_{24}$**, and **TES-ODMS$_{30}$** each with **CH$_2$=CH–PDMS-*n*-Bu** (M_n = 61,582; 62,100; 62,544 g/mol); **non-17**, **non-24**, and **non-30**, unreacted α,ω-triethoxysilylethyl-disubstituted products (M_n = 1,772; 2,290; 2,734 g/mol); and **di-17**, **di-24**, and **di-30**, the products of **ODMS$_{17}$**, **ODMS$_{24}$**, and **ODMS$_{30}$** each with **CH$_2$=CH–PDMS-*n*-Bu** (1:2 molar ratio) (M_n = 121,334; 121,852; 122,296 g/mol).

Products **non-17**, **non-24**, and **non-30** were synthesized by Rh-catalyzed hydrosilylation of **ODMS$_{17}$**, **ODMS$_{24}$**, and **ODMS$_{30}$**, respectively, with **VTEOS** (1:2 molar ratio), whereas **di-17**, **di-24**, and **di-30** were synthesized by Pt-catalyzed hydrosilylation of **ODMS$_{17}$**, **ODMS$_{24}$**, and **ODMS$_{30}$**, respectively, with **CH$_2$=CH–PDMS-*n*-Bu** (1:2 molar ratio).

In the GPC chromatographs of **mono-17**, **mono-24**, and **mono-30**, the elution peaks of **non-17**, **non-24**, and **non-30**, respectively, are absent (**Figure 3.2**). The elution peaks of **di-17**, **di-24**, and **di-30** would overlap with the elution peaks of **mono-17**, **mono-24**, and **mono-30** but must be absent as well since **non-17**, **non-24**, and **non-30** and **di-17**, **di-24**, and **di-30** would be present in equal amounts, respectively. Thus, the compositions of **mono-17**, **mono-24**, and **mono-30** may be identified as the product of monosubstituted **TES-ODMS$_{17}$**, **TES-ODMS$_{24}$**, and **TES-ODMS$_{30}$** each with **CH$_2$=CH–PDMS-*n*-Bu**. These results confirm that the Rh-catalyzed hydrosilylation reactions of **ODMS$_{17}$**, **ODMS$_{24}$**, and **ODMS$_{30}$** each with **VTEOS** were regioselective and produced only monosubstituted **TES-ODMS$_{17}$**, **TES-ODMS$_{24}$**, and **TES-ODMS$_{30}$**, respectively.

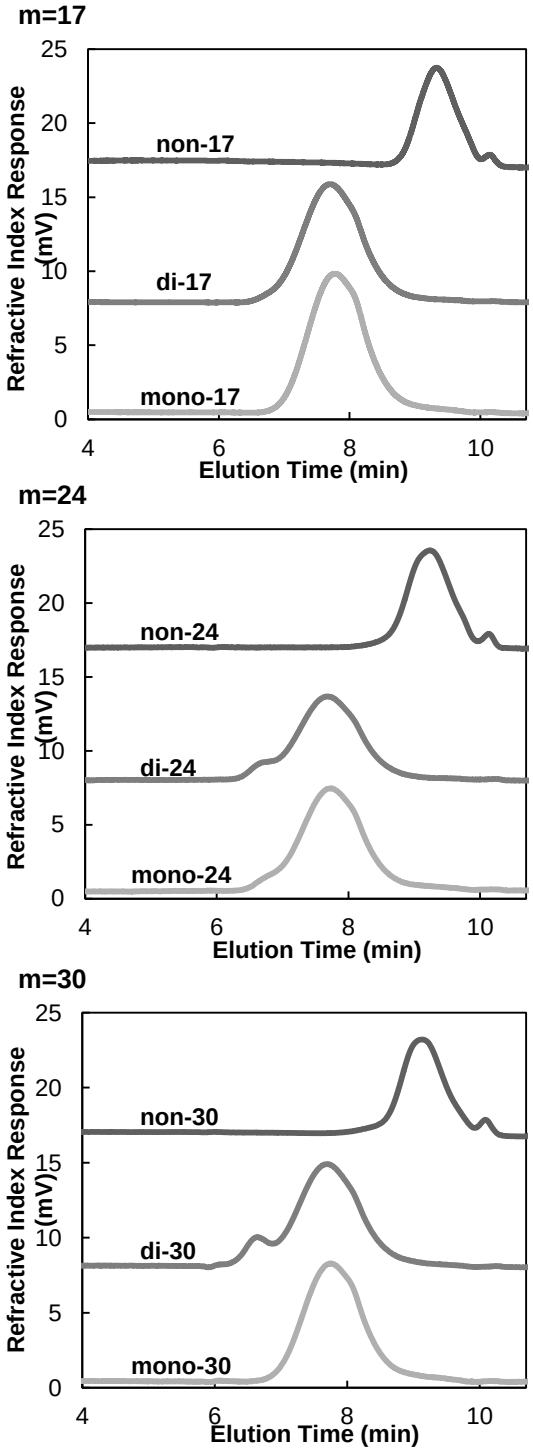

Figure 3.2. GPC chromatographs of **non-*m***, **di-*m***, and **mono-*m***. The absence of **non-*m*** (and thus **di-*m***) confirms that **mono-*m*** is the product of monosubstituted **TES-ODMS*m*** and **CH_2=CH–PDMS-*n*-Bu**.

*3.4.4 Synthesis of **m=17-30***

The Platinum-catalyzed hydrosilylation reaction of equimolar amounts of **TES-ODMS$_{17}$**, **TES-ODMS$_{24}$**, and **TES-ODMS$_{30}$** each with **A-PEO$_8$M** produced **m=17**, **m=24**, and **m=30**, respectively, in good yields (≥78%). Completion of the reaction was confirmed by IR analysis of **m=17**, **m=24**, and **m=30**, which showed no absorbance at ~2125 cm^{-1} which corresponds to unreacted Si–H bonds. The Si–H peak (~4.7 ppm) of the ^{1}H NMR spectra of **m=17**, **m=24**, and **m=30** was also absent.

3.4.5 Grafted Silicon Wafers

3.4.5.1 XPS

XPS was used to confirm successful grafting of PEO-silane amphiphiles onto silicon wafers. The elemental surface compositions of grafted silicon wafers are reported in **Table 3.1**. As expected, the Si 2p content decreased and the C 1s content increased upon surface-grafting. The Si 2p peak decreased as siloxane tether length increased, which can be explained by the lower silicon content of PDMS (25% theoretical) versus the bare wafer surface (61% measured). The HR C 1s peaks were deconvoluted using XPS software into two peaks centered at 284.5 eV (C–C and C–Si) and 286.4 eV (C–O) which was unique to PEO (**Figure 3.3**). The component of the C 1s peak corresponding to C–O decreased as the siloxane tether was lengthened, corresponding to a decrease in the PEO concentration relative to PDMS. These results confirm the presence of grafted PEO-silane amphiphiles on the silicon wafers and correlate well with differences in composition.

Table 3.1. Surface atomic % composition by XPS of surface-grafted PEO-silane amphiphiles and a PEO control (n = 8).

	C 1s	*C-Si/ C-C*	*C-O*	O 1s	Si 2p
Surface	**Total**	***284.5 eV***	***286.4 eV***		
Oxidized wafer	5	-	-	34	61
PEO control	20	19	81	36	44
m=0	10	32	68	37	52
m=4	16	31	69	39	46
m=13	22	54	46	30	48
m=17	23	66	34	34	44
m=24	38	72	28	30	32
m=30	44	68	32	27	30

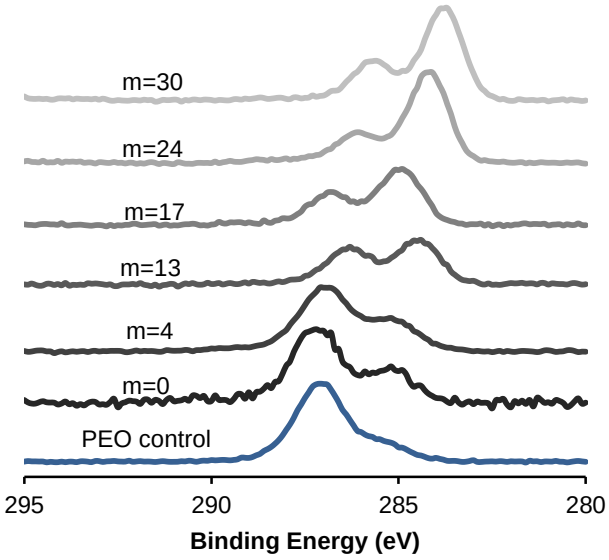

Figure 3.3. HR C 1s XPS spectra of silicon wafers grafted with PEO-silane amphiphiles and a PEO control (n = 8).

3.4.5.2 Ellipsometry

PEO-silane amphiphiles of varying siloxane tether length were grafted onto silicon wafers and the dry graft layer thicknesses (*h*) were measured (**Table 3.2**). As expected, *h* of the PEO-silane amphiphiles increased with siloxane tether length such that **m=30** yielded the thickest graft layer (2.9 nm) while **m=0** was the thinnest (1.4 nm). The *h* values were then used to calculate spacing between grafted polymer chains (*D*, **Table 3.2**) which is known to influence their conformation [170,171]. For the surface-grafted chains to have an extended conformation (brush regime), *D* must be less than twice the Flory radius (R_F) [154]. For each PEO-silane amphiphile composition, R_F was calculated using the length of one monomer unit (*a*) and the degree of polymerization (*N*) as follows: (1) $R_F = aN^{1/3}$ for the siloxane control in a poor solvent (i.e. water), where a = 0.5 nm [172] and N = 13 and (2) $R_F = aN^{3/5}$ for the PEO control in a good solvent (i.e. water), where a = 0.35 nm [39,173] and N = 8 [99,163,164]. However, due to the two-block composition of the PEO-silane amphiphiles and the differing solubility of PEO and PDMS, the R_F of the PEO segment and the siloxane tether must be calculated separately using their respective Flory equations as explained above (**Table 3.2**). For all grafted silicon wafers, the PEO-silane amphiphiles exhibited *D* less than $2R_F$ for both the PEO segment as well as for the siloxane tether. Thus, all grafted surfaces were determined to be in a brush regime. Lastly, *D* for all grafted PEO-silane amphiphiles and the siloxane control differed by less than 0.5 nm (1.05 - 1.49 nm) with the exception of the PEO control (0.67 nm). Thus, the effect of chain density could be disregarded as a variable when comparing protein resistance of grafted PEO-silane amphiphiles.

Table 3.2. Ellipsometry data for silicon wafers grafted with PEO-silane amphiphiles, a PEO control (n = 8), and a siloxane control (m = 13).

Grafted Surface	M_n (g/mol)	Density ρ (g/mL)	Thickness h (nm)	Chain Density $\sigma = (h\rho/M_n) \times N_A$ (chains/nm^2)	Graft Distance $D = (4/\pi\sigma)^{1/2}$ (nm)	PEO Flory Spacing $2R_F = 2aN^{3/5}$ (nm)	PDMS Flory Spacing $2R_F = 2aN^{1/3}$ (nm)
PEO control	588	1.06	2.2 ± 0.1	2.39	0.73	2.4	-
m=0	749	1.02	1.4 ± 0.3	1.15	1.05	2.4	-
m=4	1044	1.00	1.6 ± 0.5	0.92	1.17	2.4	1.6
m=13	1710	0.98	1.5 ± 0.2	0.52	1.57	2.4	2.3
m=17	2006	0.99	2.0 ± 0.2	0.59	1.46	2.4	2.5
m=24	2524	0.98	2.8 ± 0.1	0.65	1.39	2.4	2.9
m=30	2968	0.98	2.9 ± 0.1	0.58	1.49	2.4	3.1
Siloxane control	1286	1.01	2.5 ± 0.9	1.2 ± 0.4	1.1 ± 0.2	-	2.3

3.4.5.3 Contact Angle Analysis

θ_{static} (0 sec) and θ_{static} (2 min) of water droplets on grafted surfaces are reported in **Figure 3.4**. A silicon wafer grafted with a siloxane tether (**TES-ODMS$_{13}$**; m = 13) served as a hydrophobic control. As the siloxane tether increased, the grafted wafers exhibited an increase in θ_{static} (0 sec) and θ_{static} (2 min), indicating a decrease in surface hydrophilicity. This trend was attributed to the hydrophobic siloxane tether which created more hydrophobic surfaces as its concentration was increased. Hysteresis ($\theta_\Delta = \theta_{adv} - \theta_{rec}$) was relatively consistent among all grafted wafers, signifying that surface reorganization was not a variable.

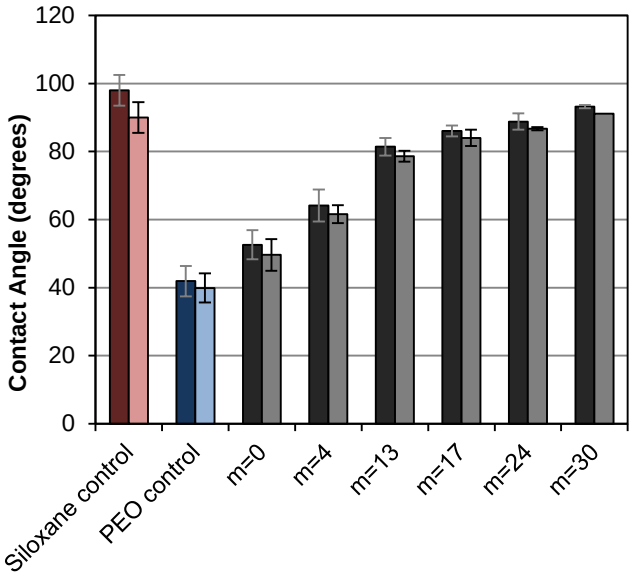

Figure 3.4. Static contact angles (θ_{static}) of silicon wafers grafted with PEO-silane amphiphiles, a PEO control (n = 8), and a siloxane control (m = 13) at 0 s (dark) and 2 min (light) following water droplet placement. Each bar represents the average and standard deviation of three measurements taken from three different areas of the same sample.

3.4.5.4 Protein Adsorption via QCM-D

Adsorbed HF plays a major role in surface-induced thrombosis by facilitating platelet adhesion and activation [9,174]. Thus, the amount of HF protein adsorbed onto grafted surfaces was analyzed via QCM-D to estimate thromboresistance (**Figure 3.5**). Due to the low dissipation of adsorbed HF [175], the adsorbed mass was calculated using Sauerbrey approximation and the seventh frequency overtone. Due to its hydrophobicity, the siloxane control adsorbed the highest amount of HF. The PEO-silane amphiphiles experienced reduced adsorption compared to the siloxane control due to their relatively reduced hydrophobicity as determined by contact angle (**Figure 3.4**). Lastly, the PEO control adsorbed significantly less HF compared to all other grafted surfaces due to its hydrophilicity. Thus, reduced HF adsorption generally correlates with

increased hydrophilicity of the grafted surfaces. Therefore, the siloxane tether is detrimental to the inherent protein resistance of surface-grafted PEO-silane amphiphiles. However, due to the absence of restructuring effects, the silicon wafer is not necessarily predictive of protein resistance for PEO-silane amphiphiles in a bulk-modified silicone network.

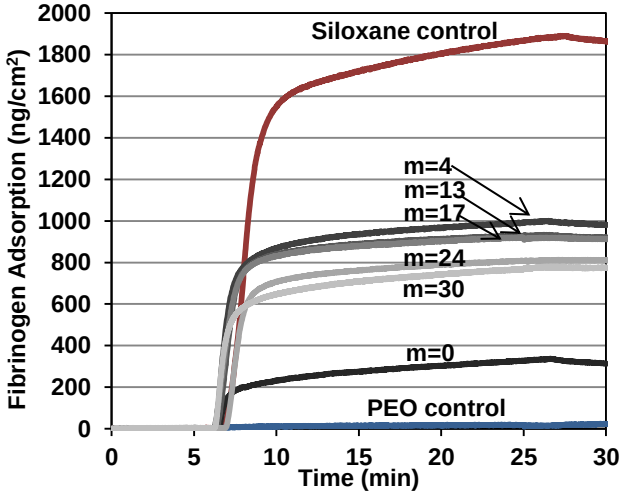

Figure 3.5. QCM-D-measured adsorption of HF onto silica-coated sensors grafted with PEO-silane amphiphiles, a PEO control (n = 8), and a siloxane control (m = 13). After equilibration for 5 min with PBS, the sensors were exposed to HF for 20 min and then to PBS for 5 min.

3.4.6 Silicone Films

3.4.6.1 Preparation of Films

A medical grade, silica-reinforced acetoxy cure RTV silicone was modified with PEO-silane amphiphiles of variable siloxane tether length (**m=0**, **m=4**, **m=13**, **m=17**, **m=24**, and **m=30**) as well as a PEO control at equivalent molar concentrations (**Figure**

3.1). Films were prepared by solvent-casting with hexane onto glass microscope slides (**Figure 3.6**).

Figure 3.6. Unmodified silicone and silicones bulk-crosslinked with PEO-silane amphiphiles and a PEO control (n = 8) before (top row) and after (bottom) soaking in water (6 days). wt% absorbed water content is displayed (blue).

3.4.6.2 TGA

Successful crosslinking of bulk silicone films was confirmed by TGA (**Figure 3.7**). The thermal degradation profiles of PEO-modified silicones were compared to that of unmodified silicone as well as the neat PEO-silane amphiphiles. In air, ~55 to 70% silica residue remained as expected due to the degradation of polysiloxanes [122]. The thermal stabilities of the PEO-modified silicones did not vary substantially from the unmodified silicone film. Additionally, the significant weight loss at lower temperatures that was observed for neat PEO-silane amphiphiles was not observed for PEO-modified silicones. Thus, PEO-silane amphiphiles were successfully crosslinked into the bulk silicone films.

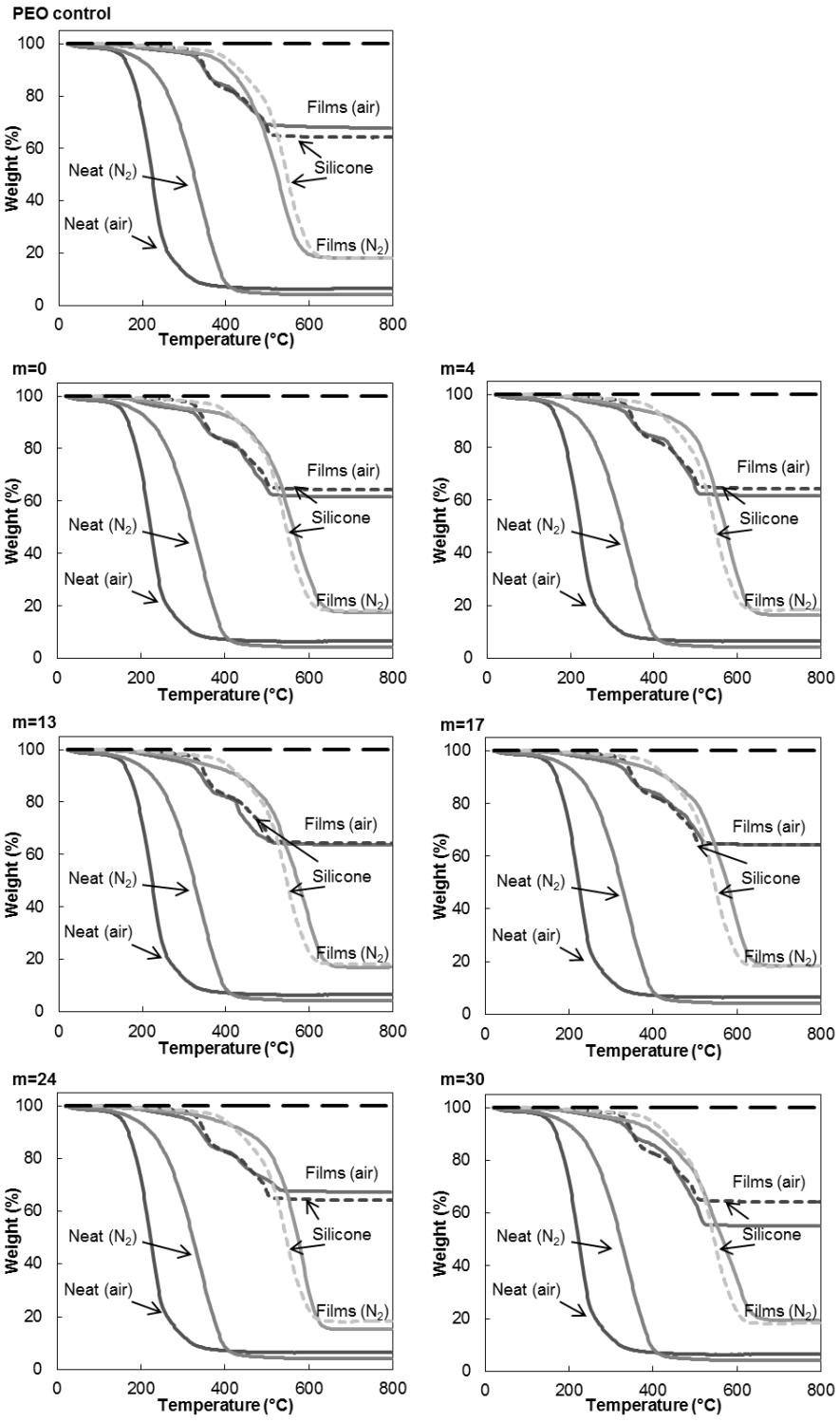

Figure 3.7. Thermal stability of silicones bulk-crosslinked with PEO-silane amphiphiles and a PEO control (n = 8) in N_2 and in air.

3.4.6.3 Contact Angle Analysis

Contact angle measurements of films cured for one day are reported in **Figure 3.8**. The contact angle was tracked for 2 min following the deposition of a water droplet to monitor surface restructuring in response to water exposure. As expected, the unmodified silicone control was hydrophobic (θ_{static} > 90°) [176] with minimal restructuring over the 2 min period. The contact angle of the PEO control was similarly hydrophobic and remained so after 2 min but did undergo greater restructuring (Δ = -15º) attributed to a small amount of hydrophilic PEO migrating from the bulk to the surface. However, all of the PEO-silane amphiphile-modified films underwent major surface reorganization as evidenced by greater increases in wettability (**m=0**, Δ = -64º; **m=4**, Δ = -72º; **m=13**, Δ = -77º; **m=17**, Δ = -75º; **m=24**, Δ = -67º; **m=30**, Δ = -69º). As the siloxane tether was lengthened from m = 0 to m = 13, the films exhibited greater restructuring capacity due to the enhanced configurational mobility of the PEO with a longer tether. However, PEO-silane amphiphile restructuring was reduced from m = 17 to m = 30. Thus, **m=13** films observed the greatest restructuring ability, beyond which the chains became too bulky to migrate to the surface-water interface as effectively due to the lengthened siloxane tether.

The films were similarly characterized during prolonged exposure to both air (30 days) and water (33 days) to assess longevity (**Figure 3.9**). For films exposed to air, restructuring behavior remained generally constant over 30 days. Alternatively, the restructuring capacity of films soaked in water was gradually reduced (higher contact angle at 2 min) over the 33 day period. Furthermore, shorter tether lengths appeared to

be more heavily influenced by water equilibration. Yet, the films containing PEO-silane amphiphiles generally remain hydrophilic even after 33 days.

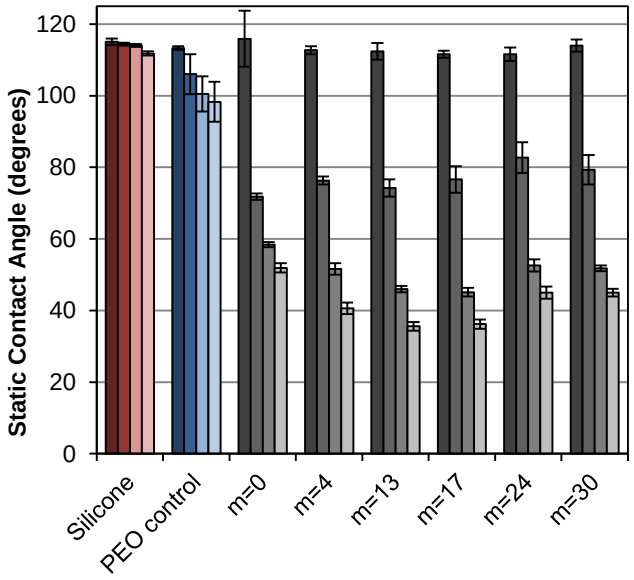

Figure 3.8. Static contact angles (θ_{static}) of unmodified silicone and silicones bulk-crosslinked with PEO-silane amphiphiles and a PEO control (n = 8) measured over 2 min. Bars are organized as the time after initial water droplet placement from dark color to light as follows: 0 sec, 15 sec, 1 min, and 2 min. Each bar represents the average and standard deviation of three measurements at the designated time point on three different areas of the same sample.

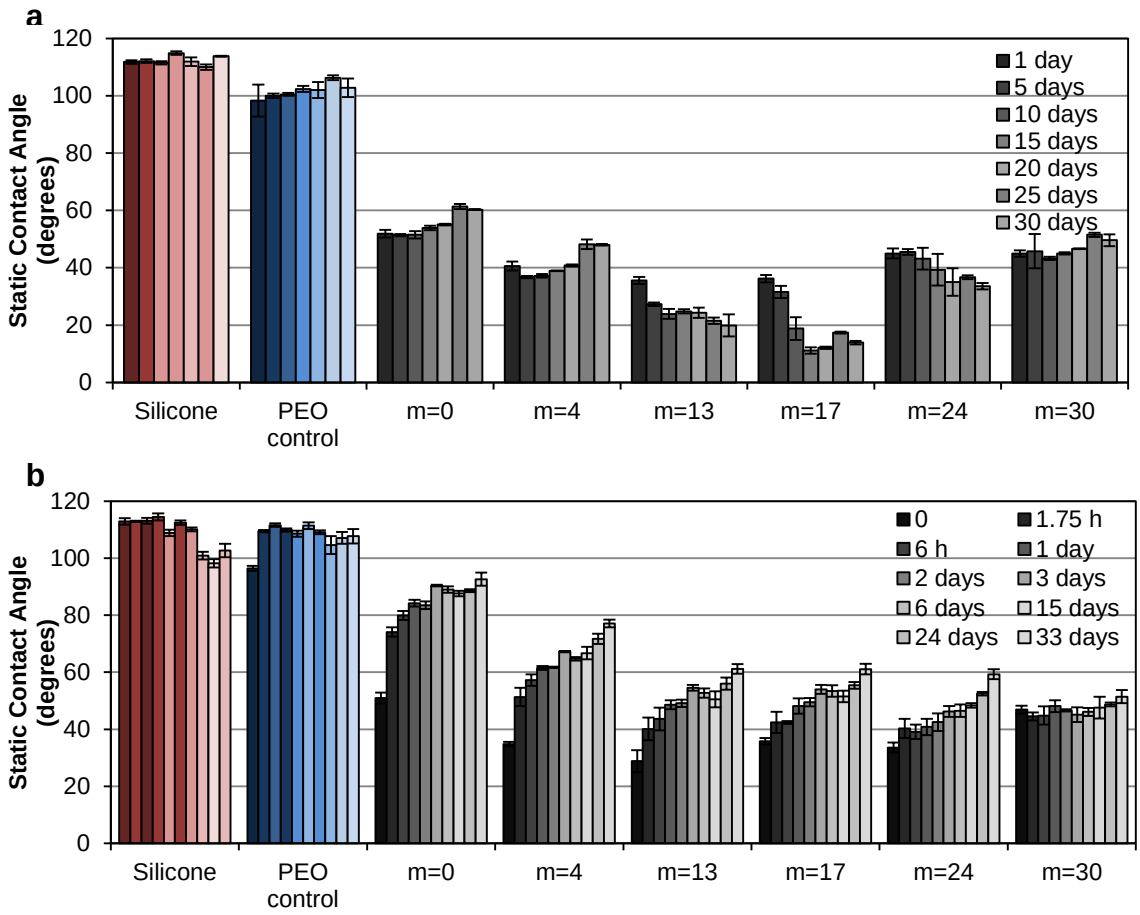

Figure 3.9. Static contact angles (θ_{static}) of unmodified silicone and silicones bulk-crosslinked with PEO-silane amphiphiles and a PEO control (n = 8) during exposure to (a) air for 30 days and (b) DI water for 33 days. Each bar represents the average and standard deviation of three measurements taken from three different areas of the same sample.

3.4.6.4 Absorbed Water Content

After soaking for six days, PEO-silane amphiphile-modified silicone films generally absorbed similar amounts of water (~6-11 wt%) versus unmodified silicone (0.3 ± 0.04 wt%) (**Figure 3.6**). Water uptake could also be observed as an increase in film opaqueness resulting from incompatibility of the silicone and the absorbed water. Water content within the film is believed to inhibit the surface restructuring capacity of

PEO-silane amphiphiles by reducing the driving force of PEO from the bulk to the surface-water interface [177].

3.4.6.5 Protein Adsorption

The amount of fluorescently-labelled HF protein adsorbed onto silicone films was measured with CLSM (**Figure 3.10**; **Table 3.3**). The results correlate well with θ_{static} measurements. The unmodified silicone control adsorbed expectedly high levels of HF due to its extreme hydrophobicity. The PEO control-modified silicone adsorbed similarly high levels due to the hydrophobicity that resulted from PEO's inability to migrate to the surface. However, the PEO-silane amphiphile films adsorbed significantly reduced amounts of HF, which coincides with their greater surface restructuring ability and subsequent hydrophilicity. Protein resistance was maximized with shorter siloxane tethers (m = 0-13), whereas longer siloxane tethers led to decreased protein resistance (m = 17-30). Thus, longer siloxane tethers appear to inhibit PEO surface migration and reduce the protein resistance of PEO-silane amphiphiles. More importantly, these results demonstrate that PEO-silane amphiphiles outperform conventional PEO-silanes (i.e. no siloxane tether) in reducing protein adsorption on silicone.

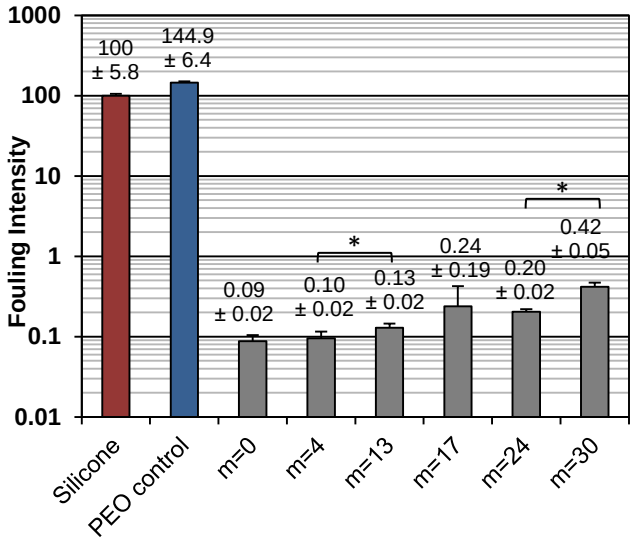

Figure 3.10. Fibrinogen adsorption on silicones bulk-modified with PEO-silane amphiphiles and a PEO control (n = 8) as measured by fluorescence intensity with confocal microscopy. Each bar represents the average and standard deviation of pixel intensity for three images normalized to unmodified silicone. Statistical significance was determined for low-fouling samples by one-way analysis of variance (Holm-Sidak method where * indicates $p < 0.05$).

Table 3.3. Fluorescence intensity measured on silicones bulk-modified with PEO-silane amphiphiles and a PEO control (n = 8) before (absolute) and after normalizing all values to the signal measured on unmodified silicone.

	Absolute	**Normalized**
Silicone	1571.8 ± 91.7	100 ± 5.8
PEO control	2276.8 ± 5.9	144.9 ± 6.4
m=0	1.4 ± 0.3	0.09 ± 0.02
m=4	1.5 ± 0.3	0.10 ± 0.02
m=13	2.0 ± 0.3	0.13 ± 0.02
m=17	6.4 ± 0.3	0.24 ± 0.19
m=24	3.2 ± 0.3	0.20 ± 0.02
m=30	11.2 ± 0.1	0.42 ± 0.05

3.5 Conclusions

New PEO-silane amphiphiles with variable lengths of the siloxane tether were synthesized to study their effect on protein resistance. Surface-grafted coatings were used to measure the inherent protein resistance of amphiphiles in the absence of surface restructuring effects. The siloxane tether of the amphiphiles, when compared to the PEO control, was found to increase the hydrophobicity of surface-grafted coatings to an extent that depended directly on the relative tether length. HF adsorption on the coatings correlated with their wettability such that more hydrophobic surfaces adsorbed the most protein. These results indicated that the inherent protein resistance of PEO-silanes is reduced with the incorporation of a siloxane tether. Next, PEO-silane amphiphiles were tested in a bulk-crosslinked medical grade silicone where surface restructuring was prevalent. The substantial surface restructuring in response to water that was observed on silicone modified with PEO-silane amphiphiles was largely absent with the PEO control-modified silicone. This was attributed to the siloxane tether enhancing the ability of PEO to migrate from the bulk to the surface-water interface. Restructuring ability correlated with protein resistance such that the same PEO-silane amphiphiles with inherently poor protein resistance actually outperformed conventional PEO in reducing fouling on modified silicone. Overall, **m=13** was most effective PEO-silane amphiphile in surface restructuring and protein resistance. These results indicate that while model substrates may be useful as an initial step in determining the antifouling potential of coatings, they are not reliable for screening chemistries intended for polymeric materials where surface restructuring effects are critical.

CHAPTER IV

BACTERIA AND DIATOM RESISTANCE OF SILICONES MODIFIED WITH PEO-SILANE AMPHIPHILES[*]

4.1 Overview

Silicone coatings with enhanced antifouling behavior towards bacteria, diatoms, and a diatom dominated slime were prepared by incorporating PEO-silane amphiphiles with varied siloxane tether lengths (a–c): α-$(EtO)_3Si(CH_2)_2$-oligodimethylsiloxane$_n$-*block*-poly(ethylene oxide)$_8$-OCH_3 [n = 0 (a), 4 (b), and 13 (c)]. Three modified silicone coatings (A–C) were prepared by the acid-catalyzed sol–gel cross-linking of a–c, respectively, each with a stoichiometric 2:3 M ratio of α, ω-bis(Si–OH)polydimethylsiloxane (M_n = 3,000 g mol^{-1}). The coatings were exposed to the marine bacterium *Bacillus* sp.416 and the diatom (microalga) *Cylindrotheca closterium*, as well as a mixed community of *Bacillus* sp. and *C. closterium*. In addition, *in situ* microfouling was assessed by maintaining the coatings in the Atlantic Ocean. Under all test conditions, biofouling was reduced to the highest extent on coating C which was prepared with the PEO-silane amphiphile having the longest siloxane tether length (c).

---

[*] Hawkins, M.L.; Faÿ, F.; Réhel, K.; Linossier, I.; Grunlan, M.A. Bacteria and diatom resistance of silicones modified with PEO-silane amphiphiles. Biofouling 2014, 30, 247-258. This is the author's accepted manuscript of an article published as the version of record in Biofouling, 2014. http://www.tandfonline.com/doi/full/10.1080/08927014.2013.862235

4.2 Introduction

Diatom slimes are compact marine biofilms comprised of bacteria and diatoms embedded in a matrix of secreted extracellular polymeric substances (EPS), often referred to as mucilage or slime [178]. Diatoms are unicellular algae that are ubiquitous in marine as well as freshwater habitats [73], and are a main eukaryotic microorganism that fouls ship hulls [78]. Development of diatom slimes on ships' hulls and other submerged structures is a dynamic process [179,180]. First, a conditioning film forms from the adsorption of ions, proteins, and other organic macromolecules (eg glycoproteins and polysaccharides) present in the water [69,70], followed by attachment of bacteria, diatoms, and other microorganisms [71,72] although as noted by Callow and Callow [179], these processes are not always sequential. Diatoms have a silica case (the frustule) comprised of two overlapping halves which completely enclose the protoplast [73]. Raphid diatoms secrete mucilaginous EPS through the elongated slit (the raphe) and pores thereby permitting attachment as well as gliding on the substratum, leaving behind deposited adhesive trails [181]. EPS consists primarily of polysaccharide as well as smaller amounts of protein [182]. In seawater, attached diatoms rapidly divide to form a slime layer or 'microfilm', which can grow up to 2 mm in thickness [68].

Slime formation (ie microfouling) results in substantial economic and environmental consequences. On ships' hulls, slime increases hydrodynamic drag leading to as much as 15% greater fuel consumption and furthermore increases maintenance costs associated with cleaning and corrosive damage [76,183,184]. Slime formation is particularly pronounced for ships in port or traveling at less than two knots

[68]. Toxic, ablative antifouling (AF) paints, including those based on copper, organotin, and organic biocides, have traditionally been used to prevent biofouling [76]. However, their accumulation in marine waters and negative impact on non-target marine life has resulted in a ban on the use of organotin-based paints, and has prompted a call for restrictions on use of some other biocides by the International Maritime Organization [77].

Foul-release (FR) coatings represent a non-toxic alternative to ablative marine coatings [78]. Rather than prevent initial attachment, these coatings weaken the attachment of biofouling organisms such that they are removed *via* hydrodynamic force (eg ship movement or cleaning regimes) [79,80]. Silicone elastomers, particularly those based on polydimethylsiloxane (PDMS), have emerged as the most popular choice for commercial FR coatings [78]. Their foul-releasing behavior is attributed to their low surface energy, low roughness, low glass transition temperature (T_g), and low modulus which minimize chemical and mechanical adhesion, and enhance release [78,86,87]. While some macrofoulers such as macroalgae [74] and barnacles [185] adhere poorly to hydrophobic, low surface energy materials such as silicones, others do not. Notably, diatoms strongly adhere to hydrophobic surfaces [74,75] including silicone-based coatings [73,186]. The hydrophobicity of silicones leads to poor AF behavior towards the protein-, glycoprotein-, and polysaccharide-based bioadhesives of marine organisms [88]. Moreover, complete detachment of fouling species, including slimes, from commercial hydrophobic FR silicones requires speeds around 30 knots [89] whereas a moderate ship speed is 10–15 knots [90].

Based on the limitation of silicone FR coatings, amphiphilic AF coating systems have emerged as a potentially effective alternative way to resist fouling by multiple organisms including diatoms. These coatings present chemically complex surfaces comprised of hydrophobic and hydrophilic domains [91-94]. Several examples of amphiphilic coatings have been explored based on the combination of hydrophilic poly(ethylene oxide) (PEO, or 'PEG') with a hydrophobic component. Polystyrene-*block*-(ethylene-*ran*-butylene)-*block*-isoprene copolymers with PDMS and PEO side chains demonstrated superior resistance to diatoms with increasing PEO content compared to a PDMS control [95]. This copolymer was also prepared with ethoxylated fluoroalkyl side chains and resulted in reduced attachment of spores of *Ulva linza*, and significantly enhanced removal of sporelings (young plants) at low-impact pressures [96]. Amphiphilic coatings containing a combination of PEO and fluoropolymers have also been studied. For instance, cross-linked hyperbranched fluoropolymer and PEO networks exhibited superior FR behavior with respect to the adhesion strength of sporeling of *U. linza* compared to a PDMS standard [97]. Also, a polystyrene-*block*-PEO diblock copolymer was modified with perfluorinated chemical moieties which reduced the settlement of spores and attachment strength of sporelings of *U. linza* [98].

The aforementioned amphiphilic coatings were comprised solely of an amphiphilic co- or multi-polymer. In contrast, a strategy for imparting amphiphilicity to hydrophobic silicones *via* the introduction of PEO-silane amphiphiles has also been reported. In this way, an amphiphilic additive is utilized, permitting a simple protocol to modify silicones. In earlier work, PEO-silane amphiphiles comprised of a linear PEO

segment distanced from the cross-linkable trialkoxysilane group by an oligodimethylsiloxane tether of varying lengths: α-$(EtO)_3Si(CH_2)_2$-oligodimethylsiloxane$_n$-*block*-$(OCH_2CH_2)_8$-OCH_3; $n = 0$ (a), M_n = 749 g mol^{-1}; $n = 4$ (b), M_n = 1,044 g mol^{-1}; $n = 13$ (c), M_n = 1,710 g mol^{-1} were reported (**Figure 4.1a**) [99]. Their siloxane tether is in contrast to the short alkane spacer (eg propyl) typical of conventional PEO alkoxysilanes useful for cross-linking with α, ω-bis(Si-OH)PDMS (eg RTV silicones) [40,41,43,47,48]. The flexible, hydrophobic siloxane tether is expected to enhance PEO configurational mobility as well as render the chain amphiphilic, properties individually associated with resistance to accumulation of molecules such as proteins. First, the high protein resistance of PEO [24,25] was attributed not only to its hydrophilicity and hydration [26], but also its configurational mobility which leads to a large excluded volume [27], steric repulsion [14,15], blockage of underlying surface adsorption sites [187], and an entropic penalty of chain compression upon protein adsorption [14,15,25]. Therefore, resistance to biomolecule attachment may be enhanced by increasing PEO chain mobility. For the PEO-silane amphiphiles (a–c), the oligodimethylsiloxane tether is highly flexible due to the wide bond angle (~143°) and low barrier to linearization (0.3 kcal mol^{-1}) of Si–O–Si of dimethylsiloxanes [120,121]. It is the dynamic flexibility of Si–O–Si that produces polymers with extremely low glass transition temperatures (T_gs) (eg PDMS, T_g = −125 °C). Second, the hydrophobicity of the siloxane tether combines with the hydrophilicity of the PEO segment to create an amphiphilic chain. Amphiphilicity, as noted in the examples above, is associated with enhanced resistance to biofouling.

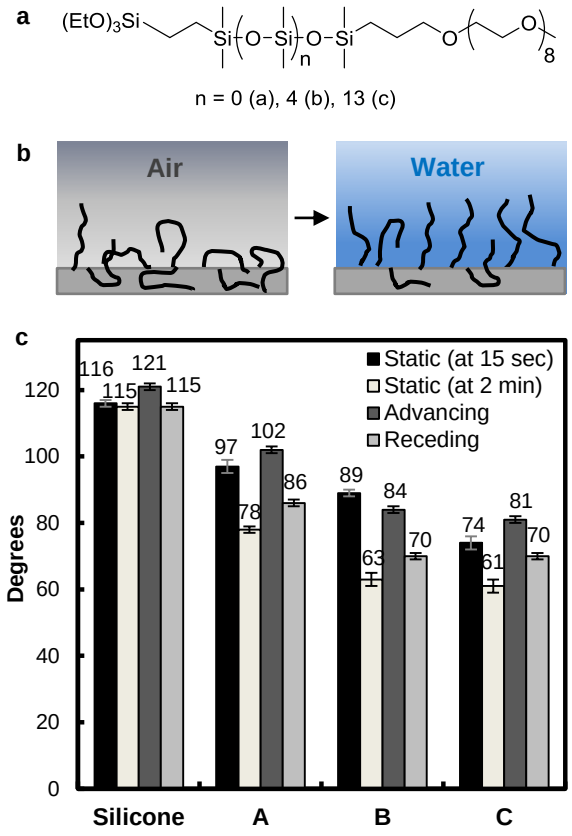

Figure 4.1. (a) Structure of PEO-silane amphiphiles. (b) Schematic representation of restructuring of PEO-silane amphiphile chains to the aqueous interface. (c) Contact angle measurements of silicone and modified silicone coatings A, B, and C prepared with PEO-silane amphiphiles a (n = 0), b (n = 4), and c (n = 13), respectively. Error bars represent the SD between three measurements taken on different areas of the same sample.

It was demonstrated previously that when PEO-silane amphiphiles (a–c) were surface-grafted onto silicon wafers, protein resistance generally increased with siloxane tether length [39]. When a–c were combined in a stoichiometric 2:3 M ratio with α, ω-bis(Si–OH)PDMS (M_n = 3,000 g mol^{-1}), protein resistance of the resulting coatings (A–C, respectively) likewise generally increased with siloxane tether length [99]. Contact angle analysis of A–C revealed that a longer siloxane tether produced more extensive restructuring of PEO chains from the air to water interface.

In this work, modified silicone coatings A–C were produced and their ability to resist microfouling was evaluated and compared to that of an unmodified silicone 'standard' ('silicone', Silastic T-2). Microfouling resistance was evaluated in terms of the settlement of the bacterium *Bacillus* sp. 4J6 and the diatom (microalga) *Cylindrotheca closterium* (formerly*Nitzschia closterium*) as well as mixtures of the two. *Bacillus* sp. 4JS is a Gram-positive bacterium which constitutes up to 20% of the total bacterial flora found in seawater [188] and which forms a 'substrate' for subsequent biofouling [189]. The bacterium used herein is most similar to *Pseudoalteromonas* sp. strain SM9913 which is a Gram-negative, psychrotolerant bacterium found in deep-sea sediment [190]. Furthermore,*Pseudoalteromonas* spp. have shown a variety of biological activities associated with the secretion of extracellular compounds [191]. *C. closterium* is a benthic marine diatom which is a major component of the diatom slimes that form on AF coatings [192]. Immersion of the coatings in the Atlantic Ocean for periods of 1, 2, and 4 weeks provided comparisons of *in situ* microfouling *via* microscopy. Finally, formation of diatom slime was evaluated by visual observation after immersion in the ocean for 6 weeks.

4.3 Materials and Methods

4.3.1 Materials

Solvents, H_3PO_4, Marine Broth (MB2216, Difco), NaCl, glutaraldehyde, and Guillard's F/2 Marine Enrichment Basal Salt Mixture were obtained from Sigma-Aldrich. Syto green was obtained from molecular probes. α, ω-Bis(Si–

OH)polydimethylsiloxane (M_n = 2,000–3,500 g mol^{-1} per specifications; M_w/M_n = 5,000/3,000 g mol^{-1} by gel permeation chromatography [99] was obtained from Gelest. Glass microscope slides (75 × 25 × 1 mm) were obtained from Fisher Scientific. Polycarbonate (PC) sheets (100 × 75 × 1 mm) were obtained from Goodfellow USA. PC sheets (1 mm thick) used to prepared spacers for fiberglass panels were obtained from McMaster Carr. Glass fiber composite panels (40 cm × 10 cm) were obtained from Nautix Corporation. Interlux Epoxy Primekote was obtained from West Marine. Silastic T-2 (a 2-part RTV silicone) was obtained from Dow Corning and served as a silicone standard. PEO-silane amphiphiles were synthesized according to the procedures previously reported [99]. The benthic diatom *C. closterium* (Diatomophyceae, AC515) was obtained from the Culture Collection of Algae of the University of Caen (France).

4.3.2 Coating Preparation

Coatings A–C were prepared and characterized as previously reported [99]. Briefly, PEO-silane amphiphiles [n = 0 (a), M_n = 749 g mol^{-1}; n = 4 (b), M_n = 1,044 g mol^{-1}; n = 13 (c), M_n = 1,710 g mol^{-1}] were each combined with α, ω-bis(Si–OH)PDMS (M_n = 3,000 g mol^{-1}) with a 2:3 M ratio of a, b, or c to α, ω-bis(Si–OH)PDMS and mixed for ~5 min. Next, 3 mol% of H_3PO_4 (based on total solid weight of the mixture) was added as a solution of H_3PO_4/EtOH (10:90 w/w) and the mixture was rapidly stirred for 3 h. Silastic T-2 was used without further modification.

Coatings A–C used for bacterial and diatom tests were formed on microscope slides (75 × 25 × 1 mm), which were sequentially cleaned with deionized (DI) H_2O, CH_2Cl_2/hexane (1:1 v/v) and acetone, and lastly dried in a 150 °C oven for 24 h [99]. One milliliter of each of the aforementioned mixtures containing a–c was applied to a microscope slide, allowed to level across the entire surface and cured in a 150 °C oven for 48 h. All coated microscope slides were leached in DI H_2O for 24 h with a water change at 12 h to aid in the removal of the acid catalyst and other leachable compounds. Coated microscope slides were subsequently dried with a stream of nitrogen and the final coating thickness was ~0.5 mm. For short-term seawater immersion tests (1–4 weeks), coatings A–C (0.5 mm thick) were prepared on PC sheets by applying 4 ml of each mixture and curing as above. For the 6-week seawater immersion tests, glass fiber composite panels were painted with two coats of epoxy primer with a foam brush, allowing the first coat to dry for 12 h at room temperature (RT) before applying the second coat. After two days, PC borders (1 cm wide × 4 mm thick) were attached with Super Glue™ to define an interior area of 10 × 7.5 cm. Each mixture containing a–c was applied (4 ml) and cured as above. Coated PC sheets and panels were not soaked in DI H_2O prior to settlement tests to better parallel the manner in which a coated ship's hull would be directly exposed to fouling organisms. 'Silicone' standard coatings (~0.6 mm thick) were formed by applying the Silastic T-2 mixture onto glass microscope slides and PC sheets with a drawdown bar (30 mil) and onto glass fiber composite panels as above and cured at RT for over 72 h.

4.3.3 Bacterial Biofilm Test Conditions

A strain of a marine bacterium, *Bacillus* sp. 4J6, was isolated from a surface of glass which had been previously immersed in natural seawater (Gulf of Morbihan, France) for 6 h [72] and was subsequently grown in Marine Broth (MB2216, Difco). Its 16S rDNA sequence (GenBank accession number FJ966949) is most closely related (95.5% identity) to that of *Pseudoalteromonas* sp. strain SM9913 [193]. Bacterial cells were harvested by centrifugation at 7000 × *g* for 10 min, washed twice with 0.15 M NaCl, and re-suspended in 0.15 M NaCl at 10^7 cells ml^{-1}. Each coated microscope slide was incubated in 20 ml of a given bacterial suspension for 6 h at 20 °C under static conditions. Next, the samples were gently rinsed three times with 0.15 M NaCl to remove non-adherent bacteria. A given coating composition was tested using three independent cultures of bacteria with three samples per culture. Bacterial biofilm formation was analyzed using confocal laser scanning microscopy (CLSM) (see below).

4.3.4 Diatom Biofilm Test Conditions

C. closterium was grown in sterile artificial seawater (SASW) medium with Guillard's F/2 Marine Enrichment Basal Salt Mixture (stored at 4 °C before use) at 18 °C [194]. Synthetic seawater was prepared before use [195]. Diatom suspensions were maintained under controlled illumination of 500 μmol photons m^2 s^{-1}white fluorescent lamps at 18 °C, cycled with 16 h of darkness, and 8 h of light. Three slides of each composition were placed in a bioreactor composed of an Erlenmeyer flask containing 2 l of SASW which was then inoculated with a pure culture of diatoms at a concentration of

3.7×10^5 cells ml^{-1}. Slides were maintained in the bioreactor at 20 °C and pH 7.6 under controlled illumination of 500 μmol photons m^2 s^{-1} cool white fluorescent lamps, cycled with 16 h of darkness, and 8 h of light. Air was flowed into the bioreactor at 1.8 l min^{-1} to agitate the medium. Each minute, 1 ml of SASW medium with Guillard's F/2 was added to the bioreactor while a peristaltic pump withdrew 1 ml in order to maintain the supply of nutrients. The growth of biofilms on the test surfaces was analyzed after 1 and 3 weeks. At each time point, all slides were collected and analyzed *via* CLSM. Sample surfaces were not rinsed prior to imaging to avoid detachment of diatoms from the surface.

4.3.5 Mixed Biofilm Test Conditions

Prior to inoculation, slides were placed in a bioreactor composed of an Erlenmeyer flask containing 2 l of SASW with 10% Marine Broth medium (MB2216, Difco). Pure cultures of the bacterium (*Bacillus* 4J6) and the diatom (*C. closterium*) were inoculated together in the bioreactor at 1×10^7 cells ml^{-1} and 1×10^5 cells ml^{-1}, respectively. All samples were maintained in the bioreactor at 20 °C and pH 7.6 under controlled illumination of 500 μmol photons m^2 s^{-1} cool white fluorescent lamps, cycled with 10 h of darkness and 14 h of light. Air was flowed into the bioreactor at 1.8 l min^{-1} to agitate the medium. Each minute, 1 ml of SASW with 10% Marine Broth was added to the bioreactor while a peristaltic pump withdrew 1 ml to maintain nutrients. At each time point (3, 16 and 23 days), three samples of each composition were collected and analyzed *via* CLSM and scanning electron microscopy (SEM).

4.3.6 Seawater Exposure Tests

Coated PC sheets were immersed in seawater at a depth of 50 cm (Atlantic Ocean, Kernevel Harbor, France; springtime) where the tide provided a flow of ~ 2 to 3 knots. A portion of each sheet was removed at 1, 2, and 4 weeks, and CLSM and SEM were performed. Coated fiberglass composite panels were similarly immersed in seawater and removed for visual observation of diatom slime formation at 6 weeks. Surfaces were rinsed with seawater to remove silt and unattached biofouling species. Photographs recorded the extent of slime formation on the coatings.

4.3.7 CLSM

Accumulated bacteria were stained with 5 μM syto green (485 nm excitation and 498 nm emission) for 10 min. Diatoms were imaged *via* autofluorescence of chlorophyll (633 nm excitation and 650–700 nm emission). Images were captured with CLSM using a DMB 6000B confocal microscope (Leica Microsystems, Germany). The percentage coverage was evaluated using ImageTool software (UTHSCSA), and the thickness and volume of the biofilm were measured using COMSTAT software [196]. For all coating samples, the reported results are an average of five measurements taken at various positions in a random manner from different areas of three microscope slides giving a total of 15 measurements. Images were collected from the center of the samples to eliminate any edge defects. Statistical analysis of biofilm formation data was performed with Matlab 7.4. *p*-values were calculated by one-way analysis of variance ($p < 0.05$).

Error bars represent the standard deviation (SD) between the fluorescence measurements of 15 randomly selected regions on three microscope slides (5 measurements per slide).

4.3.8 SEM

Samples were immersed in 3% glutaraldehyde (prepared in DI water) overnight at 4 °C and subsequently dehydrated by several washings: phosphate buffer (0.1 M; pH 7.35) (10 min, 3 times), 70% EtOH (10 min, 3 times), 90% EtOH (10 min, 3 times), and 100% EtOH (10 min, 3 times). The samples were desiccated by the carbon dioxide critical point method and were coated with gold. Images were collected using a JSM-6460LV SEM (JEOL) with a accelerated electron energy of 20 keV.

4.4 Results

4.4.1 Contact Angle Analysis

Static and dynamic contact angle analysis of coatings A–C and the unmodified silicone standard [99] are shown in **Figure 4.1c**. Surface restructuring of PEO-silane amphiphiles from the air to water interface was quantified by measuring the decrease in static contact angle (θ_{static}) at 15 s *vs* at 2 min as well as the difference between the advancing (θ_{adv}) *vs* receding (θ_{rec}) contact angles (ie hysteresis). Dynamic contact angle measurements occurred over a shorter time period (~7 s). The silicone standard was hydrophobic and exhibited minimal surface restructuring. θ_{static} (15 s) decreased and surface hydrophilicity increased in the order: A < B ≈ C. θ_{static} (2 min) values exhibited

the same trend but were significantly lower than the corresponding θ_{static} (15 s). Likewise, θ_{rec} was significantly lower *vs* the corresponding θ_{adv}.

4.4.2 Bacterial Biofilm Formation

Following incubation in the presence of *Bacillus* 4J6 (10^7 cells ml^{-1}) for 6 h, biofilm formation was quantified (**Figure 4.2**, **Table 4.1**). Bacterial percentage coverage, average thickness, and biomass decreased in the order: silicone ≈ A > B ≈ C. Maximum thickness did not vary significantly among the coatings.

4.4.3 Diatom Biofilm Formation

After exposure for 1 and 3 weeks to *C. closterium* (3.7×10^5 cells ml^{-1}), biofilm formation was observed as shown in **Figure 4.3**, **Figure 4.4**, and **Table 4.2**). At 1 week the percentage coverage decreased in the order: silicone ≈ A > B ≈ C. At 3 weeks, the percentage coverage decreased in the order: silicone > A ≈ B > C. For A, the percentage coverage at 1 week was unexpectedly higher than that at 3 weeks.

4.4.4 Mixed Biofilm Formation

Mixed biofilm formation was observed following simultaneous exposure to bacterial and diatom cells, each at the aforementioned concentrations, at 3, 16, and 23 days (**Figure 4.5a**, **Table 4.3**). At 3 and 16 days, bacterial biomass was present at low levels on coatings A–C, but was not significantly different from the silicone standard (**Figure 4.5b**). At 23 days, C exhibited significantly reduced levels of bacteria. In terms

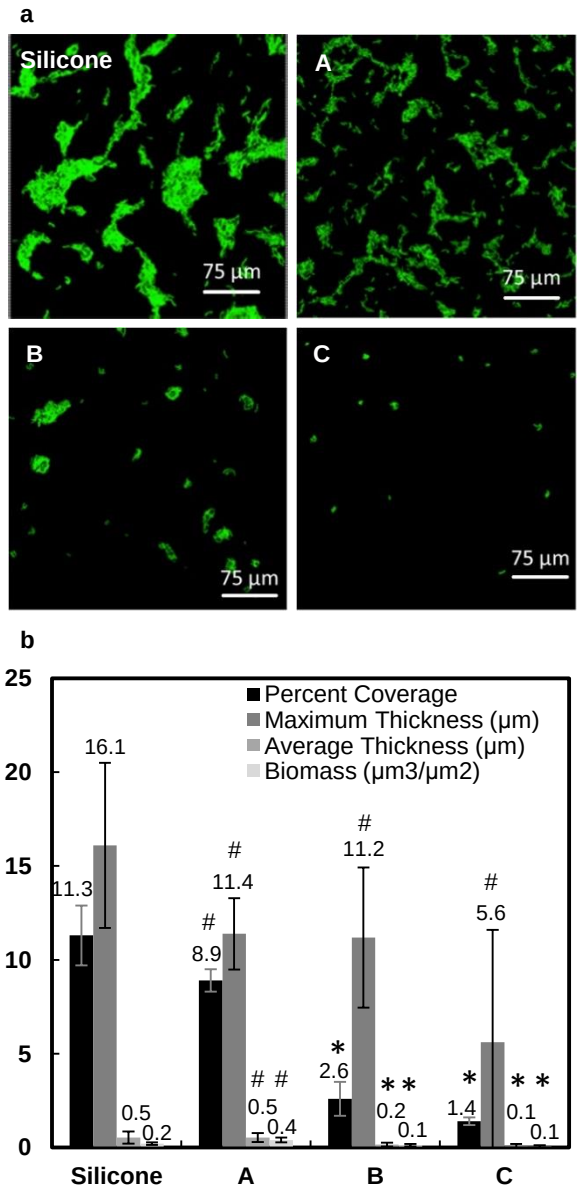

Figure 4.2. Settlement of bacterial cells on silicone and modified silicone coatings A, B, and C after 6 h *via* CLSM. Coatings A, B, and C were prepared with PEO-silane amphiphiles a (n = 0), b (n = 4), and c (n = 13), respectively. * indicates $p < 0.05$ and # indicates $p > 0.05$ when compared to silicone.

Table 4.1. *Bacillus* settlement on silicone and coatings A, B, and C after 6 h.

	Silicone	A	B	C
Percent coverage	11.3 ± 1.6	8.9 ± 0.6	2.6 ± 0.9	1.4 ± 0.2
Maximum thickness (μm)	16.1 ± 4.4	11.4 ± 1.9	11.2 ± 3.7	5.6 ± 6.0
Average thickness (μm)	0.53 ± 0.32	0.54 ± 0.24	0.16 ± 0.10	0.08 ± 0.12
Biomass ($\mu m^3\ \mu m^{-2}$)	0.21 ± 0.07	0.40 ± 0.13	0.12 ± 0.07	0.06 ± 0.07

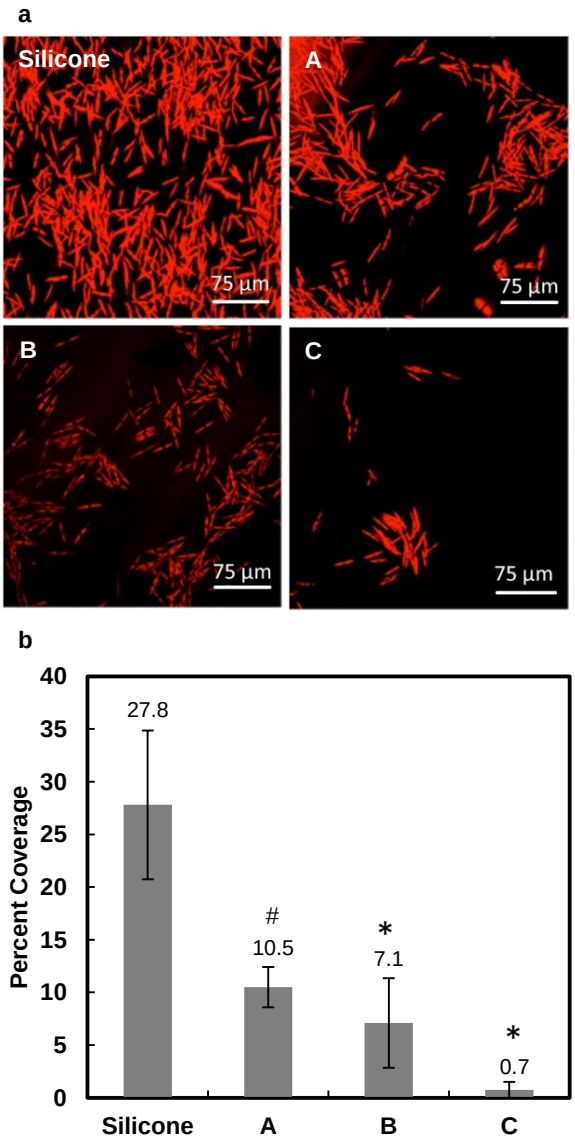

Figure 4.3. Settlement of diatom cells (*C. closterium)* on silicone and modified silicone coatings A, B, and C after 3 weeks *via* CLSM. Coatings A, B, and C were prepared with PEO-silane amphiphiles a (n = 0), b (n = 4), and c (n = 13), respectively. * indicates $p < 0.05$ and # indicates $p > 0.05$ when compared to silicone.

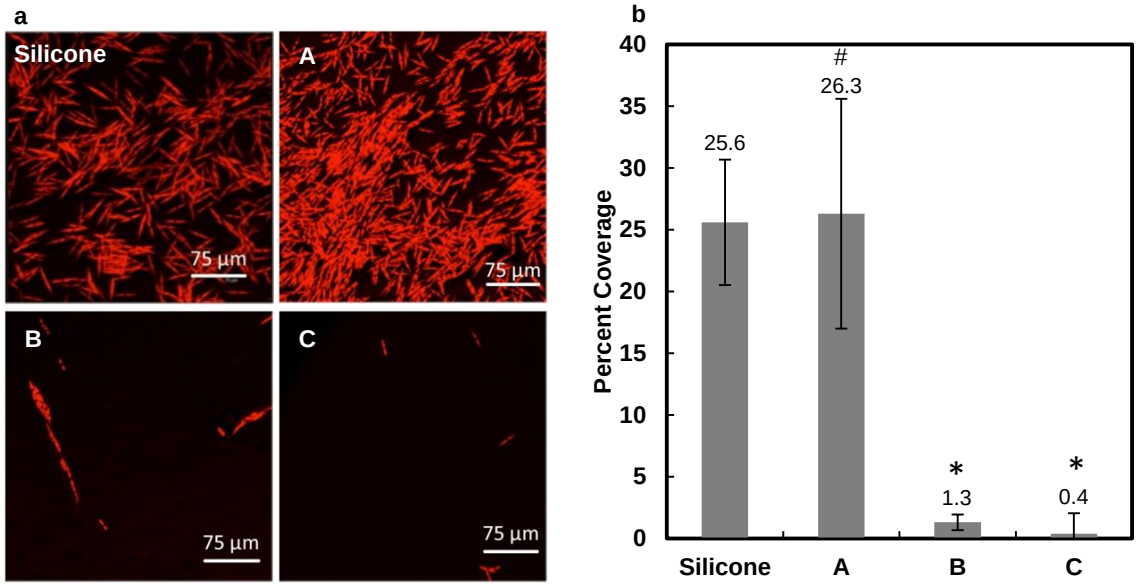

Figure 4.4. (a) *C. closterium* settlement and (b) percentage coverage on silicone and modified silicone coatings A, B, and C after 1 week *via* CLSM. Coatings A, B, and C were prepared with PEO-silane amphiphiles a (n = 0), b (n = 4), and c (n = 13), respectively. * indicates $p < 0.05$ and # indicates $p > 0.05$ when compared to silicone.

Table 4.2. *C. closterium* settlement on silicone and coatings A, B, and C after 1 and 3 weeks.

Percent coverage	Silicone	A	B	C
1 week	25.6 ± 5.1	26.3 ± 9.3	1.3 ± 0.6	0.4 ± 1.7
3 weeks	27.8 ± 7.1	10.5 ± 1.9	7.1 ± 4.3	0.7 ± 0.8

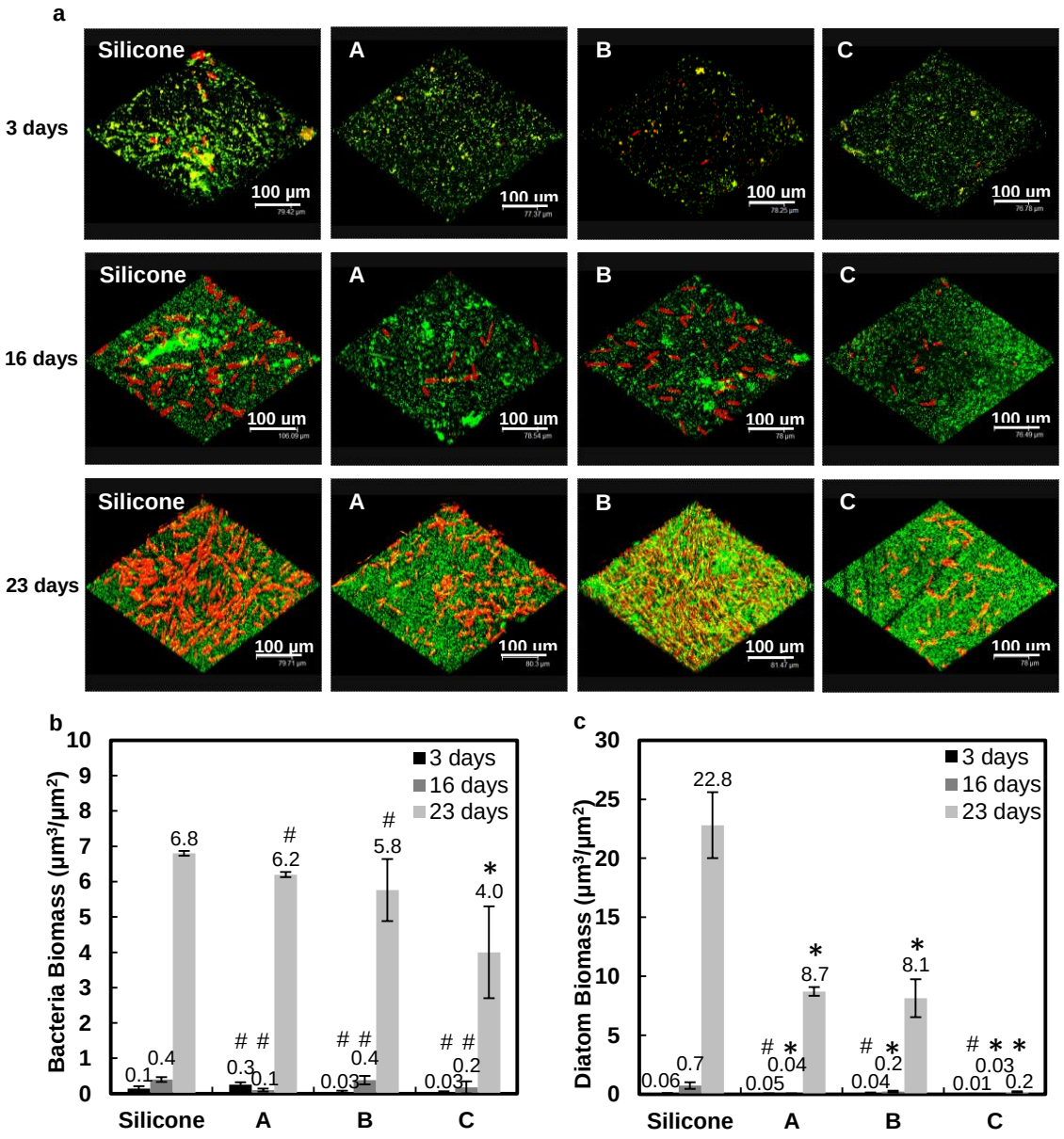

Figure 4.5. (a) Mixed biofilm (bacterium and diatom), (b) *Bacillus* biomass and (c) *C. closterium* biomass on silicone and modified silicone coatings A, B, and C after 3, 16, and 23 days *via* CLSM. Coatings A, B, and C were prepared with PEO-silane amphiphiles a ($n = 0$), b ($n = 4$), and c ($n = 13$), respectively. * indicates $p < 0.05$ and # indicates $p > 0.05$ when compared to silicone.

Table 4.3. Mixed biofilm settlement (*Bacillus* and *C. closterium*) on silicone and coatings A, B, and C after 3, 16, and 23 days *via* CLSM.

	No. of days	Silicone	A	B	C
Bacillus biomass	3	0.14 ± 0.07	0.25 ± 0.07	0.03 ± 0.05	0.03 ± 0.04
($\mu m^3\ \mu m^{-2}$)	16	0.4 ± 0.07	0.1 ± 0.04	0.38 ± 0.12	0.18 ± 0.17
	23	6.8 ± 0.07	6.2 ± 0.07	5.8 ± 0.88	4.0 ± 1.30
C. closterium biomass	3	0.06 ± 0.03	0.05 ± 0.01	0.04 ± 0.10	0.01 ± 0.03
($\mu m^3\ \mu m^{-2}$)	16	0.73 ± 0.28	0.04 ± 0.03	0.21 ± 0.08	0.03 ± 0.01
	23	22.8 ± 2.8	8.7 ± 0.37	8.14 ± 1.61	0.19 ± 0.05
Maximum thickness	3	16.8 ± 0.71	20.7 ± 4.23	20.3 ± 5.76	10.5 ± 1.17
(μm)	16	21.2 ± 1.68	23.4 ± 1.40	25.4 ± 1.40	13.9 ± 3.80
	23	18.3 ± 2.7	24.1 ± 7.40	56.9 ± 1.40	12.9 ± 2.30

of diatom biomass, after 3 days, diatoms were present on all coatings but at indistinguishably low levels, statistically similar to the silicone standard (**Figure 4.5c**). At 16 and 23 days, coatings A–C exhibited reduced amounts of diatoms *vs* the silicone standard. Notably, at 23 days, C exhibited exceptionally low diatom biomass. In addition, the maximum thickness of the mixed biofilm was significantly reduced on C *vs* the silicone standard at all time points (**Figure 4.6**). The corresponding SEM images of the mixed biofilms are shown in **Figure 4.7**.

4.4.5 Seawater Microfouling

Coated panels were immersed in the ocean, and microfouling was observed after 1, 2, and 4 weeks (**Figure 4.8**). The silicone standard rapidly accumulated a biofilm comprised of a diverse community of microorganisms, which consisted predominantly of diatoms along with bacteria and other microorganisms. For coatings A–C, the biofilm was noticeably reduced at all time points *vs* the silicone standard. Unlike silicone, at 1 and 2 weeks, A–C displayed a negligible presence of diatoms. Only after submersion for

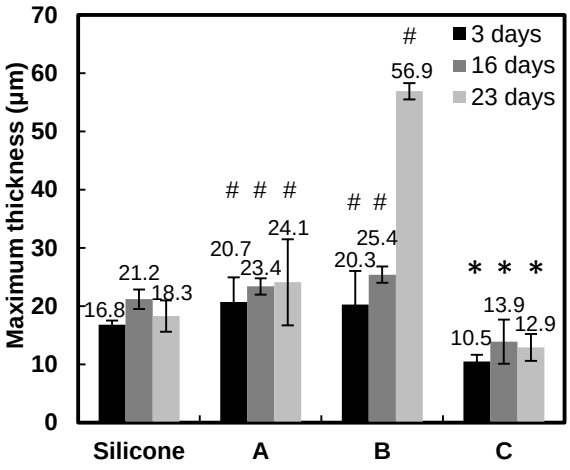

Figure 4.6. Mixed biofilm (*Bacillus* and *C. closterium*) on silicone and modified silicone coatings A, B, and C after 3, 16, and 23 days *via* CLSM. Coatings A, B, and C were prepared with PEO-silane amphiphiles a (n = 0), b (n = 4), and c (n = 13), respectively. * indicates $p < 0.05$ and # indicates $p > 0.05$ when compared to silicone.

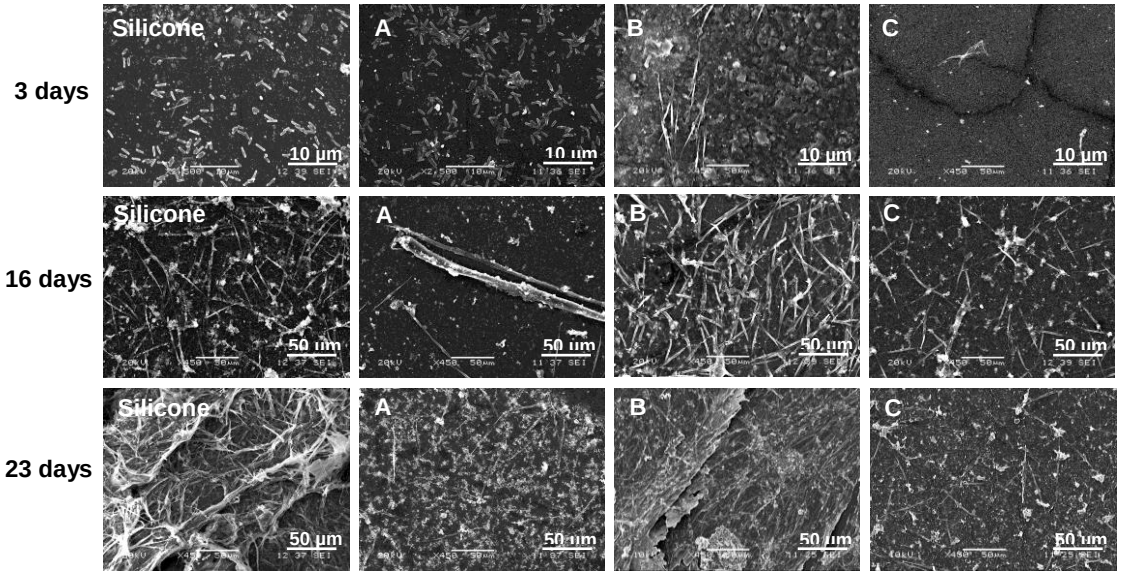

Figure 4.7. Mixed biofilm (*Bacillus* and *C. closterium*) on silicone and modified silicone coatings A, B, and C after 3, 16, and 23 days *via* SEM. Coatings A, B, and C were prepared with PEO-silane amphiphiles a (n = 0), b (n = 4), and c (n = 13), respectively.

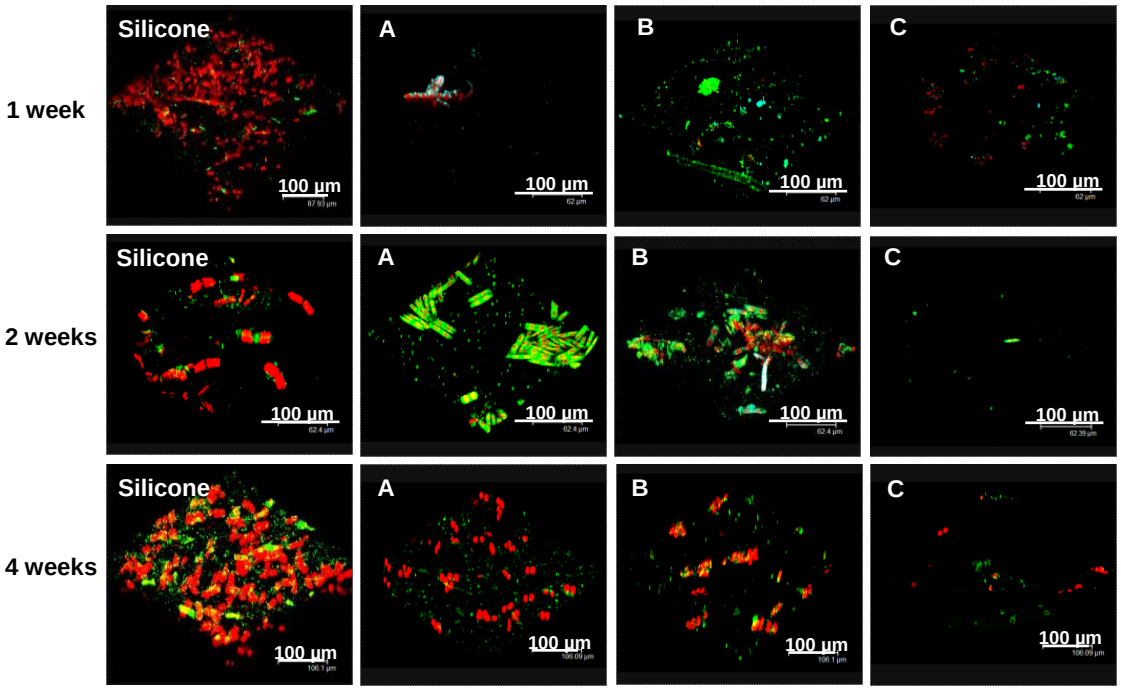

Figure 4.8. *In situ* microfouling of silicone and modified silicone coatings A, B, and C after immersion in the Atlantic Ocean for 1, 2, and 4 weeks *via* CLSM. Coatings A, B, and C were prepared with PEO-silane amphiphiles a (n = 0), b (n = 4), and c (n = 13), respectively.

4 weeks did diatoms become a significant part of the biofilm, and bacterial levels remained quite low. At 4 weeks, coating C showed exceptional resistance to microfouling. The corresponding SEM images are shown in **Figure 4.9**. After immersion for 6 weeks in the ocean, microfouling was observed by visual inspection [197] (**Figure 4.10**). While the silicone standard showed the presence of a brown slime, coatings A–C did not.

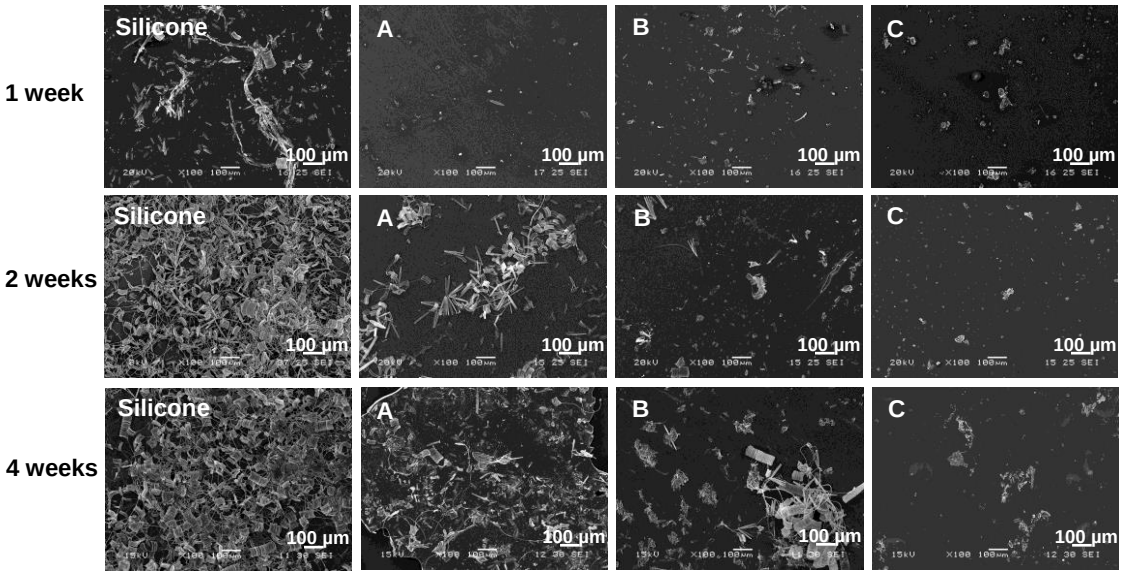

Figure 4.9. *In situ* microfouling of silicone and modified silicone coatings A, B, and C after immersion in Atlantic Ocean for 1, 2, and 4 weeks *via* SEM. Coatings A, B, and C were prepared with PEO-silane amphiphiles a (n = 0), b (n = 4), and c (n = 13), respectively.

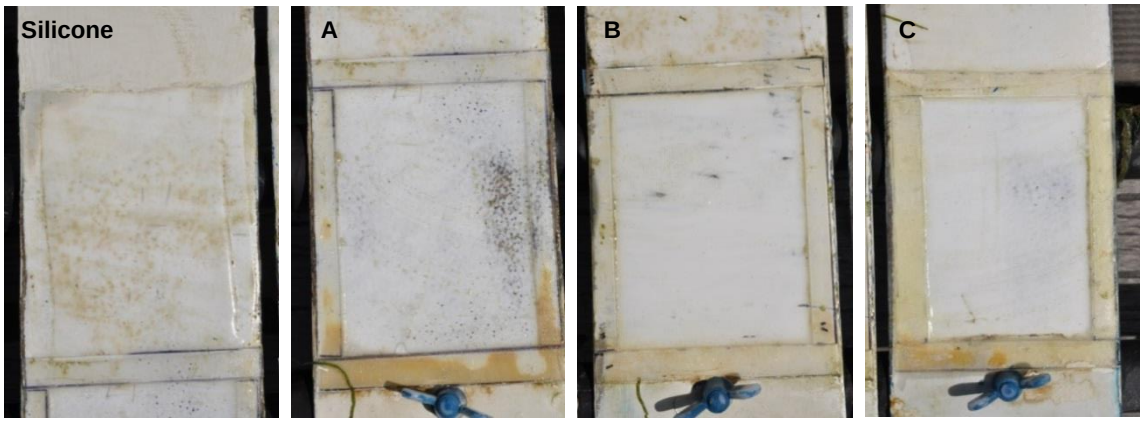

Figure 4.10. *In situ* microfouling of silicone and modified silicone coatings A, B, and C after immersion in the Atlantic Ocean for 6 weeks. Coatings A, B, and C were prepared with PEO-silane amphiphiles a (n = 0), b (n = 4), and c (n = 13), respectively.

4.5 Discussion

PEO-silane amphiphiles (a–c) containing flexible, hydrophobic siloxane tethers of varying lengths [a ($n = 0$), b ($n = 4$), and c ($n = 13$)] were used to produce three modified silicone coatings (A–C, respectively) (**Figure 4.1a**). A 2:3 stoichiometric molar ratio of a–c and α, ω-bis(Si–OH)PDMS was utilized and resulted in coatings with ≤1 wt.% of uncross-linked materials, ensuring that the coatings contained similar molar concentrations of a–c [99]. θ_{static} (15 s) and θ_{adv} values revealed that coating surface hydrophilicity at the air interface increased with siloxane tether length in the order: silicone < A < B ≈ C (**Figure 4.1c**). In addition, as noted by the decrease in the corresponding values of θ_{static} (2 min s) and θ_{rec}, PEO-silane amphiphiles rapidly restructured to the aqueous interface (**Figure 4.1b**). This process was also facilitated by a longer siloxane tether such that hydrophilicity likewise increased in the order: silicone < A < B ≈ C. Previous work demonstrated that coating resistance to bovine serum albumin protein was enhanced with increased siloxane tether length in the order A < B ≈ C [99]. Protein resistance improved further when the coatings were first equilibrated in an aqueous environment. Also, protein resistance paralleled coating hydrophilicity. These results confirmed that the mobility of PEO-silane amphiphiles to the coating surface was enhanced by a longer siloxane tether, leading to increased surface hydrophilicity and, thus, protein resistance. In addition, the combination of the hydrophobic siloxane tether and the hydrophilic PEO chain produces amphiphilic surfaces, particularly at the aqueous interface, to also enhance protein rejection.

The efficacy of A–C in diminishing the accumulation of diatom slime was measured through a series of biofouling tests. A commercial silicone (Silastic T-2) (silicone) served as a positive standard as its strong affinity to diatoms has been demonstrated [198]. Because the accumulation of bacteria often precedes diatom settlement [72], the coatings were exposed to *Bacillus* (4J6) and *C. closterium* as well as a mixture of the two using a previously reported static incubation strategy [199]. Settlement of *C. closterium* and mixed biofilms also containing *Bacillus* sp. were measured temporally for extended time periods to observe the progression of biofouling. These settlement tests collectively revealed key differences among the coatings, which often became more pronounced at the later time points. First, the percentage coverage, average thickness, and biomass of bacteria on coatings B and C were statistically lower than that on the silicone standard. The higher settlement on the silicone standard as well as the coating prepared with the PEO-silane amphiphile bearing the shortest siloxane tether (A) may be attributed to their greater hydrophobicity. Second, coatings were exposed to *C. closterium*, a known fouler of silicone-based coatings, for 1 and 3 weeks. At 1 week, coatings B and C exhibited statistically lower percentage coverage *vs* silicone. At 3 weeks, coatings A–C all exhibited statistically lower percentage coverage *vs* silicone. However, coverage was particularly low on coating C. With prolonged exposure from 1 to 3 weeks, the percentage coverage did not significantly increase for the silicone standard. In the case of A, percentage coverage at 3 weeks was lower than at 1 week, indicating weak attachment of settled diatoms. For B and C, percentage coverage was not substantially increased *vs* at 1 week. The enhanced

diatom resistance of B and, in particular, C is consistent with their greater hydrophilicity. Since natural seawater provides simultaneous exposure to bacteria and diatoms, the coatings were also exposed to a mixture of the two for 3, 16, and 23 days. Coatings prepared with PEO-silane amphiphiles having a longer siloxane tether generally exhibited reduced mixed biofilm formation *vs* the silicone standard, particularly with longer exposure times. These trends are consistent with results observed when coatings were exposed individually to bacteria and diatoms. The enhanced resistance of B and C (particularly of C to diatoms) can be likewise attributed to their higher hydrophilicity due to enhanced restructuring of the PEO-silane amphiphiles to the water interface. In future studies, the AF capacity of the coatings under dynamic conditions should also be evaluated [200,201]. Finally, the coatings were submerged for 1, 2 and 4 weeks in seawater (Atlantic Ocean) such that they would be exposed to a natural environment containing bacteria, diatoms, and other biofoulers. A biofilm dominated by diatoms was observed on the silicone standard at just 1 week and increased at 2 and 4 weeks. In contrast, coatings prepared with PEO-silane amphiphiles exhibited diminished biofilm formation. The biofilm was particularly reduced on coating C due to the enhanced restructuring of the PEO-silane amphiphiles to the water interface and the resulting increased hydrophilicity. Finally, coated panels were also immersed in the Atlantic Ocean for an extended period of 6 weeks to allow the observation of brown slime. Slime was noted on the silicone standard but not on coatings A–C, which were indistinguishable from each other. Thus, C displayed the best overall resistance to biofouling, which may be attributed to the longer siloxane tether of the PEO-silane

amphiphile (c) and associated surface properties. However, the complex interactions between bacteria, diatoms and other microorganisms in biofilms developed on coatings immersed in the ocean will also impact on their long-term performance [202-204].

In conclusion, PEO-silane amphiphiles containing siloxane tethers of varying length [$n = 0$ (a), $n = 4$ (b), $n = 13$ (c)] may be used as additives to form modified silicones (A–C) by simply blending with a α, ω-bis(Si–OH)PDMS. As the length of the siloxane tether is increased (a < b < c), surface restructuring of the amphiphiles to the aqueous interface is enhanced as confirmed by an increase in surface hydrophilicity. As a result, the modified silicone coating (C) prepared with the PEO-silane amphiphile comprised of the longest siloxane tether (c) exhibited the greatest AF behavior to microfouling by bacteria and diatoms. The FR behavior of a coating is known to be enhanced by a low modulus [205-207]. As expected for modified silicones, coatings A–C exhibited low modulus values that decreased slightly as the PEO-silane amphiphile siloxane tether was lengthened: 27.4 MPa (A), 5.4 MPa (B) and 4.9 MPa (C) [99]. As a result, the low modulus of coatings A–C may also contribute to their FR behavior. Thus, PEO-silane amphiphiles may be used to produce silicones with a high capacity to control diatom slimes and possibly other categories of marine biofouling. Such coatings would represent potential alternatives to toxic, ablative marine coatings.

4.5.1 Acknowledgements

Financial support from Texas A&M Engineering and Experiment Station is gratefully acknowledged. M.L. Hawkins thanks the Texas A&M University Diversity

Fellowship for financial support. The authors thank Fabrice Azemar for photographing the ocean panels. The performance of diatom and bacteria assay experiments by Fabienne Faÿ, Karine Réhel, and Isabelle Linossier is gratefully acknowledged.

CHAPTER V

ZWITTERIONIC PEO-SILANE AMPHIPHILES FOR ENHANCED BLOOD PROTEIN RESISTANCE

5.1 Overview

A new PEO-silane amphiphile chemistry was prepared by modification with a zwitterionic sulfobetaine end group: triethoxysilylethyl-oligodimethylsiloxane$_{13}$-*block*-poly(ethylene oxide)$_{11}$-sulfobetaine. The sulfobetaine end group is expected to provide enhanced hydration to the PEO segment versus the methoxy end group to further reduce protein adsorption. In addition to the zwitterionic PEO$_8$-silane amphiphile (**TES-ODMS$_{13}$-PEO$_{11}$-SB**), a series of controls were also prepared which contain one or more key structural features, including: PEO$_8$-silane amphiphile control [α-(EtO)$_3$Si(CH$_2$)$_2$-oligodimethylsiloxane$_{13}$-*block*-(OCH$_2$CH$_2$)$_8$-OCH$_3$; **TES-ODMS$_{13}$-PEO$_8$**], PEO-zwitterion control [α-(EtO)$_3$Si(CH$_2$)$_3$-*block*-(OCH$_2$CH$_2$)$_{11}$-SB; **TES-PEO$_{11}$-SB**], PEO-silane control [α-(EtO)$_3$Si(CH$_2$)$_3$-*block*-(OCH$_2$CH$_2$)$_8$-OCH$_3$; **TES-PEO$_8$**], siloxane control [α-(EtO)$_3$Si(CH$_2$)$_2$-oligodimethylsiloxane$_{13}$-SiH; **TES-ODMS$_{13}$**], and potentially a zwitterion control [α-(MeO)$_3$Si(CH$_2$)$_3$-SB; **TMS-SB**]. This series may be surface-grafted onto a model substrate and incorporated into bulk-modified silicones to determine the impact on protein resistance in the absence and in the presence of water-driven surface restructuring.

5.2 Introduction

Silicones, such as crosslinked polydimethylsiloxane (PDMS), are commonly used in biomedical applications [11-13] due to their unique properties including thermal and oxidative stability, gas permeability, flexibility and ease of processing [11,12]. However, silicones typically exhibit poor resistance to blood proteins due to its extreme hydrophobicity [7,8,14-16]. Adsorbed proteins initiate platelet adhesion and activation of coagulation pathways, which ultimately leads to thrombosis thereby compromising device efficacy and safety [7-10].

Zwitterionic polymers are neutral polymers with a positive and negative electrical charge at different locations within the molecule. They achieve excellent hydration via electrostatic interactions [49,50], specifically when compared to other protein-resistant polymers such as poly(ethylene oxide) (PEO; or poly(ethylene glycol) (PEG)) which achieves hydration via hydrogen-bonding. Water is believed to be an important factor in surface resistance to protein adsorption due to the resulting repulsive forces that prevent proteins from adsorbing to hydrated surfaces [51-54]. Thus, zwitterions are expected to be excellent candidates for protein-resistant materials due to their ability to bind a significant amount of water molecules.

Poly(sulfobetaine) is a commonly used zwitterion due to its simple synthesis [60] and chemical stability and has been shown to exhibit excellent non-fouling properties [55-58]. A zwitterionic siloxane composed of sulfobetaine [3-(dimethyl-(3-(trimethoxysilyl)propyl)ammonio)propane-1-sulfonate] has been used to coat silica [107,208], iron oxide [209,210], and gold [211] nanoparticles for enhanced stability and

biocompatibility, reduced cytotoxicity, and reduced nonspecific protein adsorption for increased circulation times in blood. When compared to silica nanoparticles coated with PEO, those coated with the zwitterionic siloxane were shown to have greater stability against particle disintegration at various temperatures [208].

Additionally, zwitterionic polymers have been covalently attached to low molecular weight PEO_n (i.e. oligoethylene oxide) (n = 0-4) to produce phosphorylcholine-oligoethylene oxide-alkane thiols which were subsequently used to form self-assembled monolayers (SAMs) on gold surfaces [58]. Protein resistance was enhanced by as much as 62% when compared to the corresponding oligoethylene oxide-alkane thiols. In limited reports, silicone surfaces have been surface-modified with carboxybetaine and sulfobetaine by surface ozone-induced grafting as well as by covalent silanization to reduce protein adsorption and platelet adhesion [63-65] as well as to form coatings with enhanced stability against hydrophobic recovery (i.e. migration of grafted zwitterion chains below the surface) [66].

Previously, Grunlan and co-workers reported new PEO-silane amphiphiles prepared with a short siloxane tether [α-$(EtO)_3Si(CH_2)_2$-oligodimethylsiloxane$_m$-*block*-$(OCH_2CH_2)_8$-OCH_3; m = 0, 4, and 13] [39,99]. As discussed in Chapter IV, the siloxane tether length was increased further (m = 17, 24, and 30) [212]. The flexibility and similarly hydrophobic nature of the siloxane tether was anticipated to enhance reorganization of PEO to the surface-water interface and reduce protein adsorption. Indeed, compared to a PEO-silane control (i.e. no siloxane tether), PEO-silane amphiphiles demonstrated a higher capacity to organize to the surface-water interface,

thereby enhancing protein resistance, with intermediate siloxane tether lengths achieving optimal results [99,163,212].

In this study, PEO-silane amphiphiles were modified with a zwitterionic sulfobetaine end group (**Figure 5.1**) with the goal of enhancing PEO hydration while maintaining the improved ability of the PEO to migrate through a silicone coating matrix. Due to its previously exhibited superior ability to undergo water-driven surface-restructuring, a siloxane tether (m = 13) was utilized in the synthesis of the zwitterionic PEO-silane amphiphile. In addition, a series of controls were also prepared which contained one or more key structural features, including: PEO_8-silane amphiphile control (**TES-ODMS$_{13}$-PEO$_8$**), PEO-zwitterion control (**TES-PEO$_{11}$-SB)**, PEO-silane control (**TES-PEO$_8$)**, siloxane control (**TES-ODMS$_{13}$**), and potentially a zwitterion control (**TMS-SB**) (**Figure 5.2**). As in previous studies [212,213], the zwitterionic PEO-silane amphiphile as well as and the controls may be used to prepare surface-grafted coatings on silicon wafers as well as bulk-modified silicone coatings such that surface hydrophilicity, water-driven restructuring, and protein resistance can be evaluated.

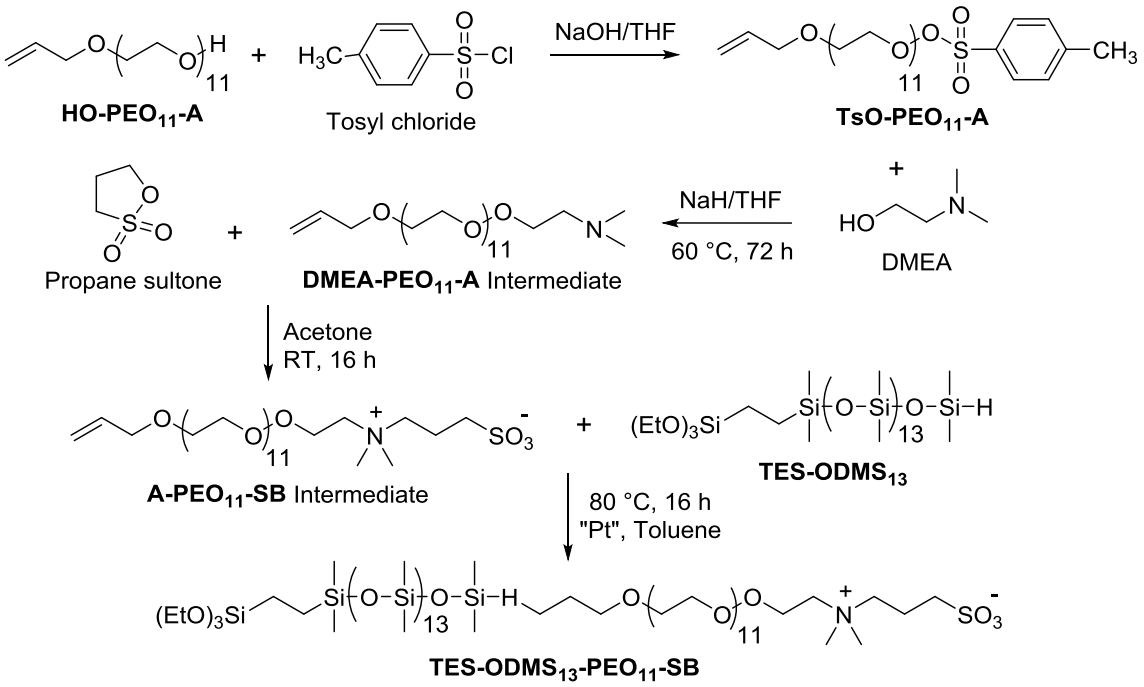

Figure 5.1. Synthesis of zwitterionic PEO-silane amphiphile.

Zwitterionic PEO-silane amphiphile (**TES-ODMS$_{13}$-PEO$_{11}$-SB**)

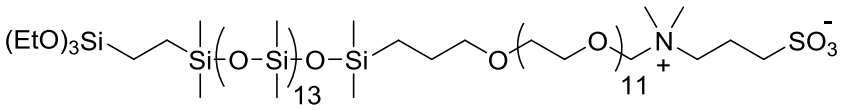

PEO-silane amphiphile control (**TES-ODMS$_{13}$-PEO$_{8}$**)

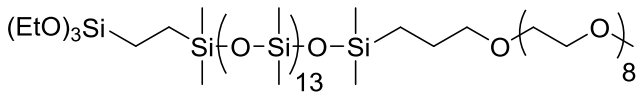

PEO-zwitterion control (**TES-PEO$_{11}$-SB**)

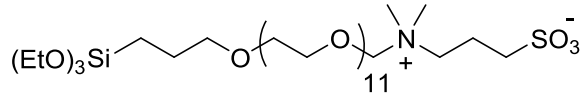

PEO-silane control (**TES-PEO$_{8}$**)

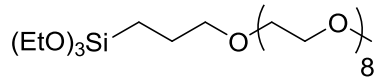

Siloxane control (**TES-ODMS$_{13}$**)

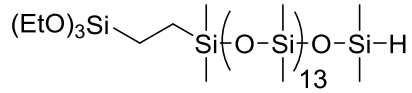

Zwitterion control (**TMS-SB**)

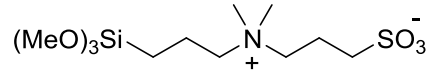

Figure 5.2. Structures of PEO-silane amphiphiles and PEO controls (with and without zwitterion), siloxane control, and zwitterion control.

5.3 Materials and Methods

5.*3.1 Materials*

p-Toluene sulfonyl chloride (tosyl chloride, TsCl), sodium hydroxide (NaOH), N,N'-dimethylethanolamine (DMEA), sodium hydride (NaH), propane sultone, $RhCl(Ph_3P)_3$ (Wilkinson's catalyst), ACS-grade dichloromethane (CH_2Cl_2), acetone,

hexane, and ethyl acetate, HPLC-grade tetrahydrofuran (THF), toluene, and chloroform ($CHCl_3$), NMR grade $CDCl_3$, and dimethyl sulfoxide-d_6 (DMSO) were obtained from Sigma-Aldrich. Allyloxy poly(ethylene oxide) (**HO-PEO$_{11}$-A**) [M_n = ~480 g/mol per manufacturer's specifications; M_n = 554 g/mol per ^{1}H NMR end group analysis; ^{1}H NMR (δ, ppm): 2.66 (s, 1H, O*H*), 3.55-3.70 (m, 44H, CH_2CH_2O), 3.98-4.01 (dt, 2H, CH_2═CHCH_2O), 5.12-5.28 (m, 2H, CH_2═CHCH_2O), 5.82-5.95 (m, 1H, CH_2═C*H*CH_2O)], Pt-divinyltetramethyldisiloxane complex in xylene (Karstedt's catalyst), triethoxysilane, α,ω-bis-(SiH)oligodimethylsiloxane$_{13}$ (**ODMS$_{13}$**) [M_n = 1000 – 1100 g/mol per manufacturer's specifications; M_n = 1096 g/mol per ^{1}H NMR end group analysis; ^{1}H NMR (*δ*, ppm): 0.05 – 0.10 (m, 78H, SiCH_3), 0.185 (d, *J* = 2.7 Hz, 12H, SiCH_3), 4.67 – 4.73 (m, 2H, Si*H*)], vinyltriethoxysilane (**VTEOS**), and (*N*,*N*-dimethyl-3-aminopropyl)trimethoxysilane (**DMA-TMS**) were obtained from Gelest. Allyl methyl PEO (**A-PEO$_8$-M**) [Polyglykol AM 450, M_n = 292 – 644 g/mol per manufacturer's specifications; M_n = 424 g/mol per ^{1}H NMR end group analysis; ^{1}H NMR (*δ*, ppm): 3.35 (s, 3H, OCH_3), 3.51 – 3.66 (m, 32H, OCH_2CH_2), 4.00 (d, *J* = 5.4 Hz, 2H, CH_2=CHCH_2O), 5.13 – 5.28 (m, 2H, CH_2=CHCH_2O), 5.82 – 5.96 (m, 1H, CH_2=C*H*CH_2O)] was provided by Clariant. Magnesium sulfate ($MgSO_4$) and activated charcoal were obtained from Fisher Scientific. The PEO-silane amphiphile control (**TES-ODMS$_{13}$-PEO$_8$**), siloxane control (**TES-ODMS$_{13}$**), and PEO-silane control (**TES-PEO$_8$**) were synthesized according to the procedures previously reported [99]. The zwitterion control (**TMS-SB**) may be synthesized as reported by Estephan et al. [107].

5.3.2 NMR

^{1}H spectra were obtained on a Mercury 300 MHz spectrometer operating in the Fourier transform mode. Five percent (w/v) $CDCl_3$ (dried over 4 Å molecular sieves) solutions were used to obtain spectra. Residual $CDCl_3$ was used as an internal standard set to 7.26 ppm.

5.3.3 IR Spectroscopy

IR spectra of neat liquids on NaCl plates were recorded using a Bruker TENSOR 27 Fourier transform infrared spectrometer.

5.3.4 Materials Synthesis

5.3.4.1 Synthesis of **TsO-PEO$_{11}$-A** Intermediate

Tosylated allyloxy PEO (**TsO-PEO$_{11}$-A**) was synthesized by the reaction of **HO-PEO$_{11}$-A** and TsCl in the presence of NaOH based on procedures previously reported [117,214]. **HO-PEO$_{11}$-A** (30.0 g, 60.2 mmol) in 120 mL of THF was added quickly dropwise over 5 min to a solution of NaOH (3.4 g, 84.3 mmol) in 180 mL of deionized (DI) water and 135 mL of THF. This mixture was allowed to stir for 2 h at RT before cooling to 0 °C and then TsCl (13.7 g, 72.2 mmol) in 280 mL of THF was added dropwise over 3 h (0 °C) and allowed to stir overnight at RT. The mixture was then poured over 200 mL of ice and extracted with 3 x 200 mL of CH_2Cl_2 and subsequently dried with $MgSO_4$. All volatiles were removed under reduced pressure to isolate the final product. In this way, **TsO-PEO$_{11}$-A** (25.3 g, 61% yield) was obtained. ^{1}H-NMR (δ,

ppm): 2.44-2.50 (d, 3H, C_6H_4─CH_3), 3.57-3.73 (m, 44H, OCH_2CH_2), 4.00-4.02 (dt, 2H, CH_2═CHCH_2O), 5.14-5.30 (m, 2H, CH_2═CHCH_2O), 5.84-5.97 (m, 1H, CH_2═CHCH_2O), 7.32-7.42 (m, 2H, C_6H_4), 7.77-7.93 (m, 2H, C_6H_4).

5.3.4.2 Synthesis of **DMEA-PEO$_{11}$-A** Intermediate

Dimethylethanolamino allyl PEO (**DMEA-PEO$_{11}$-A**) was prepared by the reaction of DMEA and **TsO-PEO$_{11}$-A** in the presence of NaH according to procedures previously reported [117,214]. DMEA (2.9 g, 32.6 mmol) in 10 mL of THF was added dropwise to a suspension of NaH (60% dispersion in mineral oil) (2.6 g, 65.0 mmol) in 10 mL of THF at 0 °C under an atmosphere of N_2. After the addition of DMEA, the mixture was stirred for 3 h until no bubbling of H_2 gas was observed. Next, a solution of **TsO-PEO$_{11}$-A** (4.4 g, 6.6 mmol) in 10 mL of THF was slowly added dropwise. This mixture was then heated to 60 °C and stirred for 72 h. Next, the reaction mixture was allowed to cool and sodium tosylate salts were filtered and all volatiles removed under reduced pressure. The resulting product was dissolved in 10 mL of toluene, and the organic layer was extracted with 3 x 10 mL of DI water. Next, the aqueous layer was extracted with 3 x 10 mL of $CHCl_3$. The organic layers were combined and dried with $MgSO_4$, and the solvent was removed under reduced pressure to isolate the final product. In this way, **DMEA-PEO$_{11}$-A** (1.7 g, 44% yield) was obtained. ^{1}H-NMR (δ, ppm): 2.24 (s, 6H, N^+─CH_3CH_3), 2.47-2.51 (t, 2H, OCH_2CH_2N^+), 3.63-3.64 (m, 46H, CH_2CH_2O─OCH_2CH_2N^+), 3.99-4.02 (dt, 2H, CH_2═CHCH_2O), 5.14-5.29 (m, 2H, CH_2═CHCH_2O), 5.83-5.96 (m, 1H, CH_2═CHCH_2O).

5.3.4.3 Synthesis of **A-PEO$_{11}$-SB** Intermediate

Allyl-ether-poly(ethylene oxide)$_{11}$-sulfobetaine (**A-PEO$_{11}$-SB**) was prepared by the reaction of **DMEA-PEO$_{11}$-A** and propane sultone [107,215]. DMEA-PEO$_{11}$-A (1.1 g, 1.8 mmol) and propane sultone (0.24 g, 2.0 mmol) were combined with 20 mL of acetone under an atmosphere of N_2. The reaction was stirred at RT for 16 h. Volatiles were removed under reduced pressure to isolate the final product. In this way, **A-PEO$_{11}$-SB** (1.3 g, 97% yield) was obtained. ^{1}H-NMR (δ, ppm): 2.21-2.31 (m, 2H, $CH_2CH_2CH_2SO_3^-$), 2.87-2.91 (t, 2H, $CH_2CH_2CH_2SO_3^-$), 3.22 (s, 6H, N^+─CH_3CH_3), 3.59-3.66 (m, 48H, CH_2CH_2O─$OCH_2CH_2N^+$), 3.95-3.97 (m, 2H, $CH_2CH_2CH_2SO_3^-$), 4.0-4.03 (dt, 2H, CH_2═$CHCH_2O$), 5.14-5.30 (m, 2H, CH_2═$CHCH_2O$), 5.84-5.97 (m, 1H, CH_2═$CHCH_2O$).

5.3.4.4 Synthesis of **TES-ODMS$_{13}$-PEO$_{11}$-SB**

Triethoxysilylethyl-oligodimethylsiloxane$_{13}$-*block*-poly(ethylene oxide)$_{11}$-sulfobetaine (**TES-ODMS$_{13}$-PEO$_{11}$-SB**) was prepared by the hydrosilylation of equimolar amounts of α-triethoxysilylethyl-ω-silane-oligodimethylsiloxane$_{13}$ (**TES-ODMS$_{13}$**) with **A-PEO$_{11}$-SB** similar to procedures previously reported [99,117]. **TES-ODMS$_{13}$** (2.2 g, 1.7 mmol) and **A-PEO$_{11}$-SB** (1.3 g, 1.7 mmol) were combined with 15 μL of Karstedt's catalyst and 20 mL of toluene and heated to 80 °C under an atmosphere of N_2 and allowed to stir for 16 h. The progress of the reaction was monitored with IR spectroscopy by the disappearance of the Si-H peak (~2125 cm^{-1}). In the case of an incomplete reaction, additional Karstedt's catalyst (15 μL) was added and the reaction

continued for another ~6 h. This cycle was repeated until no Si-H absorbance was observed in the IR spectrum. The catalyst was removed from the reaction mixture by refluxing with activated charcoal for 3 h at 80 °C. After filtration, the volatiles were removed under reduced pressure to isolate the final product. In this way, **TES-ODMS$_{13}$-PEO$_{11}$-SB** (1.9 g, 54% yield) was obtained. ^{1}H-NMR (δ, ppm): 0.04-0.09 (m, 92H, SiC*H*$_3$─C*H*$_2$CH$_2$CH$_2$), 0.48-0.55 (m, 3H, SiC*H*$_2$C*H*$_2$), 1.07-1.10 (d, 1H, SiC*H*$_2$C*H*$_2$), 1.18-1.25 (m, 9H, SiOCH$_2$C*H*$_3$), 1.55-1.65 (m, 2H, SiCH$_3$─CH$_2$C*H*$_2$CH$_2$), 2.23-2.31 (m, 2H, CH$_2$C*H*$_2$CH$_2$SO$_3^-$), 2.88-2.94 (t, 2H, CH$_2$CH$_2$C*H*$_2$SO$_3^-$), 3.23 (s, 6H, N$^+$─C*H*$_3$C*H*$_3$), 3.38-3.43 (t, 2H, SiCH$_3$─CH$_2$CH$_2$C*H*$_2$), 3.57-3.66 (m, 48H, C*H*$_2$C*H*$_2$O─OC*H*$_2$C*H*$_2$N$^+$), 3.71-3.73 (m, 2H, C*H*$_2$CH$_2$CH$_2$SO$_3^-$), 3.78-3.84 (m, 6H, SiOC*H*$_2$CH$_3$).

5.3.4.5 Synthesis of PEO$_8$-Silane Amphiphile Control (**TES-ODMS$_{13}$-PEO$_8$**)

Triethoxysilylethyl-oligodimethylsiloxane$_{13}$-*block*-poly(ethylene oxide)$_8$ (**TES-ODMS$_{13}$-PEO$_8$**) was prepared as previously reported [99] by the hydrosilylation of equimolar amounts of **A-PEO$_8$-M** with α-triethoxysilylethyl-ω-silane-oligodimethylsiloxane$_{13}$ (**TES-ODMS$_{13}$**). **A-PEO$_8$-M** (3.42 g, 8.0 mmol) and **TES-ODMS$_{13}$** (10.37 g, 8.0 mmol) were combined with 50 μL of Karstedt's catalyst and 50 mL of toluene and heated to 80 °C under an atmosphere of N_2 and allowed to stir for 16 h. The progress of the reaction was monitored with IR spectroscopy by the disappearance of the Si-H peak (~2125 cm^{-1}). In the case of an incomplete reaction, additional Karstedt's catalyst (15 μL) was added and the reaction continued for another ~6 h. This cycle was repeated until no Si-H absorbance was observed in the IR spectrum.

The catalyst was removed from the reaction mixture by refluxing with activated charcoal for 3 h at 80 °C. After filtration, the volatiles were removed under reduced pressure to isolate the final product. In this way, **TES-ODMS$_{13}$-PEO$_8$** (12.1 g, 88% yield) was obtained. ^{1}H-NMR (δ, ppm): -0.002-0.05 (m, 90H, SiC*H*$_3$), 0.09 (m, 2H, SiC*H*$_2$CH$_2$CH$_2$), 0.51 (m, 3H, SiC*H*$_2$C*H*$_2$), 1.05 (m, 1H, SiC*H*$_2$C*H*$_2$), 1.18 (m, 9H, SiOCH$_2$C*H*$_3$), 1.55 (m, 2H, SiCH$_2$C*H*$_2$CH$_2$), 3.34 (s, 3H, OC*H*$_3$), 3.52 (m, 2H, SiCH$_2$CH$_2$C*H*$_2$), 3.60 (m, 32H, OC*H*$_2$C*H*$_2$), 3.78 (m, 6H, SiOC*H*$_2$CH$_3$).

5.3.4.6 Synthesis of PEO-Zwitterion Control (**TES-PEO$_{11}$-SB**)

Triethoxysilylpropyl-poly(ethylene oxide)$_{11}$-sulfobetaine (**TES-PEO$_{11}$-SB**) was prepared by the hydrosilylation of **A-PEO$_{11}$-SB** with triethoxysilane. **A-PEO$_{11}$-SB** (0.7 g, 0.9 mmol) and triethoxysilane (0.17 g, 1.0 mmol) were combined with 15 μL of Karstedt's catalyst and 20 mL of THF in a pressure tube equipped with a Teflon bushing as a pressure seal. The tube was quickly purged with N_2, sealed, and heated to 80 °C. After 6 h, the reaction was cooled to RT, and the catalyst was removed by refluxing the reaction mixture with activated charcoal at 80 °C for 3 h. After filtration, the volatiles were removed under reduced pressure to isolate the final product. In this way, the **TES-PEO$_{11}$-SB** (0.8 g, 92% yield) was obtained. ^{1}H-NMR (δ, ppm): 1.18-1.25 (m, 9H, OCH$_2$C*H*$_3$), 1.78-1.86 (m, 2H, OCH$_2$C*H*$_2$CH$_2$), 2.20-2.32 (m, 2H, CH$_2$C*H*$_2$CH$_2$SO$_3^-$), 2.88-2.93 (m, 2H, CH$_2$CH$_2$C*H*$_2$SO$_3^-$), 3.22-3.26 (m, 6H, N^+─C*H*$_3$C*H*$_3$), 3.38-3.43 (m, 2H, OC*H*$_2$CH$_2$CH$_2$), 3.58-3.72 (m, 48H, C*H*$_2$C*H*$_2$O─OC*H*$_2$C*H*$_2N^+$), 3.93-3.98 (m, 2H, C*H*$_2$CH$_2$CH$_2$SO$_3^-$), 4.01-4.03 (dt, 6H, OC*H*$_2$CH$_3$).

5.3.4.7 Synthesis of PEO-Silane Control (**TES-PEO$_8$**)

Triethoxysilylpropyl-poly(ethylene oxide)$_8$ (**TES-PEO$_8$**) was prepared by the hydrosilylation of **A-PEO$_8$-M** with excess triethoxysilane similar to procedures previously reported [99]. **A-PEO$_8$-M** (4.73 g, 11.2 mmol) and triethoxysilane (2.01 g, 12.3 mmol) were combined with 25 μL of Karstedt's catalyst and 40 mL of THF in a pressure tube equipped with a Teflon bushing as a pressure seal. The tube was quickly purged with N_2, sealed, and heated to 80 °C. After 6 h, the reaction was cooled to RT, and the catalyst was removed by refluxing the reaction mixture with activated charcoal at 80 °C for 3 h. After filtration, the volatiles were removed under reduced pressure to isolate the final product. In this way, **TES-PEO$_8$** (4.8 g, 71% yield) was obtained. ^{1}H NMR (δ, ppm): 0.59 (m, 2H, SiC*H*$_2$CH$_2$CH$_2$), 1.18 (m, 9H, SiOCH$_2$C*H*$_3$), 1.61 (m, 2H, SiCH$_2$C*H*$_2$CH$_2$), 3.34 (m, 3H, OC*H*$_3$), 3.40 (m, 2H, SiCH$_2$CH$_2$C*H*$_2$), 3.61 (m, 32H, OC*H*$_2$C*H*$_2$), 3.78 (m, 6H, SiOC*H*$_2$CH$_3$).

5.3.4.8 Synthesis of Siloxane Control (**TES-ODMS$_{13}$**)

Triethoxysilylethyl-oligodimethylsiloxane$_{13}$ (**TES-ODMS$_{13}$**) was prepared by the regioselective hydrosilylation of **ODMS$_{13}$** with **VTEOS** according to procedures previously reported [99]. **ODMS$_{13}$** (20.1 g, 20.0 mmol) and **VTEOS** (3.5 g, 20.0 mmol) were combined with Wilkinson's catalyst (10 mg) and 50 mL of toluene and heated to 80 °C under an atmosphere of N_2 and allowed to stir for 16 h. The product was purified by flash column chromatography on silica gel with hexanes/ethyl acetate (2:1 v/v), and volatiles were removed under reduced pressure. In this way, **TES-**

ODMS$_{13}$ (23.2 g, 90% yield) was obtained. ^{1}H NMR (δ, ppm): 0.001−0.17 (m, 78H, SiCH_3), 0.53 (m, 3H, SiCH_2CH_2), 1.05 (m, 1H, SiCH_2CH_2), 1.19 (m, 9H, SiOCH$_2$CH_3), 3.78 (m, 6H, SiOCH_2CH$_3$), 4.68 (m, 1H, Si*H*).

5.3.4.9 Proposed Synthesis of Zwitterion Control (**TMS-SB**)

Trimethoxysilylpropyl-sulfobetaine (**TMS-SB**) may be prepared by the ring-opening addition of propane sultone by aminoalkylsiloxane as previously reported [107].

5.4 Results and Discussion

5.*4.1 Synthesis of **TsO-PEO$_{11}$-A** Intermediate*

Tosylation of **HO-PEO$_{11}$-A** produced **TsO-PEO$_{11}$-A** in good yields (~61%). ^{1}H-NMR spectra confirmed the presence of tosyl peaks at ~7.3-7.9 ppm.

5.*4.2 Synthesis of **DMEA-PEO$_{11}$-A** Intermediate*

TsO-PEO$_{11}$-A was reacted with DMEA to produce **DMEA-PEO$_{11}$-A** with ~44% yield. The relatively low yield is attributed to product loss during filtration. ^{1}H-NMR spectra confirmed the presence of a dimethylamine peak at ~2.2 ppm.

5.*4.3 Synthesis of **A-PEO$_{11}$-SB** Intermediate*

DMEA-PEO$_{11}$-A was reacted with propane sultone to produce **A-PEO$_{11}$-SB** in good yields (~97%). ^{1}H-NMR spectra confirmed the presence of CH_2CH_2CH_2SO$_3^-$ peaks at ~4.0, ~2.2-2.3, and ~2.9 ppm, respectively.

5.4.4 Synthesis of ***TES-ODMS$_{13}$-PEO$_{11}$-SB***

A-PEO$_{11}$-SB was reacted with **TES-ODMS$_{13}$** to produce **TES-ODMS$_{13}$-PEO$_{11}$-SB** in good yields (~54%). Using IR analysis, reaction completion was confirmed by the absence of an absorbance peak at ~2125 cm^{-1} which signifies the disappearance of Si─H bonds. ^{1}H-NMR spectra further confirmed the absence of an Si─H peak (~4.7 ppm) as well as the lack of vinyl peaks (~5.1-5.3 and ~5.8-6.0 ppm) from unreacted **TES-ODMS$_{13}$** and **A-PEO$_{11}$-SB**, respectively.

5.4.5 Synthesis of *PEO$_8$*-Silane Amphiphile Control (***TES-ODMS$_{13}$-PEO$_8$***)

A-PEO$_8$-M was reacted with **TES-ODMS$_{13}$** to produce **TES-ODMS$_{13}$-PEO$_8$** in good yields (~88%). Using IR analysis, reaction completion was confirmed by the absence of an absorbance peak at ~2125 cm^{-1} which signifies the disappearance of Si─H bonds. ^{1}H-NMR spectra further confirmed the absence of an Si─H peak (~4.7 ppm) as well as the lack of vinyl peaks (~5.1-5.3 and ~5.8-6.0 ppm) from unreacted **TES-ODMS$_{13}$** and **A-PEO$_8$-M**, respectively.

5.4.6 Synthesis of PEO-Zwitterion Control (***TES-PEO$_{11}$-SB***)

A-PEO$_{11}$-SB was reacted with triethoxysilane to produce the **TES-PEO$_{11}$-SB** control in good yields (~92%). Using IR analysis, reaction completion was confirmed by the absence of an absorbance peak at ~2125 cm^{-1} which signifies the disappearance of Si─H bonds. ^{1}H-NMR spectra further confirmed the absence of an Si─H peak (~4.7

ppm) as well as the lack of vinyl peaks (~5.1-5.3 and ~5.8-6.0 ppm) from unreacted triethoxysilane and **A-PEO$_{11}$-SB**, respectively.

5.*4.7 Synthesis of PEO-Silane Control (**TES-PEO$_8$**)*

A-PEO$_8$-M was reacted with triethoxysilane to produce the **TES-PEO$_8$** control in good yields (~71%). Using IR analysis, reaction completion was confirmed by the absence of an absorbance peak at ~2125 cm^{-1} which signifies the disappearance of Si─H bonds. ^{1}H-NMR spectra further confirmed the absence of an Si─H peak (~4.7 ppm) as well as the lack of vinyl peaks (~5.1-5.3 and ~5.8-6.0 ppm) from unreacted triethoxysilane and **A-PEO$_8$-M**, respectively.

5.*4.8 Synthesis of Siloxane Control (**TES-ODMS$_{13}$**)*

ODMS$_{13}$ was reacted with **VTEOS** to produce **TES-ODMS$_{13}$** in good yields (~90%). ^{1}H-NMR spectra confirm a reduction in the Si─H peak integration value by one-half compared to the starting material.

5.*4.8 Proposed Synthesis of Zwitterion Control (**TMS-SB**)*

Propane sultone may be reacted with **DMA-TMS** to produce **TMS-SB**. This zwitterion control would be a useful addition to the series so as to compare the new zwitterionic PEO-silane amphiphile (**TES-ODMS$_{13}$-PEO$_{11}$-SB**) to a conventional zwitterion.

5.5 Conclusions

Towards the goal of achieving enhanced PEO hydration, a PEO-silane amphiphile was modified with a zwitterionic sulfobetaine end group (**TES-ODMS$_{13}$-PEO$_{11}$-SB**, **Figure 5.1**). A series of controls containing one or more features of **TES-ODMS$_{13}$-PEO$_{11}$-SB** were also prepared. In future work, this zwitterionic amphiphile and controls may be used to prepare surface-grafted coatings on a model substrate (e.g. silicon wafer) to evaluate surface hydrophilicity and protein resistance in the absence of surface restructuring. In addition, these may also be utilized to prepare bulk-modified coatings to evaluate water-driven surface-restructuring which may be measured by temporal contact angle analyses with water droplets. The protein resistance of these modified silicones could then be related to the specific structure of the PEO and corresponding ability to migrate to the surface-water interface as well as inherent protein resistance.

CHAPTER VI

CONCLUSIONS AND FUTURE DIRECTIONS

6.1 Conclusions

In these studies, a strategy was developed to effectively reduce biofouling onto silicones for the purpose of enhancing the performance of blood-contacting medical devices and marine coatings. Ultimately, these strategies could diminish the need for heparanization of patients as well as permit the replacement of toxic, ablative marine coatings. Towards this goal, a series of novel PEO-silane amphiphiles [α-$(EtO)_3$Si-$(CH_2)_2$-oligodimethylsiloxane$_m$-*block*-poly(ethylene oxide)$_8$-OCH_3] were prepared as additives for the simple bulk-modification of RTV silicones, both coatings and free-standing materials. Compositions were prepared with varying siloxane tether length (*m*) and optional inclusion of a zwitterionic PEO end group. Studies were designed to assess the impact of these structural features on the antifouling potential of corresponding bulk-modified silicones.

Chapter II described the preparation of silicones modified with varying amounts of a single PEO-silane amphiphile composition (m = 13). Films with ≥5 wt% of the PEO-silane amphiphile revealed substantial water-driven surface hydrophilicity which led to enhanced protein resistance versus the unmodified silicone. Thus, a minimal amount of the amphiphile effectively produced hydrophilic, protein resistant films.

In Chapter III, PEO-silane amphiphiles of varying siloxane tether lengths (m = 0, 4, 13, 17, 24, and 3) were prepared along with a PEO_8-silane control. Protein resistance

in the absence and presence of water-driven surface restructuring was assessed by surface-grafting of silanes to silicon wafer and by bulk-modifying silicone, respectively. When surface-grafted, the PEO control exhibited superior and ultra-low protein adsorption whereas protein adsorption increased with siloxane tether length for the PEO-silane amphiphiles. In contrast, protein adsorption on a silicone modified with the PEO control was similarly high versus unmodified silicone. PEO-silane amphiphiles exhibited an enhanced capacity to migrate to the surface-water interface to increase hydrophilicity and reduce protein adsorption. It was shown that an intermediate siloxane tether length (m = 13) was optimal. The distinctively different results of surface-grafted model substrates highlight their failure to effectively predict antifouling behavior of chains incorporated into polymer matrices such as silicones.

In Chapter IV, silicones bulk-modified with PEO-silane amphiphiles (m = 0, 4 and 13), previously evaluated for plasma protein resistance, were tested against marine bacteria and diatoms in lab assays as well as in a natural ocean environment. Surface restructuring to the surface-water interface was enhanced with increasing siloxane tether length. As observed for plasma protein tests, the PEO-silane amphiphile (m = 13) exhibited the greatest resistance to microfouling by bacteria and diatoms.

In Chapter V, the chemistry of a PEO-silane amphiphile was modified such that the methoxy PEO end group was replaced with a zwitterionic end group. In this way, the hydration of the PEO is expected to be enhanced due to the stronger binding of water to zwitterions, ultimately leading to decreased protein adsorption. This zwitterionic PEO-silane amphiphile may likewise be incorporated into silicones.

6.2 Future Directions

In future studies, new silane crosslinking chemistries will be explored (**Figure 6.1**). While a triethoxy group is useful for modification of acetoxy-cure silicones via condensation reaction, it will not crosslink with platinum-cure silicones, the other major type of silicone used for blood-contacting medical devices. This shortcoming limits the application potential for the PEO-silane amphiphiles. However, PEO-silane amphiphiles bearing vinyl end groups would effectively crosslink in platinum-cure silicone systems. In addition, methacrylate end groups would be useful for the modification of UV-curable silicones and other materials, including hydrogel contact lenses.

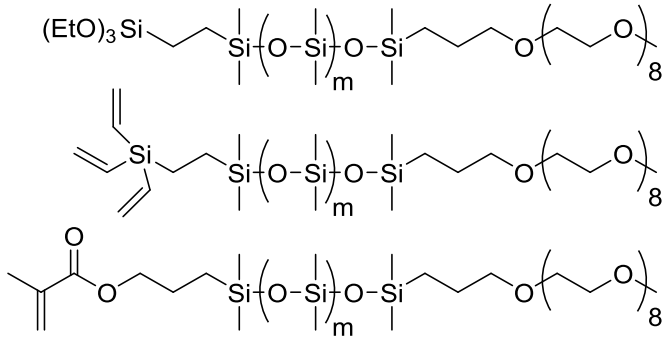

Figure 6.1. Modification of the PEO-silane amphiphile end-group to trivinyl silane and methacrylate would permit the modification of platinum-cure silicone systems and UV-cure materials, respectively.

A broader objective for future studies will explore the application of PEO-silane amphiphile-modified silicone coatings to actual medical devices. Of particular interest to our group are hemodialysis catheters. In order to screen the efficacy of the modified silicone coatings, coated catheter segments may be subjected to whole blood under static

and pulsatile flow (shear stress = 5 dynes/cm^2 for external surface; shear stress = 60 dynes/cm^2 for intraluminal surface) conditions with the use of a bioreactor (**Figure 6.2**). Thrombogenicity could be measured in terms of adherent platelet count via lactate dehydrogenase (LDH) assays, as well as surface-coverage, aggregation, and activation of platelets via scanning electron microscopy (SEM) imaging. The results of catheter segments coated with PEO-silane amphiphile-modified silicones could be compared to those of unmodified as well as heparin-coated catheters currently on the market (e.g. Decathlon Gold®).

Figure 6.2. Thrombogenicity testing of catheter sections in a bioreactor under flow.

To advance their potential as marine coatings, studies of PEO-modified silicone coatings could include efforts to improve their adhesion to common marine structure materials (e.g. fiberglass, steel, and aluminum). Initial lab assay and ocean tests did not employ a tie coat for enhanced adhesion and, in only some cases, an epoxy primer was used to prepare the surface. While delamination was not a major issue, superior adhesion could be important in some situations. Improved adhesion may be accomplished by the use of silane coupling agents, different primers, and/or physical treatment of surfaces

(e.g. sandblasting). Adhesion could be tested with shear or peel testing. Additionally, the mechanical properties (e.g. tensile strength and abrasion resistance) of the coatings will be examined and compared to those of commercial marine coatings (e.g. Intersleek® 700 or 900) with the goal of enhancing coating robustness for longer lifetime of use. Additional lab assays and field tests could confirm the efficacy of these coatings against a broad spectrum of biofoulers. Ultimately, "commercial-ready" versions of these coatings will best be prepared by partnering with a coatings company. Preliminary tests on coated marine structures such as ship hulls and buoys would be essential prior to commercialization. This endeavor is expected to be successful due to the coatings' desirable characteristics including non-toxicity, simplicity, low cost, and superior effectiveness.

REFERENCES

1. Norde W. Driving forces for protein adsorption at solid surfaces. Macromol Symp 1996;103:5.

2. Lassen B, Malmsten M. Competitive protein adsorption at plasma polymer surfaces. J Colloid Interf Sci 1997;186:9.

3. Vroman L, Adams AL. Findings with the recording ellipsometer suggesting rapid exchange of specific plasma proteins at liquid/solid interfaces. Surf Sci 1969;16:438.

4. Savage B, Saldívar E, Ruggeri ZM. Initiation of platelet adhesion by arrest onto fibrinogen or tanslocation on von Willebrand factor. Cell 1996;84:289.

5. Horbett TA. Principles underlying the role of adsorbed plasma proteins in blood interactions with foreign materials. Cardiovasc Pathol 1993;2:137.

6. Gorbet MB, Sefton MV. Biomaterial-associated thrombosis: roles of coagulation factors, complement, platelets and leukocytes. Biomaterials 2004;25:5681.

7. Bartzoka V, McDermott MR, Brook MA. Protein-silicone interactions. Adv Mater 1999;11:257.

8. Hron P. Hydrophilisation of silicone rubber for medical applications. Polym Int 2003;52:1531.

9. Pitt WG, Park K, Cooper SL. Sequential protein adsorption and thrombus deposition on polymeric biomaterials. J Colloid Interf Sci 1986;111:343.

10. Sharma CP. Blood-compatible materials: a perspective. J Biomater Appl 2001;15:359.

11. Curtis J, Colas A. In Biomaterials Science: An Introduction to Materials in Medicine, 2nd ed. Ratner BD, Hoffman AS, Schoen FJ, Lemons JE, Eds. Elsevier Academic Press: San Diego, CA, 2004, p 697.

12. VanDyke ME, Clarson SJ, Arshady R. In An Introduction to Polymeric Biomaterials Arshady R, Ed. Citrus Books: London, 2003, Vol. 1, p 109.

13. El-Zaim HS, Heggers JP. In Polymeric Biomaterials, 2nd ed. Dumitriu S, Ed. Marcel Dekker, Inc.: New York, NY, 2002, p 79.

14. Jeon SI, Andrade JD. Protein-surface interactions in the presence of polyethylene oxide: II. Effect of protein size. J Colloid Interf Sci 1991;142:159.

15. Jeon SI, Lee JH, Andrade JD, DeGennes PG. Protein-surface interactions in the presence of polyethylene oxide: I. Simplified theory. J Colloid Interf Sci 1991;142:149.

16. Anderson JM, Ziats NP, Azeez A, Brunstedt MR, Stack S, Bonfield TL. Protein adsorption and macrophage activation on poly(dimethyl siloxane) and silicone rubber. J Biomater Sci Polym Ed 1995;7:159.

17. Coelho G, Sequeira H, Rios L, Azevedo L, Zenha H, Cardoso A, Costa H. Revascularization of the hand by intra-arterial injection of heparin. Eur J Plast Surg 2012;35:195.

18. Krauel K, Hackbarth C, Fürll B, Greinacher A. Heparin-induced thrombocytopenia: in vitro studies on the interaction of dabigatran, rivaroxabana, and low-sulfated heparin, with platelet factor 4 and anti-PF_4/heparin antibodies. Blood 2012;119:1248.

19. Linhardt RJ. Claude S. Hudson award address in carbohydrate chemistry. Heparin: structure and activity. J Med Chem 2003;46:2551.

20. Ni X, Castanares M, Mukherjee A, Lupold SE. Nucleic acid aptamers: clinical applications and promising new horizons. Curr Med Chem 2011;18:4206.

21. Ginsberg RJ, Kearon C, Ginsberg J, Hirsh J. Critical Decisions in Thrombosis and Hemostasis PMPH USA, 1998.

22. Hietala E-M, Maasilta P, Välimaa T, Harjula ALJ, Törmälä P, Salminen U-S, Lassila R. Platelet responses and coagulation activation on polylactide and heparin-polycaprolactone-L-lactide -coated polylactide stent struts. J Biomed Mater Res 2003;67A:785.

23. Niimi Y, Ichinose F, Ishiguro Y, Terui K, Uezono S, Morita S, Yamane S. The effects of heparin coating of oxygenator fibers on platelet adhesion and protein adsorption. Anesth Analg 1999;89:573.

24. Gombotz WR, Guanghui W, Horbett TA, Hoffman AS. Protein adsorption to poly(ethylene oxide) surfaces. J Biomed Mater Res 1991;25:1547.

25. Lee JH, Lee HB, Andrade JD. Blood compatibility of polyethylene oxide surfaces. Prog Polym Sci 1995;20:1043.

26. Elbert DL, Hubbell JA. Surface treatments of polymers for biocompatibility. Annu Rev Mater Sci 1996;26:365.

27. Knoll D, Hermans J. Polymer-protein interactions. Comparison of experiment and excluded volume theory. J Biol Chem 1983;258:5710.

28. Oesterberg E, Bergstroem K, Holmberg K, Riggs JA, VanAlstine JM, Schuman TP, Burns NL, Harris JM. Comparison of polysaccharide and poly(ethylene glycol) coatings for reduction of protein adsorption on polystyrene surfaces. Colloid Surface A 1993;77:159.

29. Prime KL, Whitesides GM. Adsorption of proteins onto surfaces containing end-attached oligo(ethylene oxide): a model system using self-assembled monolayers. J Am Chem Soc 1993;115:10714.

30. Pale-Grosdemange C, Simon ES, Prime KL, Whitesides GM. Formation of self-assembled monolayers of chemisorption of derivatives of oligo(ethylene glycol) of structure $HS(CH_2)_{11}(OCH_2CH_2)_mOH$ on gold. J Am Chem Soc 1991;113:12.

31. Yuang Y-W, Gupta VK. Influence of polymer flux and chain length on adsorption of poly(ethylene oxide) on physically heterogeneous surfaces. Langmuir 2002;18:2280.

32. Ruiz-Taylor LA, Martin TL, Zaugg FG, Witte K, Indermuhle P, Nock S, Wagner P. Monolayers of derivatized poly(L-lysine)-grafted poly(ethylene glycol) on metal oxides as a class of biomolecular interfaces. Proc Natl Acad Sci U S A 2001;3:852.

33. Desai NP, Hubbell JA. Solution technique to incorporate polyethylene oxide and other water-soluble polymers into surfaces of polymeric biomaterials. Biomaterials 1991;12:144.

34. Desai NP, Hubbell JA. Surface physical interpenetrating networks of poly(ethylene terephthalate) and poly(ethylene oxide) with biomedical applications. Macromolecules 1992;25:226.

35. Ikada Y. Surface modification of polymers for medical applications. Biomaterials 1994;15:725.

36. Gombotz WR, Gunaghiu W, Hoffman AS. Immobilization of poly(ethylene oxide on poly(ethylene terephthalate) using a plasma polymerization process. J Appl Polym Sci 1989;37:91.

37. Sofia SJ, Premnath V, Merrill EW. Poly(ethylene oxide) grafted to silicon surfaces: grafting density and protein adsorption. Macromolecules 1998;31:5059.

38. Malmsten M, Emoto K, Alstine JMV. Effect of chain density on inhibition of protein adsorption by poly(ethylene glycol) based coatings. J Colloid Interf Sci 1998;202:507.

39. Murthy R, Shell CE, Grunlan MA. The influence of poly(ethylene oxide) grafting via siloxane tethers on protein adsorption. Biomaterials 2009;30:2433.

40. Delamarche E, Donzel C, Kamounah FS, Wolf H, Geissler M, Stutz R, Schmidt-Winkel P, Michel B, Mathieu HJ, Schaumburg K. Microcontact printing using poly(dimethylsiloxane) stamps hydrophilized by poly(ethylene oxide) silanes. Langmuir 2003;19:8749.

41. Sui G, Wang J, Lee C-C, Lu W, Lee SP, Leyton JV, Wu AM, Tseng H-R. Solution-phase surface modification in intact poly(dimethylsiloxane) microfluidic channels. Anal Chem 2006;78:5543.

42. Papra A, Bernard A, Juncker D, Larsen NB, Michel B, Delamarche E. Microfluidic networks made of poly(dimethylsiloxane), Si, and Au coated with polyethylene glycol for patterning proteins onto surfaces. Langmuir 2001;17:4090.

43. Chen H, Zhang Z, Chen Y, Brook MA, Sheardown H. Protein repellant silicone surfaces by covalent immobilization of poly(ethylene oxide). Biomaterials 2005;26:2391.

44. Kato K, Uchida E, Kang E-T, Uyama Y, Ikada Y. Polymer surfaces with graft chains. Prog Polym Sci 2003;28:209.

45. Bhattacharya A, Misra BN. Grafting: a versatile means to modify polymers. Techniques, factors, and applications. Prog Polym Sci 2004;29:767.

46. Uyama Y, Kato K, Ikada Y. Surface modification of polymers by grafting. Adv Polym Sci 1998;137:3.

47. Chen H, Brook MA, Chen Y, Sheardown H. Surface properties of PEO-silicone composites: reducing protein adsorption. J Biomater Sci Polym Ed 2005;16:531.

48. Chen H, Brook MA, Sheardown H. Silicone elastomers for reduced protein adsorption. Biomaterials 2004;25:2273.

49. Chen S, Zheng J, Li L, Jiang S. Strong resistance of phosphorylcholine self-assembled monolayers to protein adsorption: insights into nonfouling properties of zwitterionic materials. J Am Chem Soc 2005;127:14473.

50. Cao Z, Jiang S. Super-hydrophilic zwitterionic poly(carboxybetaine) and amphiphilic non-ionic poly(ethylene glycol) for stealth nanoparticles. Nano Today 2012;7:404.

51. Harder P, Grunze M, Dahint R, Whitesides GM, Laibinis PE. Molecular conformation in oligo(ethylene glycol)-terminated self-assembled monolayers on gold and silver surfaces determines their ability to resist protein adsorption. J Phys Chem B 1998;201:426.

52. Zheng J, Li L, Chen S, Jiang S. Molecular simulation study of water interactions with oligo(ethylene glycol)-terminated alkanethiol self-assembled monolayers. Langmuir 2004;20:8931.

53. Li L, Chen S, Zheng J, Ratner BD, Jiang S. Protein adsorption on oligo(ethylene glycol)-terminated alkanethiolate self-assembled monolayers: the molecular basis for nonfouling behavior. J Phys Chem B 2005;109:2934.

54. He Y, Hower J, Chen S, Bernards MT, Chang Y, Jiang S. Molecular simulation studies of protein interactions with zwitterionic phosphorylcholine self-assembled monolayers in the presence of water. Langmuir 2008;24:10358.

55. Jiang S, Cao Z. Ultralow-fouling, functionalizable, and hydrolyzable zwitterionic materials and their derivatives for biological applications. Adv Mater 2010;22:920.

56. Cao Z, Brault N, Xue H, Keefe A, Jiang S. Manipulating sticky and non-sticky properties in a single material. Angew Chem Int Edit 2011;50:6102.

57. Feng W, Gao X, McClung G, Zhu S, Ishihara K, Brash JL. Methacrylate polymer layers bearing poly(ethylene oxide) and phosphorylcholine side chains as non-fouling surfaces: *in vitro* interactions with plasma proteins and platelets. Acta Biomater 2011;7:3692.

58. Tanaka M, Sawaguchi T, Sato Y, Yoshioka K, Niwa O. Synthesis of phosphorylcholine-oligoethylene glycol-alkane thiols and their suppressive effect on non-specific adsorption of proteins. Tetrahedron Lett 2009;50:4092.

59. Yoshimoto K, Hirase T, Madsen J, Armes SP, Nagasaki Y. Non-fouling character of poly[2-(methacryloyloxy)ethyl phosphorylcholine]-modified gold surfaces fabricated by the 'grafting to' method: comparison of its protein

resistance with poly(ethylene glycol)-modified gold surfaces. Macromol Rapid Comm 2009;30:2136.

60. Zhang Z, Chen S, Chang Y, Jiang S. Surface grafted sulfobetaine polymers via atom transfer radical polymerization as superlow fouling coatings. J Phys Chem B 2006;110:10799.

61. Zhang Z, Chen S, Jiang S. Dual-functional biomimetic materials: nonfouling poly(carboxybetaine) with active functional groups for protein immobilization. Biomacromolecules 2006;7:3311.

62. Zhang Z, Vaisocherová H, Cheng G, Yang W, Xue H, Jiang S. Nonfouling behavior of polycarboxybetaine-grafted surfaces: structural and environmental effects. Biomacromolecules 2008;9:2686.

63. Zhou J, Yuan J, Zang X, Shen J, Lin S. Platelet adhesion and protein adsorption on silicone rubber surface by ozone-induced grafted polymerization with carboxybetaine monomer. Colloid Surface B 2005;41:55.

64. Yuan Y, Zang X, Ai F, Zhou J, Shen J, Lin S. Grafting sulfobetaine monomer onto silicone surface to improve haemocompatibility. Polym Int 2004;53:121.

65. Yeh S-B, Chen C-S, Chen W-Y, Huang C-J. Modification of silicone elastomer with zwitterionic silane for durable antifouling properties. Langmuir 2014;

66. Keefe AJ, Brault ND, Jiang S. Suppressing surface reconstruction of superhydrophobic PDMS using a superhydrophilic zwitterionic polymer. Biomacromolecules 2012;13:1683.

67. Callow ME, Callow JA. Marine biofouling: a sticky problem. Biologist 2002;49:1.

68. Edyvean R. In Biofouling Dürr S, Thomason J, Eds. Wiley-Blackwell: West Sussex, United Kingdom, 2010, p 218.

69. Pradier CM, Bertrand P, Bellon-Fontaine MN, Compere C, Costa D, Marcus P, Poleunis C, Rondot B, Walls MG. Adsorption of proteins on an AISI 316 stainless-steel surface in natural seawater. Surf Interface Anal 2000;30:45.

70. Compere C, Bellon-Fontaine M-N, Bertrand P, Costa D, Marcus P, Poleunis C, Pradier C-M, Rondot B, Walls MG. Kinetics of conditioning layer formation on stainless steel immersed in seawater. Biofouling 2001;17:129.

71. Dang H, Lovell RC. Bacterial primary colonization and early succession on surfaces in marine waters as determined by amplified rRNA gene restriction analysis and sequence analysis of 16S rRNA genes. Appl Environ Microbiol 2000;66:467.

72. Grasland B, Mitalane J, Briandet R, Quemener E, Meylheuc T, Linossier I, Vallee-Rehel K, Haras D. Bacterial biofilm in seawater: cell surface properties of early-attached marine bacteria. Biofouling 2003;19:307.

73. Molino PJ, Wetherbee R. The biology of biofouling diatoms and their role in the development of microbial slimes. Biofouling 2008;24:365.

74. Finlay JA, Callow ME, Ista LK, Lopez GP, Callow JA. The influence of surface wettability on the adhesion strength of settled spores of the gree alga *Enteromorpha* and the diatom *Amphora*. Integr Comp Biol 2002;42:1119.

75. Finlay JA, Bennett SM, Brewer LH, Sokolova A, Clay G, Gunari N, Meyer AE, Walker GC, Wendt DE, Callow ME, Callow JA, Detty MR. Barnacle settlement and the adhesion of protein and diatom microfouling to xerogel films with varying surface energy and water wettability. Biofouling 2010;26:657.

76. Yebra DM, Kiil S, Dam-Johansen K. Anti-fouling technology - past, present and future steps towards efficient and environmentally friendly antifouling coatings. Prog Org Coatings 2004;50:75.

77. Chambers LD, Stokes KR, Walsh FC, Wood RJK. Modern approaches to marine antifouling coatings. Surf Coat Tech 2006;201:3642.

78. Lejars M, Marigaillan A, Bressy C. Foul release coatings: A nontoxic alternative to biocidal antifouling coatings. Chemical Rev 2012;112:4347.

79. Swain GW, Schultz MP. The testing and evaluation of non-toxic antifouling coatings. Biofouling 1996;10:187.

80. Kavanagh CJ, Quinn RD, Swain GW. Observations of barnacle detachment from silicones using high-speed video. J Adhes 2005;81:843.

81. Finnie AA, Williams DN. In Biofouling Dürr S, Thomason J, Eds. Wiley-Blackwell: West Sussex, United Kingdom, 2010, p 194.

82. Webster DC, Chisholm BJ. In Biofouling Dürr S, Thomason J, Eds. Wiley-Blackwell: West Sussex, United Kingdom, 2010, p 371.

83. Liu X, Li H. Effect of diatomite/polyethylene glycol binary processing aid on the melt fracture and the rheology of polyethylenes. Polym Eng Sci 2005;45:898.

84. Hori H, Yamamoto A, Hayakawa E, Taniyasu S, Yamashita N, Kutsuna S. Efficient decomposition of environmentally persistent perfluorocarboxylic acids by use of persulfate as a photochemical oxidant. Environ Sci Technol 2005;39:2383.

85. Ellis DA, Mabury SA, Martin JW, Muir DCG. Thermolysis of fluoropolymers as a potential source of halogenated organic acids in the environment. Nature 2001;412:321.

86. Brady RF. Foul-release coatings for warships. Def Sci J 2005;55:75.

87. Krishnan S. In Polymer adhesion, friction, and lubrication Zeng H, Ed. Wiley: New Jersey and Canada, 2013, p 266.

88. Krishnan S, Weinman CJ, Ober CK. Advances in polymers for anti-biofouling surfaces. J Mater Chem 2008;18:3405.

89. Ltd IC. Drag resistance and foul-release coatings: the influence of slime. Propeller 2001;12:8.

90. Youngblood JP, Andruzzi L, Ober CK, Hexemer A, Kramer EJ, Callow JA, Finlay JA, Callow ME. Coating based on side-chain ether-linked poly(ethylene glycol) and fluorocarbon polymer for the control of marine biofouling. Biofouling 2003;19:91.

91. Krishnan S, Wang N, Ober C, Finlay J, Callow M, Callow J, Fischer D. Anti-biofouling properties of comb-like block copolymers with amphiphilic side chains. Langmuir 2006;22:5075.

92. Martinelli E, Agostini S, Galli G, Chiellini E, Glisenti A, Pettitt M, Callow M, Callow J, Graf K, Bartels F. Nanostructured films of amphiphilic fluorinated block copolymers for fouling release application. Langmuir 2008;24:13138.

93. Martinelli E, Sarvothaman MK, Galli G, Pettitt ME, Callow ME, Callow JA, Conan SL, Clare AS, Sugiharto AB, Davies C, Williams D. Poly(dimethyl siloxane) (PDMS) network blends of amphiphilic acrylic copolymers with poly(ethylene glycol)-fluoroalkyl side chains for fouling-release coatings. II. Laboratory assays and field immersion trials. Biofouling 2012;28:571.

94. Park D, Weinman C, Finlay J, Fletcher B, Paik M, Sundaram H, Dimitriou M, Sohn K, Callow M, Callow J. Amphiphilic surface active triblock copolymers

with mixed hydrophobic and hydrophilic side chains for tuned marine fouling-release properties. Langmuir 2010;26:9772.

95. Sundaram HA, Cho Y, Dimitriou MD, Weinman CJ, Finlay JA, Cone G, Callow ME, Callow JA, Kramer EJ, Ober CK. Fluorine-free mixed amphiphilic polymers based on PDMS and PEG side chains for fouling release applications. Biofouling 2011;27:589.

96. Weinman CJ, Finlay JA, Park D, Paik MY, Krishnan S, Sundaram HS, Dimitriou M, Sohn KE, Callow ME, Callow JA, Handlin DL, Willis CL, Kramer EJ, Ober CK. ABC triblock surface active block copolymer with grafted ethoxylated fluoroalkyl amphiphilic side chains for marine antifouling/fouling-release applications. Langmuir 2009;25:12266.

97. Gudipati CS, Finlay JA, Callow JA, Callow ME, Wooley KL. The antifouling and fouling-release performance of hyperbranched fluoropolymer (HBFP)-poly(ethylene glycol) (PEG) composite coatings evaluated by adsorption of biomacromolecules and the green fouling alga *Ulva*. Langmuir 2005;21:3044.

98. Dimitriou MD, Zhou Z, Yoo H-S, Killops KL, Finlay JA, Cone G, Sundaram HS, Lynd NA, Barteau KP, Campos LM, Fischer DA, Callow ME, Callow JA, Ober CK, Hawker CJ, Kramer EJ. A general approach to controlling the surface composition of poly(ethylene oxide)-based block copolymers for antifouling coatings. Langmuir 2011;27:13762.

99. Murthy R, Cox CD, Hahn MS, Grunlan MA. Protein-resistant silicones: incorporation of poly(ethylene oxide) via siloxane tethers. Biomacromolecules 2007;8:3244.

100. Lee S-W, Laibinis PE. Protein-resistant coatings for glass and metal oxide surfaces derived from oligo(ethylene glycol)-terminated alkyltrichlorosilanes. Biomaterials 1998;19:1669.

101. Zhang M, Ferrari M. Hemocompatible polyethylene glycol films on silicon. Biomed Microdevices 1998;1:81.

102. Feldman K, Hähner G, Spencer ND, Harder P, Grunze M. Probing resistance to protein adsorption of oligo(ethylene glycol)-terminated self-assembled monolayers by scanning force microscopy. J Amer Chem Soc 1999;121:10134.

103. Jo S, Park K. Surface modification using silanated poly(ethylene glycol)s. Biomaterials 2000;21:605.

104. Du YJ, Klement P, Berry LR, Tressel P, Chan AKC. *In vivo* rabbit acute model tests of polyurethane catheters coated with a novel antithrombin-heparin covalent complex. Thromb Haemost 2005;94:366.

105. Park K, Shim HS, Dewanjee MK, Eigler NL. In vitro and in vivo studies of PEO-grafted blood-contacting cardiovascular prostheses. J Biomater Sci Polym Ed 2000;11:1121.

106. Yasuda H, Sharma AK. Effect of orientation and mobility of polymer molecules at surfaces on contact angle and its hysteresis. J Polym Sci Part B: Polym Phys 1981;19:1285.

107. Estephan ZG, Jaber JA, Schlenoff JB. Zwitterion-stabilized silica nanoparticles: toward nonstick nano. Langmuir 2010;26:16884.

108. Niimi Y, Ichinose F, Ishiguro Y, Terui K, Uezono S, Morita S, Yamana S. The effects of heparin coating of oxygenator fibers on platelet adhesion and protein adsorption. Anesth Analg 1999;89:573.

109. Gudipati CS, Greenlief CM, Johnson JA, Prayongpan P, Wooley KL. Hyperbranched fluoropolymer and linear poly(ethylene glycol) based amphiphilic crosslinked networks as efficient antifouling coatings: An insight into the surface compositions, topographies, and morphologies. J Polym Sci Pol Chem 2004;42:6193.

110. Uilk J, Johnston EE, Bullock S, Wynne KJ. Surface characterization, microstructure, and wetting of networks from a,w-dihydroxy(polydimethylsiloxane) and 1,1,2,2-tetrahydrtridecafluoro octyltriethoxysilane. Macromol Chem Physic 2002;203:1506.

111. Uchida K, Otsuka H, Kaneko M, Kataoka K, Nagasaki Y. A rective poly(ethylene glycol) layer to achieve specific surface plasmon resonance sensing with a high S/N ratio: the substantial role of a short underbrushed PEG layer in minimizing nonspecific adsorption. Anal Chem 2005;77:1075.

112. Singh N, Cui X, Boland T, Husson SM. The role of independently variable grafting density and layer thickness of polymer nanolayers on peptide adsorption and cell adhesion. Biomaterials 2007;28:763.

113. Abbasi F, Mirzadeh H, Katbab A-A. Modification of polysiloxane polymers for biomedical applications: a review. Polym Int 2001;50:1279.

114. Bodas D, Khan-Malek C. Formation of more stable hydrophilic surfaces of PDMS by plasma and chemical treatments. Microelectron Eng 2006;83:1277.

115. Yao K, Huang X-D, Huang X-J, Xu Z-K. Improvement of the surface biocompatibility of silicone intraocular lens by the plasma-induced tethering of phospholipid moieties. J Biomed Mater Res, Part A 2006;78A:684.

116. Zhang H, Annich GM, Miskulin J, Osterholzer K, Merz SI, Bartlett RH, Meyerhoff ME. Nitric oxide releasing silicone rubbers with improved blood compatibility: preparation, characterization, and in vivo evaluation. Biomaterials 2002;23:1485.

117. Murthy R, Bailey BM, Valentin-Rodriguez C, Ivanisevic A, Grunlan MA. Amphiphilic silicones prepared from branched PEO-silanes with siloxane tethers. J Polym Sci Part A: Polym Chem 2010;48:4108.

118. Brook MA. Silicon in Organic, Organometallic, and Polymer Chemistry John Wiley & Sons, Inc.: New York, 2000.

119. Owen MJ, Smith PJ. Plasma treatment of polydimethylsiloxanes. J Adhes Sci Technol 1994;8:1063.

120. Lane TH, Burns SA. In Immunology of silicones Potter M, Rose NR, Eds. Springer: Berlin, 1996.

121. Mark JE. In Silicon-based polymer science: a comprehensive resource. Advances in chemistry series Zeigler JM, Fearon FWG, Eds. American Chemical Society: Washington, D. C., 1990, Vol. 224.

122. Dvornic PR. In Silicon-Containing Polymers: The Science and Technology of Their Synthesis and Applications Jones RG, Ando W, Chojnowski J, Eds. Kluwer Academic Publishers: Dordrecht, The Netherlands, 2000, p 200.

123. Sperling LH. In Introduction to Physical Polymer Science, 3 ed. John Wiley & Sons: New York, 2001, p 308.

124. Menard KP. In Dynamic Mechanical Analysis: A Practical Introduction CRC Press: Boca Raton, FL, 1999, p 95.

125. Roach P, Farrar D, Perry CC. Interpretation of protein adsorption: surface-induced conformational changes. J Am Chem Soc 2005;127:8168.

126. Taylor M, Urquhart AJ, Anderson DG, Williams PM, Langer R, Alexander MR, Davies MC. A methodology for investigating protein adhesion and adsorption to microarrayed combinatorial polymers. Macromol Rapid Commun 2008;29:1298.

127. Fukai R, Dakwa PHR, Chen W. Strategies toward biocompatible artificial implants: grafting of functionalized poly(ethylene glycol)s to poly(ethylene terephthalate) surfaces. J Polym Sci Pol Chem 2004;42:5389.

128. Fujimoto K, Tadokoro H, Ueda Y, Ikada Y. Polyurethane surface modification by graft polymerization of acrylamide for reduced protein adsorption and platelet adhesion. Biomaterials 1993;14:442.

129. Alauzun JG, Young S, D'Souza R, Liu L, Brook MA, Sheardown HD. Biocompatible, hyaluronic acid modified silicone elastomers. Biomaterials 2010;31:3471.

130. Chen H, Song W, Zhou F, Wu Z, Huang H, Zhang J, Lin Q, Yang B. The effect of surface microtopography of poly(dimethylsiloxane) on protein adsorption, platelet and cell adhesion. Colloid Surface B 2009;71:275.

131. Lin FYH, Policova Z, Yueh HK, Moy E, Neumann AW. Application of freezing front technique and axisymmetric drop shape analysis-profile for the determination of surface tensions of adsorbed proteins. Colloids Surf B Biointerfaces 1993;1:23.

132. Absolom DR, Zingg W, Neumann AW. Protein adsorption to polymer particles: Role of surface properties. J Biomed Mater Res 1987;21:161.

133. El-Zaim HS, Heggers JP. In Polymeric Biomaterials, 2nd Edition Dumitriu S, Ed. Marcel Dekker, Inc.: New York, NY, 2002, p 79.

134. Bartzoka V, McDermott MR, Brook MA. Protein-silicone interactions. Adv. Mater. 1999;11:257.

135. Hron P. Hydrophilisation of silicone rubber for medical applications. Polym. Int. 2003;52:1531.

136. Kenausis GL, Voros J, Elbert DL, Huang N, Hofer R, Ruiz-Taylor L, Textor M, Hubbell JA, Spencer ND. Poly(L-lysine)-*g*-poly(ethylene glycol) layers on metal oxide surfaces: attachment mechanism and effects of polymer architecture on resistance to protein adsorption. J Phys Chem B 2000;104:3298.

137. Sharma CP. Blood-compatible materials: a perspective. J. Biomater. Appl. 2001;15:359.

138. Abbasi F, Mirzadeh H, Katbab A-A. Modification of polysiloxane polymers for biomedical applications: a review. Polym. Int. 2001;50:1279.

139. Bodas D, Khan-Malek C. Formation of more stable hydrophilic surfaces of PDMS by plasma and chemical treatments. Microelectron. Eng. 2006;83:1277.

140. Yao K, Huang X-D, Huang X-J, Xu Z-K. Improvement of the surface biocompatibility of silicone intraocular lens by the plasma-induced tethering of phospholipid moieties. J. Biomed. Mater. Res., Part A 2006;78A:684.

141. Gombotz WR, Guanghui W, Horbett TA, Hoffman AS. Protein adsorption to poly(ethylene oxide) surfaces. J Biomed Mater Res 1991;25:1547.

142. Lee JH, Lee HB, Andrade JD. Blood compatibility of polyethylene oxide surfaces. Prog Polym Sci 1995;20:1043.

143. Elbert DL, Hubbell JA. Surface treatments of polymers for biocompatibility. Annu. Rev. Mater. Sci. 1996;26:365.

144. Knoll D, Hermans J. Polymer-protein interactions. Comparison of experiment and excluded volume theory. J. Biol. Chem. 1983;258:5710.

145. Harris JM. Poly(ethylene glycol) chemistry: biotechnical and biomedical applications. Plenum Press: New York, 1992.

146. Browning MB, Cereceres SN, Luong PT, Cosgriff-Hernandez EM. Determination of the *in vivo* degradation mechanism of PEGDA hydrogels. J Biomed Mater Res A 2014.

147. Prime KL, Whitesides GM. Adsorption of proteins onto surfaces containing end-attached oligo(ethylene oxide): a model system using self-assembled monolayers. J. Am. Chem. Soc. 1993;115:10714.

148. Pale-Grosdemange C, Simon ES, Prime KL, Whitesides GM. Formation of self-assembled monolayers by chemisorption of derivatives of oligo(ethylene glycol) of structure HS(CH2)11(OCH2CH2)mOH on gold. J. Am. Chem. Soc. 1991;113:12.

149. Zhang M, Desai T, Ferrari M. Proteins and cells on PEG immobilized silicon surfaces. Biomaterials 1998;19:953.

150. Papra A, Gadegaard N, Larsen NB. Characterization of ultrathin poly(ethylene glycol) monolayers on silicon substrates. Langmuir 2001;17:1457.

151. Malmsten M, Emoto K, Alstine JMV. Effect of chain density on inhibition of protein adsorption by poly(ethylene glycol) based coatings. J Colloid Interf Sci 1998;202:507.

152. Sofia SJ, Premnath V, Merrill EW. Poly(ethylene oxide) grafted to silicon surfaces: grafting density and protein adsorption. Macromolecules 1998;31:5059.

153. Yasuda H, Sharma AK, Yasuda T. Effect of orientation and mobility of polymer molecules at surfaces on contact angle and its hysteresis. J Polym Sci Pol Phys 1981;19:1285.

154. Owen MJ, Smith PJ. Plasma treatment of polydimethylsiloxane. J Adhes Sci Technol 1994;8:1063.

155. Owen MJ. In Silicon-based polymer science: a comprehensive resource Zeigler JM, Fearon FWG, Eds. American Chemical Society: Washington, D.C., 1990, p 705.

156. Owen MJ. In Siloxane Polymers Clarson SJ, Semlyen JA, Eds. Prentice Hall: Englewood Cliffs, 1993, p 309.

157. Chen H, Brook MA, Chen Y, Sheardown H. Surface properties of PEO-silicone composites: reducing protein adsorption. J Biomater Sci Polym Ed 2005;16:531.

158. Thompson DB, Fawcett AS, Brook MA. In Silicon Based Polymers Ganachaud F, Boileau S, Boury B, Eds. Springer: 2008, p 29.

159. Sui G, Wang J, Lee C-C, Lu W, Lee SP, Leyton JV, Wu AM, Tseng H-R. Solution-phase surface modification in intact poly(dimethylsiloxane) microfluidic channels. Anal. Chem. 2006;78:5543.

160. Delamarche E, Donzel C, Kamounah FS, Wolf H, Geissler M, Stutz R, Schmidt-Winkel P, Michel B, Mathieu HJ, Schaumburg K. Microcontact printing using poly(dimethylsiloxane) stamps hydrophilized by poly(ethylene oxide) silanes. Langmuir 2003;19:8749.

161. Uilk J, Johnston EE, Bullock S, Wynne KJ. Surface characterization, microstructure, and wetting of networks from a,w-dihydroxy(polydimethylsiloxane) and 1,1,2,2-tetrahydrtridecafluoro octyltriethoxysilane. Macromol. Chem. Physic. 2002;203:1506.

162. Gudipati CS, Greenlief CM, Johnson JA, Prayongpan P, Wooley KL. Hyperbranched fluoropolymer and linear poly(ethylene glycol) based amphiphilic crosslinked networks as efficient antifouling coatings: An insight into the surface compositions, topographies, and morphologies. J. Polym. Sci. Pol. Chem. 2004;42:6193.

163. Hawkins ML, Fäy F, Réhel K, Linossier I, Grunlan MA. Bacteria and diatom resistance of silicones modified with PEO-silane amphiphiles. Biofouling 2014;30:247.

164. Grunlan MA, Mabry JM, Weber WP. Synthesis of fluorinated copoly(carbosiloxane)s by Pt-catalyzed hydrosilylation copolymerization. Polymer 2003;44:981.

165. Kohli P, Blanchard GJ. Applying polymer chemistry to interfaces: layer-by-layer and spontaneous growth of covalently bound multilayers. Langmuir 2000;16:4655.

166. Fang SJ, Chen W, Yamanaka T, Helms CR. Influence of interface roughness on silicon oxide thickness measured by ellipsometry. J. Electrochem. Soc. 1997;144:L231.

167. Guhathakurta S, Subramanian A. Effect of hydrofluoric acid in oxidizing acid mixtures on the hydroxylation of silicon surface. J Electrochem Soc 2007;154:P136.

168. Unsworth LD, Tun Z, Sheardown H, Brash JL. Chemisorption of thiolated poly(ethylene oxide) to gold: surface chain densities measured by ellipsometry and neutron reflectometry. J Colloid Interf Sci 2005;281:112.

169. Murthy R, Bailey BM, Valentin-Rodriguez C, Ivanisevic A, Grunlan MA. Amphiphilic silicones prepared from branched PEO-silanes with siloxane tethers. J. Polym. Sci. Part A: Polym. Chem. 2010;48:4108.

170. Allen C, Dos Santos N, Gallagher R, Chiu GNC, Shu Y, Li WM, Johnstone SA, Janoff AS, Mayer LD, Webb MS, Bally MB. Controlling the physical behavior and biological performance of liposome formulations through use of surface grafted poly(ethylene glycol). Bioscience Rep 2002;22:225.

171. Ligoure C, Leibler L. Thermodynamics and kinetics of grafting end-functionalized polymers to an interface. J Phys 1990;51:1313.

172. Zengin A, Caykara T. Formation and properties of surface-anchored amine-terminated poly(dimethylsiloxane) assemblies with tunable physico-chemical characteristics. Thin Solid Films 2011;519:3135.

173. Wagner ML, Tamm LK. Tethered polymer-supported planar lipid bilayers for reconstitution of integral membrane proteins: silane-polyethyleneglycol-lipid as a cushion and covalent linker. Biophys J 2000;79:1400.

174. Roach P, Farrar D, Perry CC. Interpretation of protein adsorption: surface-induced conformational changes. J Amer Chem Soc 2005;127:8168.

175. Hemmersam AG, Foss M, Chevallier J, Besenbacher F. Adsorption of fibrinogen on tantalum oxide, titanium oxide and gold studied by the QCM-D technique. Colloid Surface B 2005;43:208.

176. Sangermano M, Bongiovanni R, Malucelli G, Priola A, Pollicino A, Recca A. Fluorinated epoxides as surface modifying agents of UV-curable systems. J Appl Polym Sci 2003;89:1524.

177. Hawkins ML, Grunlan MA. The protein resistance of silicones prepared with a PEO-silane amphiphile. J. Mater. Chem. 2012;22:19540.

178. Hoagland KD, Rosowski JR, Gretz MR, Roemer SC. Diatom extracellular polymeric substances: Function, fine structure, chemistry and physiology. J Phycol 1993;29:537.

179. Callow JA, Callow ME. Trends in the development of environmentally friendly fouling-resistant marine coatings. Nat Commun 2011;2:1.

180. Mieszkin S, Martin-Tanchereau P, Callow ME, Callow JA. Effect of bacterial biofilms formed on fouling-release coatings from natural seawater and *Cobetia marina*, on the adhesion of two marine algae. Biofouling 2012;28:953.

181. Wetherbee R, Lind JL, Burke J, Quatrano RS. The first kiss: Establishment and control of initial adhesion by raphid diatoms. J Phycol 1998;34:9.

182. Staats N, Winder BD, Stal L, Mur L. Isolation and characterization of extracellular polysaccharides from the epipelic diatoms *Cylidrotheca closterium* and *Navicula salinarum*. Eur J Phycol 1999;34:161.

183. Schultz MP. Effects of coating roughness and biofouling on ship resistance and powering. Biofouling 2007;23:331.

184. Schultz MP, Bendick JA, Holm ER, Hertel WM. Economic impact of biofouling on a naval surface ship. Biofouling 2011;27:87.

185. Dahlstrom M, Jonsson H, Jonsson PR, Elwing H. Surface wettability as a determinant in ite settlement of the barnacle *Balanus Improvisus* (DARWIN). J Exp Mar Biol Ecol 2004;305:223.

186. Molino PJ, Campbell E, Wetherbee R. Development of the initial diatom microfouling layer on antifouling and fouling-release surfaces in temperate and tropical Australia. Biofouling 2009;25:685.

187. McPherson T, Kidane A, Szleifer I, Park K. Prevention of protein adsorption by tethered poly(ethylene oxide) layers: experiments and single-chain mean-field analysis. Langmuir 1998;14:176.

188. Priest FG. In Bacillus Harwood CR, Ed. Plenum Press: New York, 1989, p 33.

189. Bhosale SH, Nagle VL, Jagtap TG. Antifouling potential of some marine organisms from India against species of *Bacillus* and *Pseudomonas*. Mar Biotechnol 2002;4:111.

190. Qin G, Zhu L, Chen X, Wang PG, Zhang Y. Structural characterization and ecological roles of a novel exopolysaccharide from the deep-sea psychrotolerant becterium *Pseudoalteromonas* sp. SM9913. Microbiology 2007;153:1566.

191. Dheilly A, Soum-Soutéra E, Klein GL, Compère C, Haras D, Dufour A. Antibiofilm activity of the marine bacterium *Pseudoalteromonas* sp. strain 3J6. Appl Environ Microb 2010;76:3452.

192. Briand J-F. Marine antifouling laboratory bioassays: an overview of their diversity. Biofouling 2009;25:297.

193. Qiu D, Eisinger VM, Rowen DW, Yu HD. Regulated proteolysis controls mucoid conversion in *Pseudomonas aeruginosa*. National Acad Sciences 2007;104:8107.

194. Ryther JH, Guillard RRL. Studies of marine planktonic diatoms: II. use of cyclotella nana hustedt for assays of vitamin B_{12} in sea water. Can J Microbiol 1962;8:437.

195. Berges JA, Franklin DJ, Harrison PJ. Evolution of an artificial seawater medium: improvements in enriched seawater, artificial water over the last two decades. J Phycol 2001;37:1138.

196. Heydorn A, Nielsen AT, Hentzer M, Sternberg C, Givskov M, Ersbøll BK, Molin S. Quantification of biofilm structures by the novel computer program COMSTAT. Microbiology 2000;146:2395.

197. Almeida E, Diamantino TC, Sousa Od. Marine paints: the particular case of antifouling paints. Prog Org Coat 2007;59:2.

198. Holland R, Dugdale TM, Wetherbee R, Brennan AB, Finlay JA, Callow JA, Callow ME. Adhesion and motility of fouling diatoms on a silicone elastomer. Biofouling 2004;20:323.

199. Doiron K, Linossier I, Fay F, Yong J, Wahid EA, Hadjiev D, Bourgougnon N. Dynamic approaches of mixed species biofilm formation using modern technologies. Mar Environ Res 2012;78:40.

200. Hodson OM, Monty JP, Molino PJ, Wetherbee R. Novel whole cell adhesion assays of three isolates of the fouling diatom *Amphora coffeaeformis* reveal diverse responses to surfaces of different wettability. Biofouling 2012;28:381.

201. Finlay JA, Schultz MP, Cone G, Callow ME, Callow JA. A novel biofilm channel for evaluating the adhesion of diatoms to non-biocidal coatings. Biofouling 2013;29:401.

202. Briand J-F, Djeridi I, Jamet D, Coupé S, Bressy C, Molmeret M, Berre BL, Rimet F, Bouchez A, Blache Y. Pioneer marine biofilms on artificial surfaces including antifouling coatings immersed in two contrasting French Mediterranean coast sites. Biofouling 2012;28:453.

203. Dobretsov S, Abed RMM, Teplitski M. Mini-review: Inhibition of biofouling by marine microorganisms. Biofouling 2013;29:423.

204. Mieszkin S, Callow ME, Callow JA. Interactions between microbial biofilms and marine fouling algae: a mini review. Biofouling 2013;29:1097.

205. Kendall K. The adhesion and surface energy of elastic solids. Phys D: Appl Phys 1971;4:1186.

206. Newby BZ, Chaudhury MK, Brown HR. Macroscopic evidence of the effect of interfacial slippage on adhesion. Science 1995;269:1407.

207. Sokolova A, Cilz N, Daniels J, Stafslien SJ, Brewer LH, Wendt DE, Bright FV, Detty MR. A comparison of the antifouling/foul-release characteristics of non-biocidal xerogel and commercial coatings toward micro- and macrofouling organisms. Biofouling 2012;28:511.

208. Estephan ZG, Schlenoff PS, Schlenoff JB. Zwitteration as an alternative to PEGylation. Langmuir 2011;27:6794.

209. Rouhana LL, Schlenoff JB. Aggregation resistant zwitterated superparamagnetic nanoparticles. J Nanopart Res 2012;14:1.

210. Estephan ZG, Hariri HH, Schlenoff JB. One-pot, exchange-free, room-temperature synthesis of sub-10 nm aqueous, noninteracting, and stable zwitterated iron oxide nanoparticles. Langmuir 2013;29:2572.

211. Rouhana LL, Jaber JA, Schlenoff JB. Aggregation-resistant water-soluble gold nanoparticles. Langmuir 2007;23:12799.

212. Hawkins ML, Schott SM, Grigoryan B, Rufin MA, Raymond ES, Raymond JE, Grunlan MA. Pitfalls of PEO modification of silicones: PEO-silane amphiphiles' superior ability to reduce protein adsorption. in preparation.

213. Rufin MA, Gruetzner JA, Hurley MJ, Hawkins ML, Raymond ES, Raymond JE, Grunlan MA. Overcoming the poor ability of PEO to reduce protein adsorption onto silicone: PEO-silane amphiphiles with variable PEO length. submitted.

214. Hooper R, Lyons LJ, Mapes MK, Schumacher D, Moline DA, West R. Highly conductive siloxane polymers. Macromolecules 2001;34:931.

215. Litt M, Matsuda T. Siloxane zwitterions: synthesis and surface properties of crosslinked polymers. J Appl Polym Sci 1975;19:1221.

APPENDIX

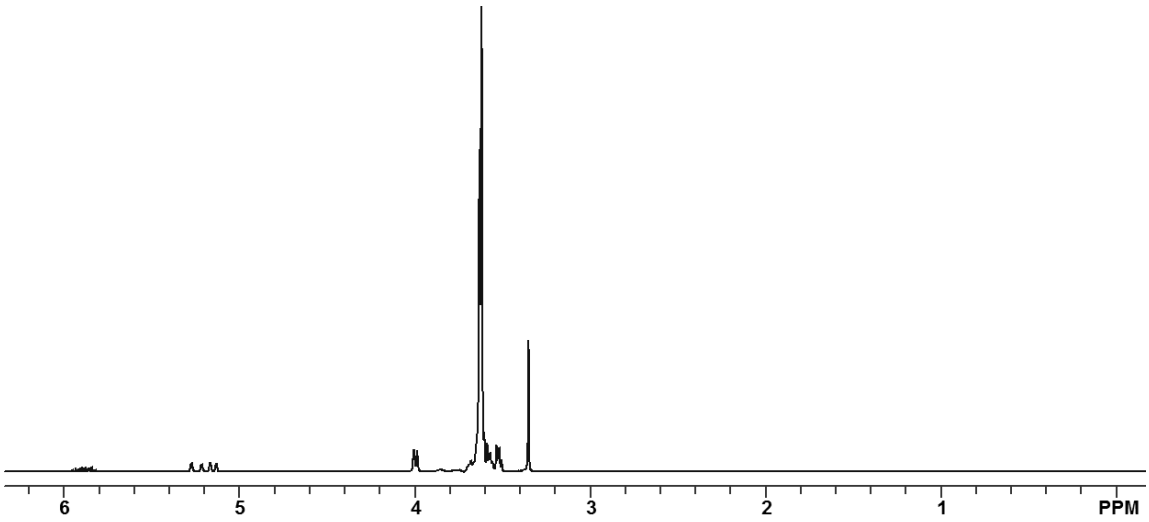

^{1}H NMR of poly(ethylene oxide)$_{8}$ allyl methyl ether (**A-PEO$_{8}$M**) [From Chapters II, III, IV, and V]

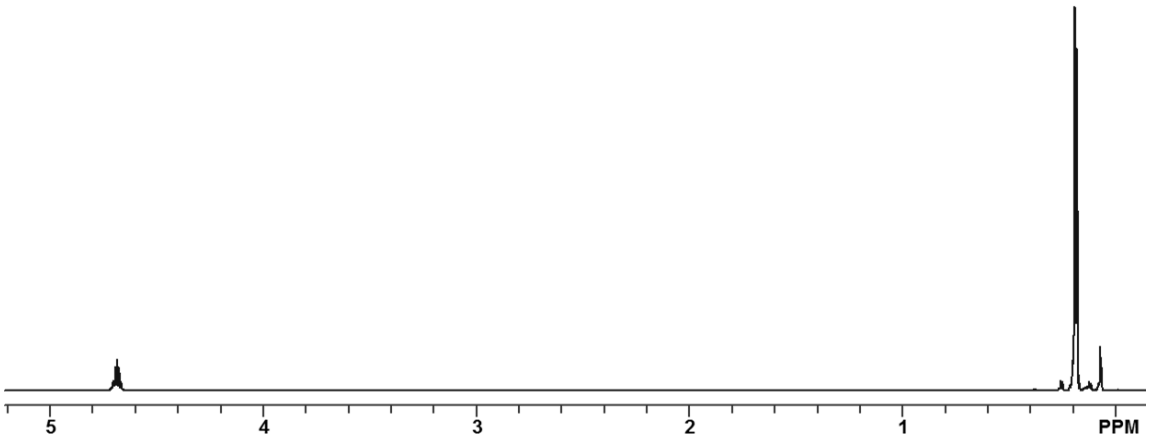

^{1}H NMR of **ODMS$_{0}$** (TMDS) [From Chapters III and IV]

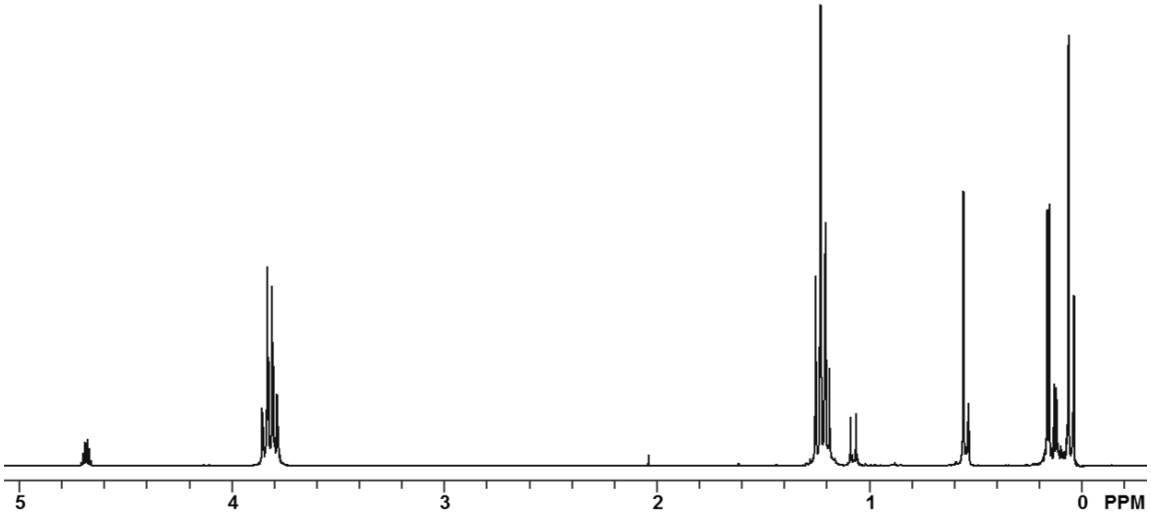

^{1}H NMR of triethoxysilylethyl-ODMS$_0$ (**TES-ODMS$_0$**) [From Chapters III and IV]

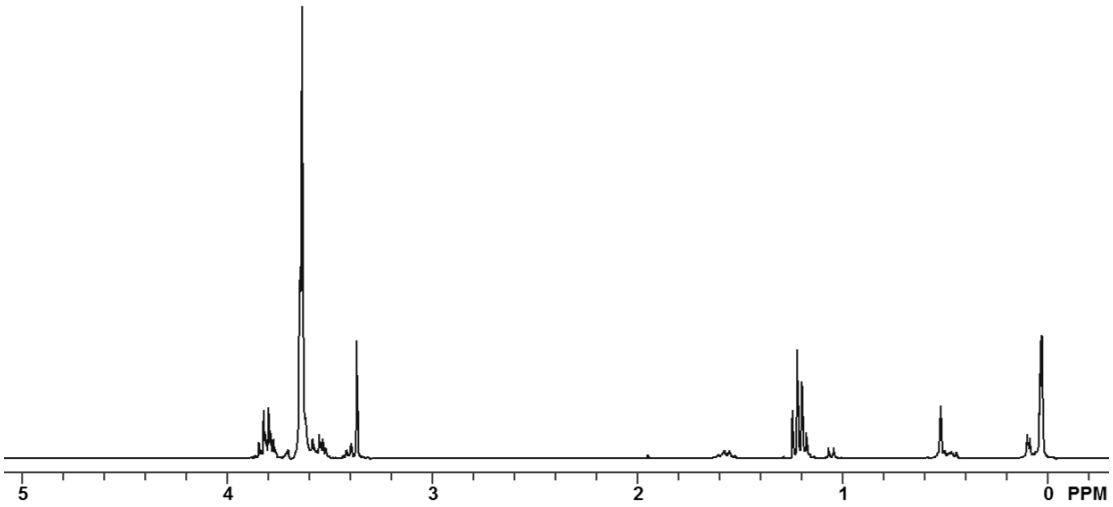

^{1}H NMR of triethoxysilylethyl-ODMS$_0$-*block*-poly(ethylene oxide)$_8$ (**m=0**) [From Chapters III and IV]

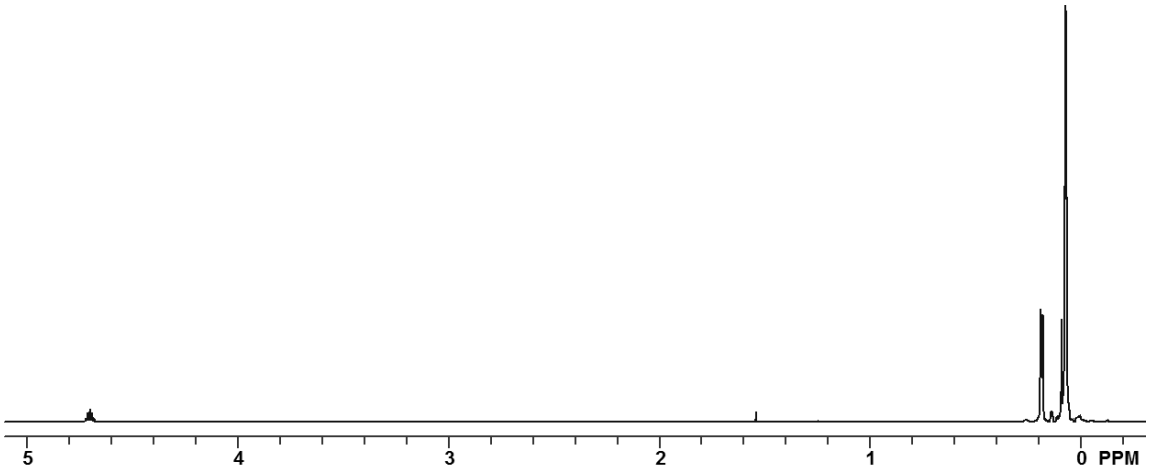

^{1}H NMR of **ODMS$_4$** [From Chapters III and IV]

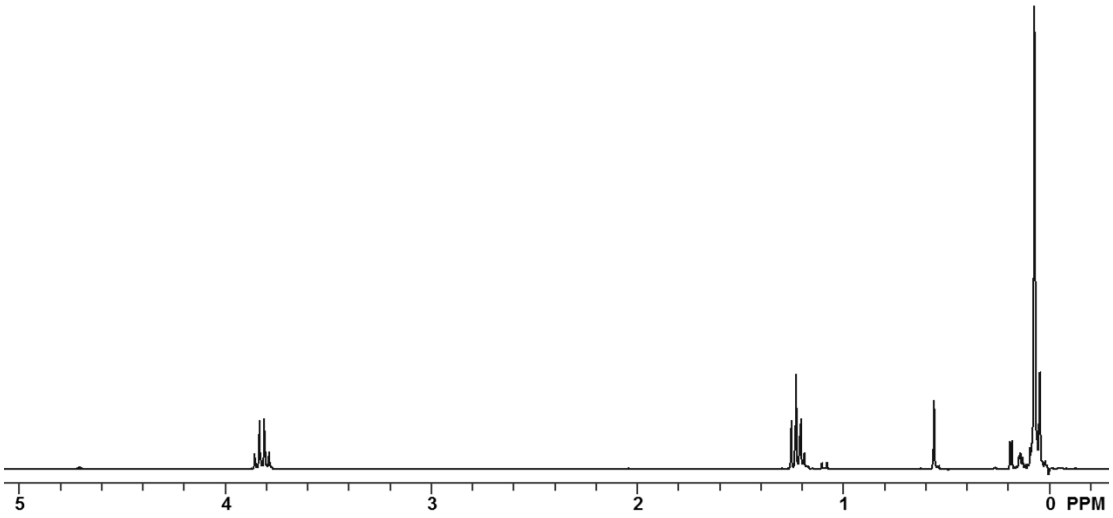

^{1}H NMR of triethoxysilylethyl-ODMS$_4$ (**TES-ODMS$_4$**) [From Chapters III and IV]

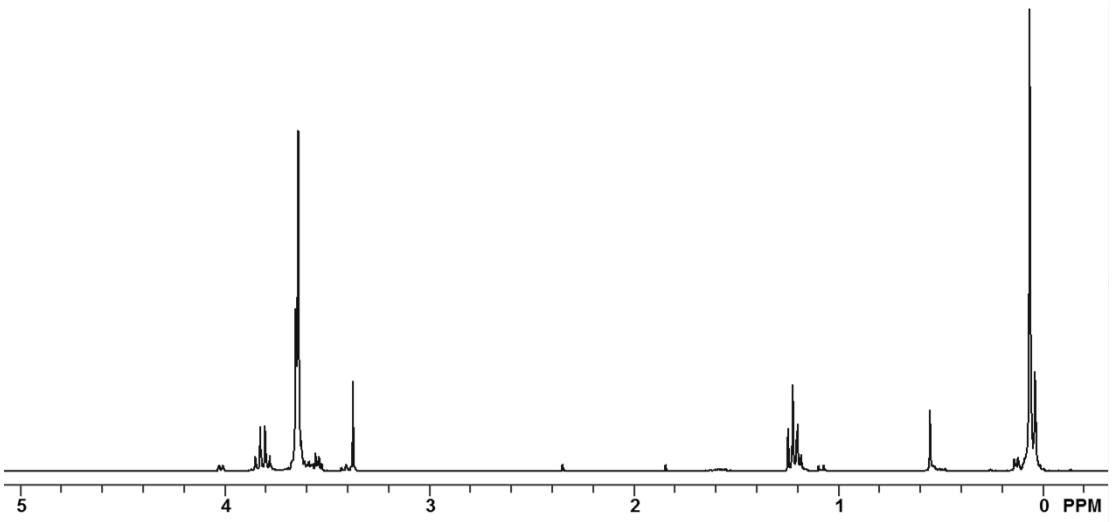

^{1}H NMR of triethoxysilylethyl-ODMS$_4$-*block*-poly(ethylene oxide)$_8$ (**m=4**) [From Chapters III and IV]

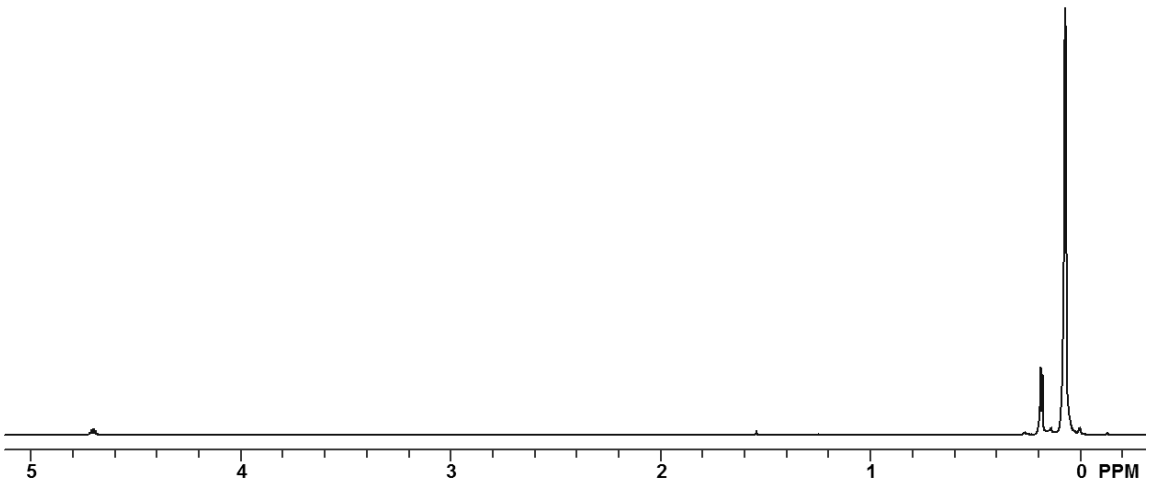

^{1}H NMR of **ODMS$_{13}$** [From Chapters II, III, IV, and V]

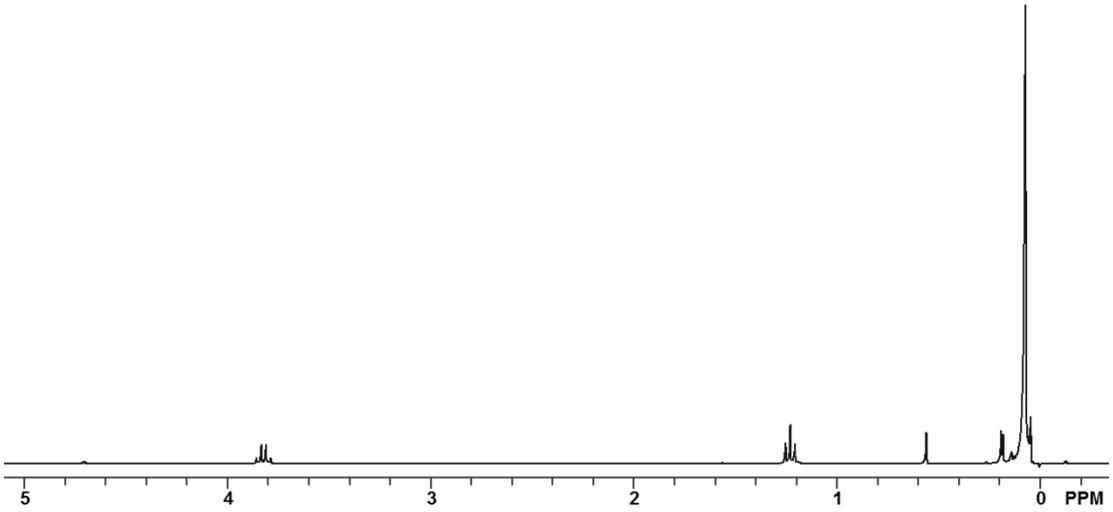

^{1}H NMR of triethoxysilylethyl-ODMS$_{13}$ (**TES-ODMS$_{13}$**) [From Chapters II, III, IV, and V]

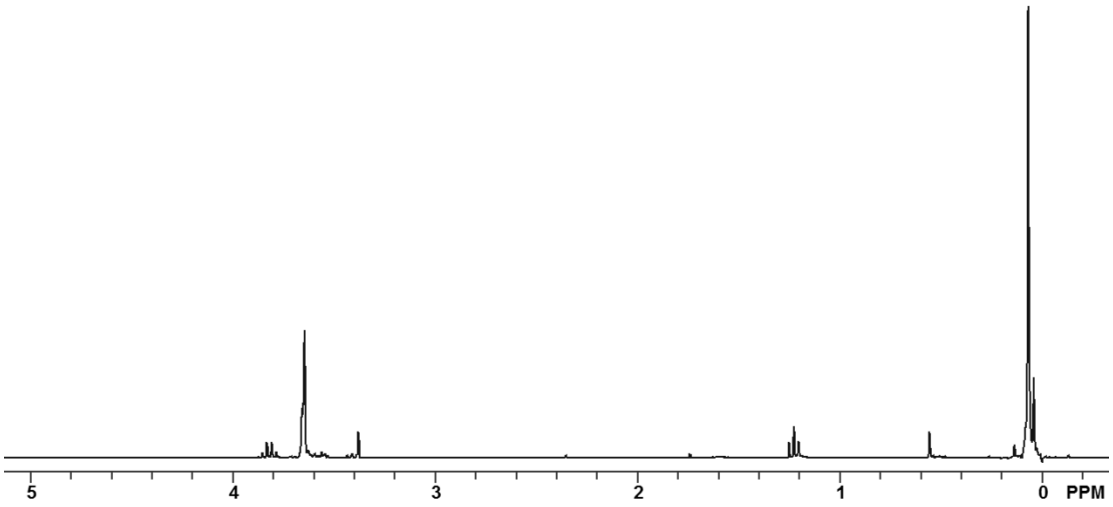

^{1}H NMR of triethoxysilylethyl-ODMS$_{13}$-*block*-poly(ethylene oxide)$_{8}$ (**m=13**; **TES-ODMS$_{13}$-PEO$_{8}$**) [From Chapters II, III, IV, and V]

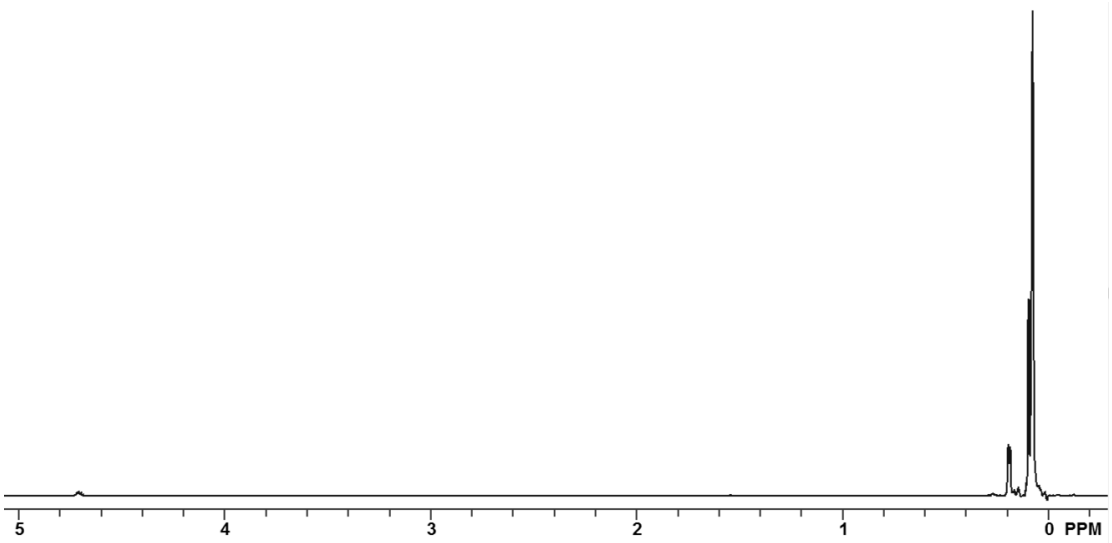

^{1}H NMR of **ODMS$_{17}$** [From Chapter III]

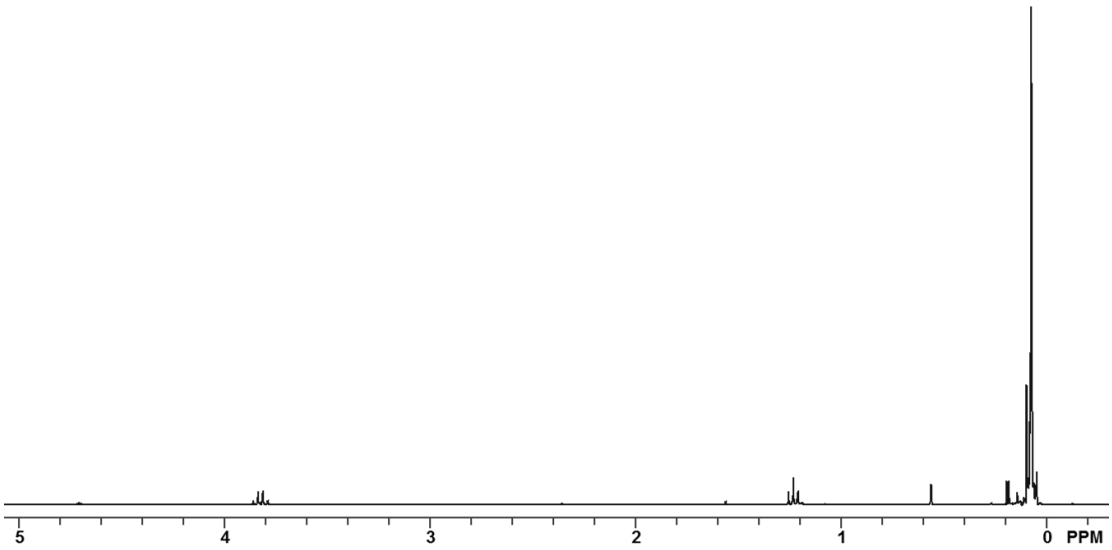

^{1}H NMR of triethoxysilylethyl-ODMS$_{17}$ (**TES-ODMS$_{17}$**) [From Chapter III]

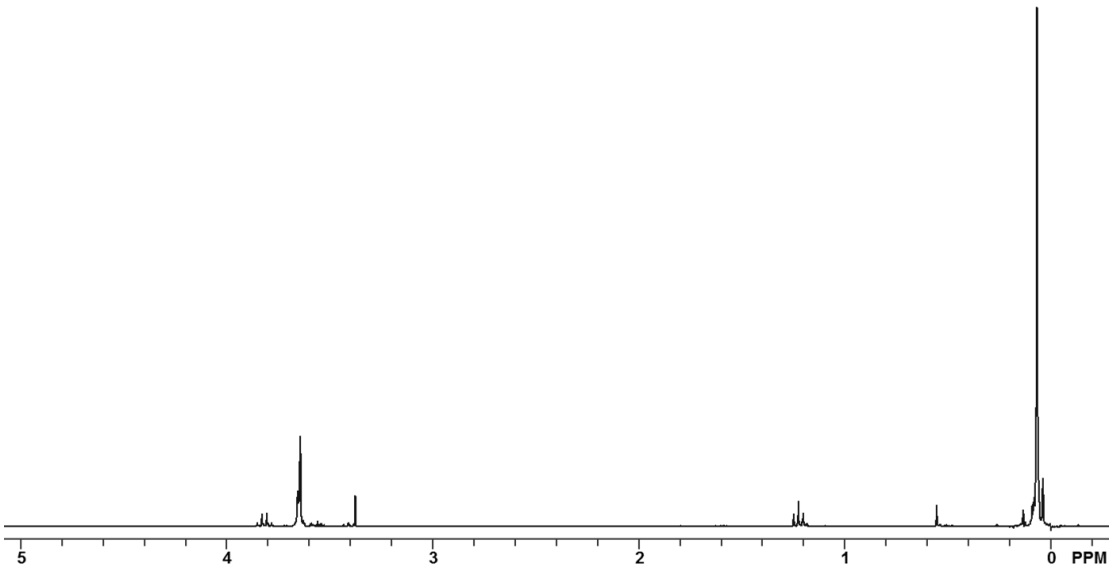

^{1}H NMR of triethoxysilylethyl-ODMS$_{17}$-*block*-poly(ethylene oxide)$_{8}$ (**m=17**) [From Chapter III]

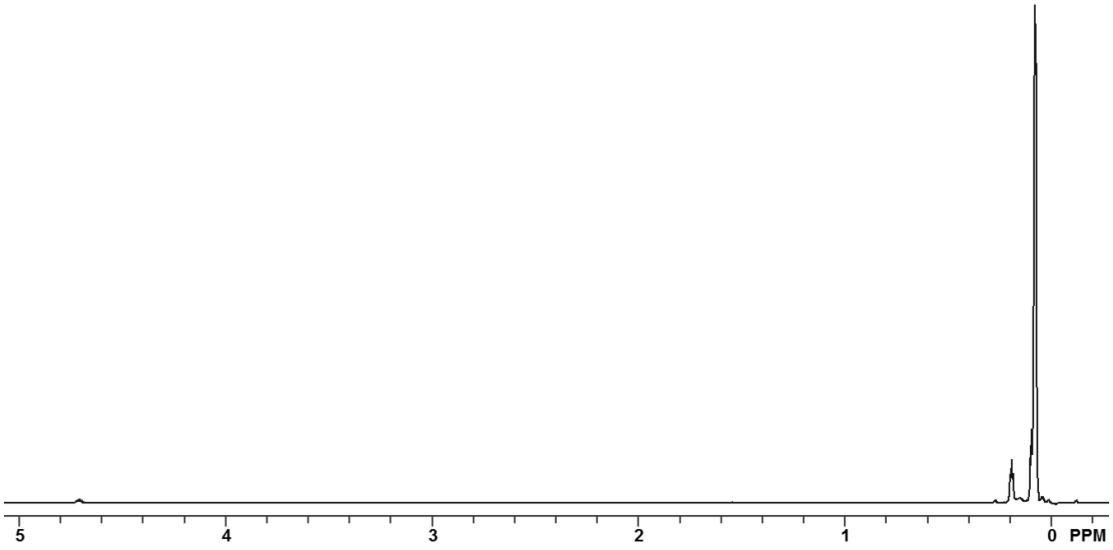

^{1}H NMR of **ODMS$_{24}$** [From Chapter III]

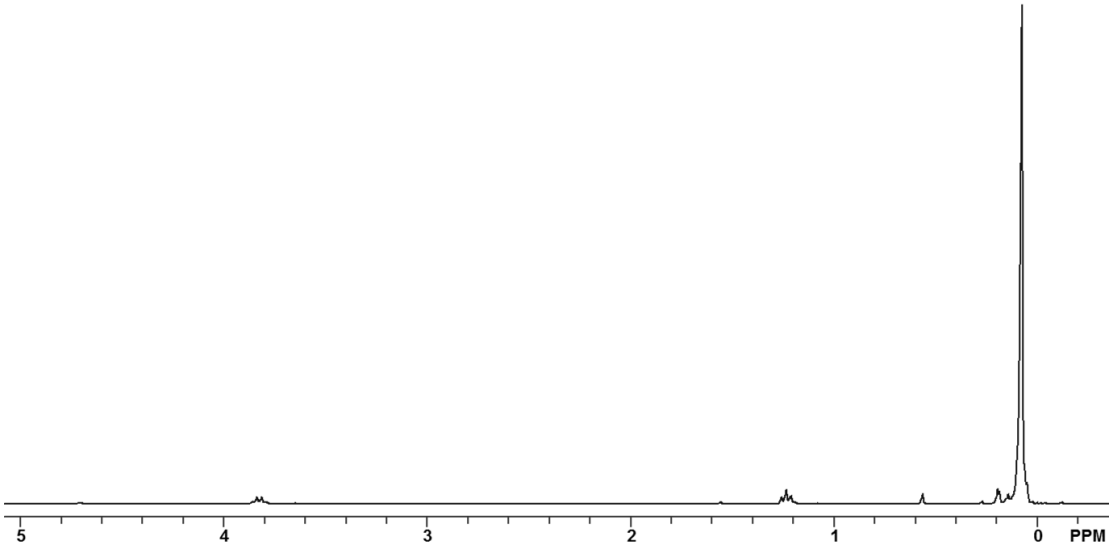

^{1}H NMR of triethoxysilylethyl-ODMS$_{24}$ (**TES-ODMS$_{24}$**) [From Chapter III]

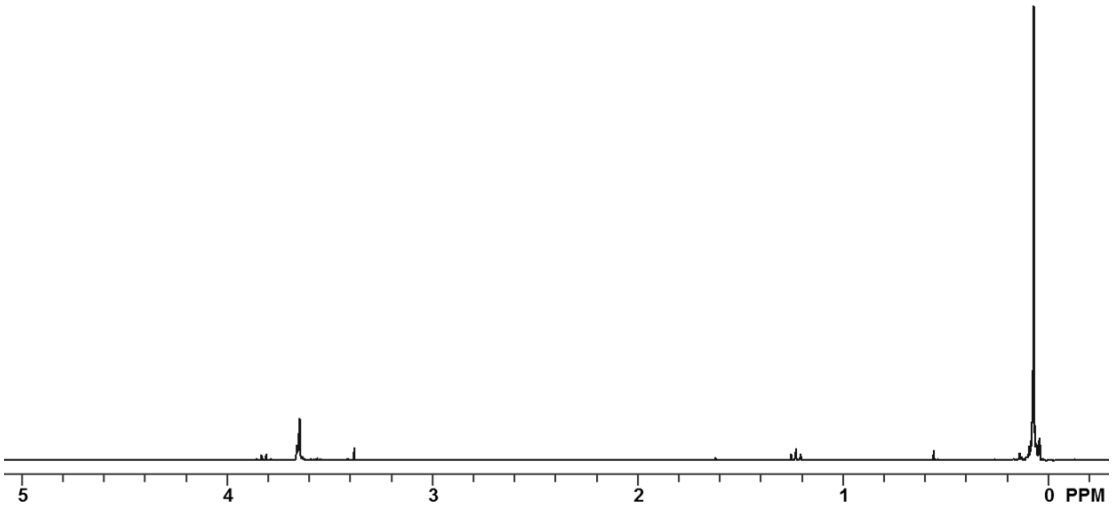

^{1}H NMR of triethoxysilylethyl-ODMS$_{24}$-*block*-poly(ethylene oxide)$_{8}$ (**m=24**) [From Chapter III]

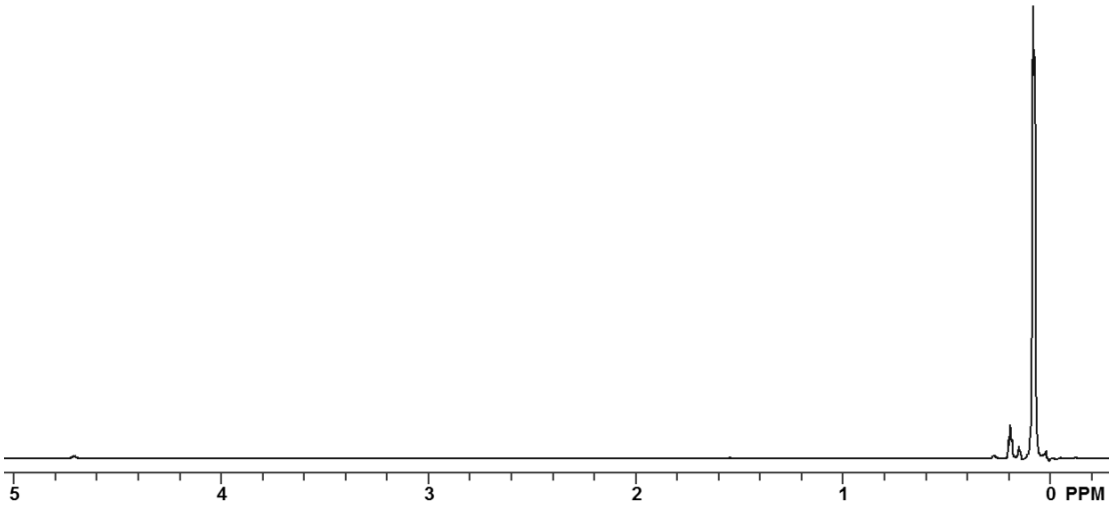

^{1}H NMR of **ODMS$_{30}$** [From Chapter III]

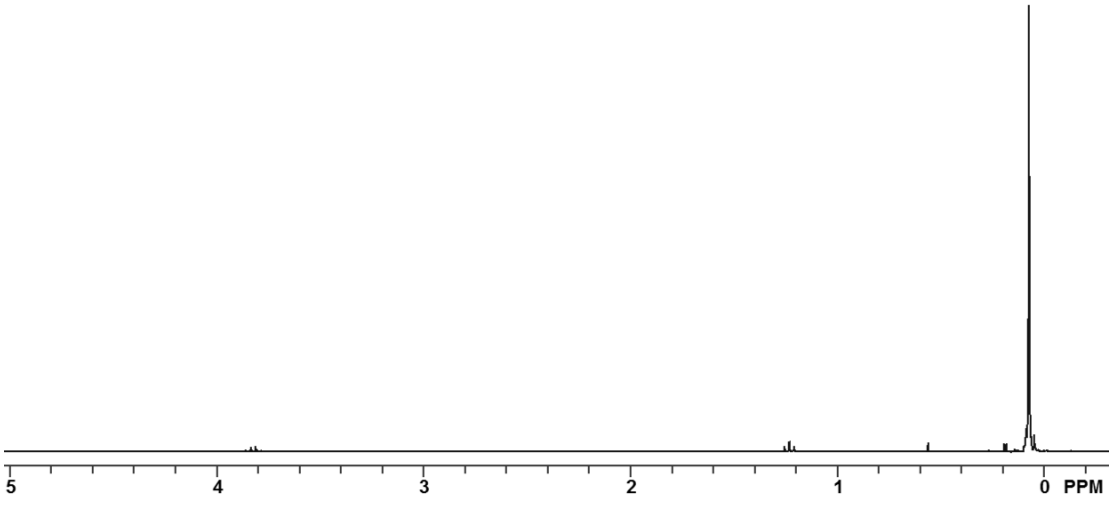

^{1}H NMR of triethoxysilylethyl-ODMS$_{30}$ (**TES-ODMS$_{30}$**) [From Chapter III]

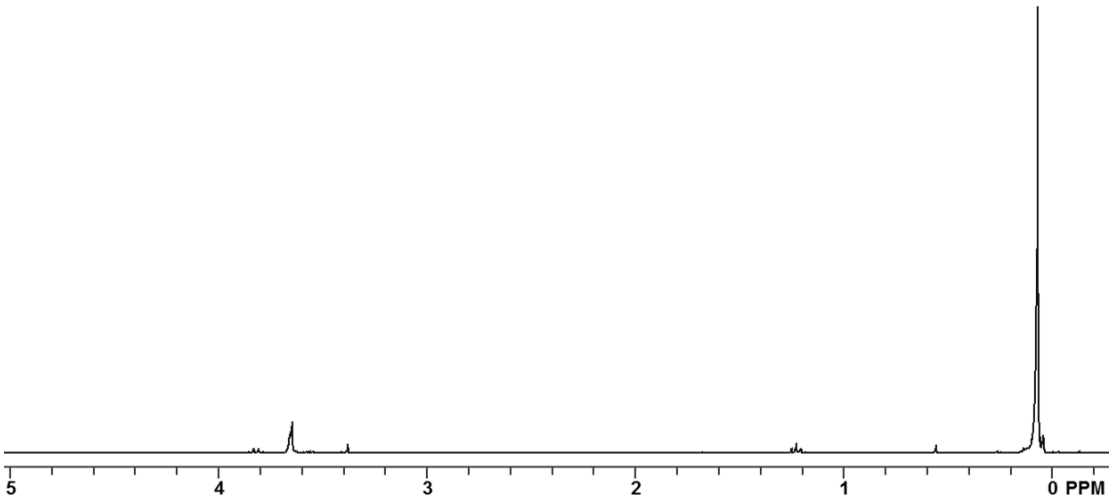

^{1}H NMR of triethoxysilylethyl-ODMS$_{30}$-*block*-poly(ethylene oxide)$_{8}$ (**m=30**) [From Chapter III]

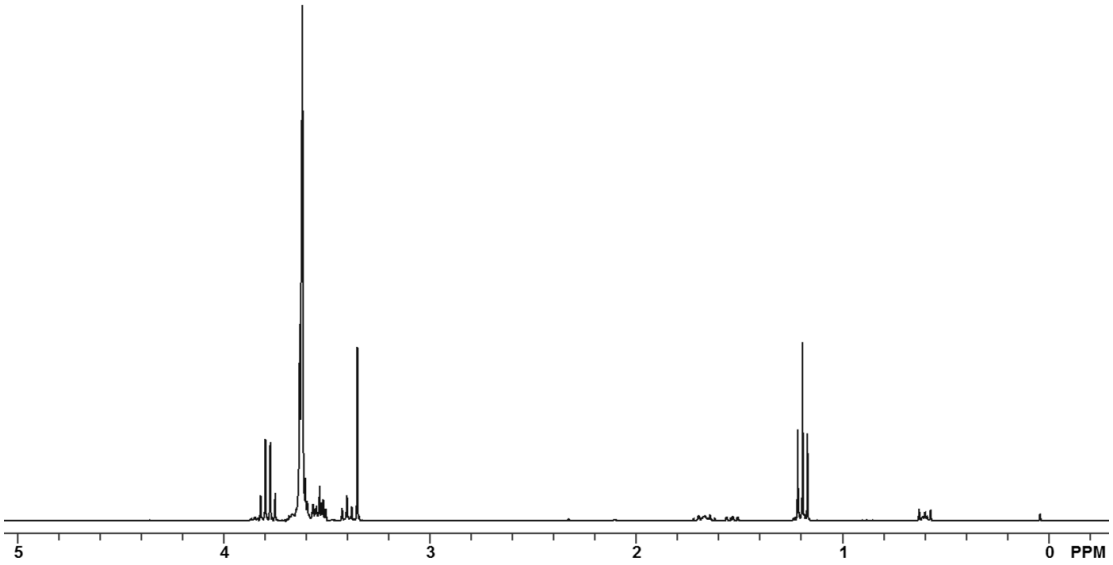

^{1}H NMR of triethoxysilylethyl-*block*-poly(ethylene oxide)$_{8}$ (**PEO control**; **TES-PEO$_{8}$**) [From Chapters III and V]

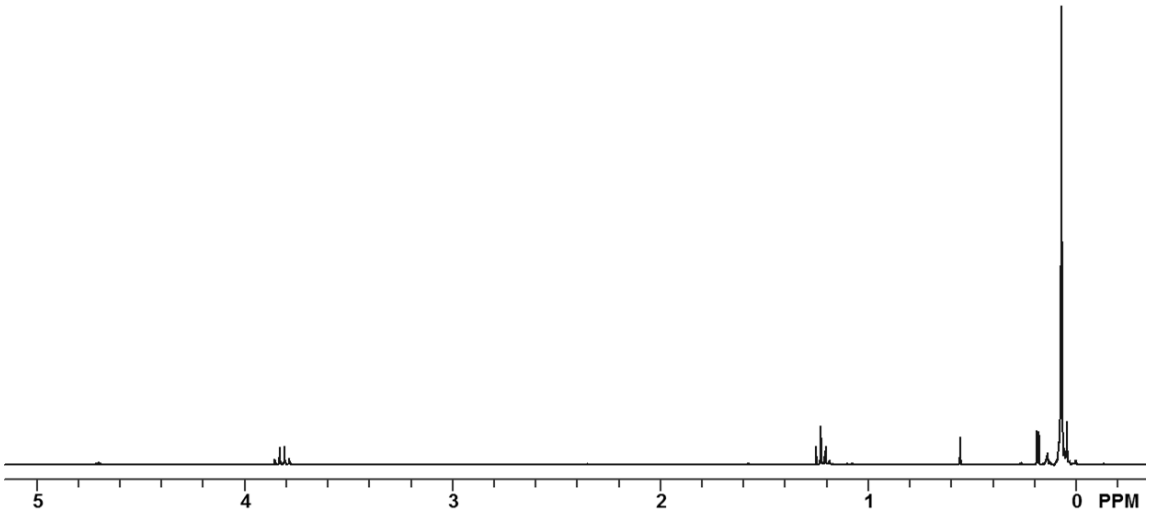

^{1}H NMR of α-triethoxysilylethyl-ω-silane-oligodimethylsiloxane$_{13}$ (**siloxane control**; **TES-ODMS$_{13}$**) [From Chapters III and V]

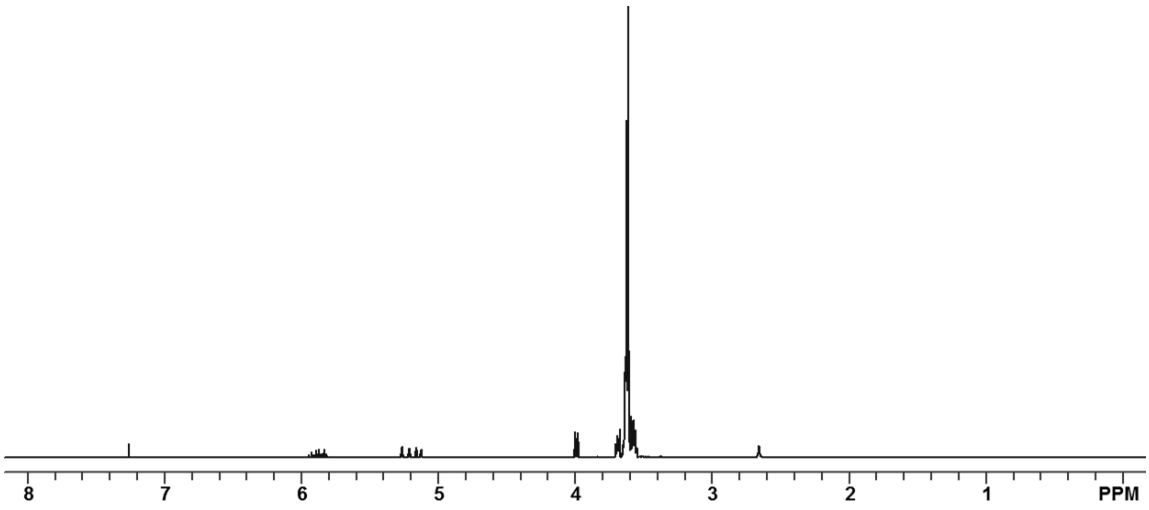

^{1}H NMR of allyloxy poly(ethylene oxide) (**HO-PEO$_{11}$-A**) [From Chapter V]

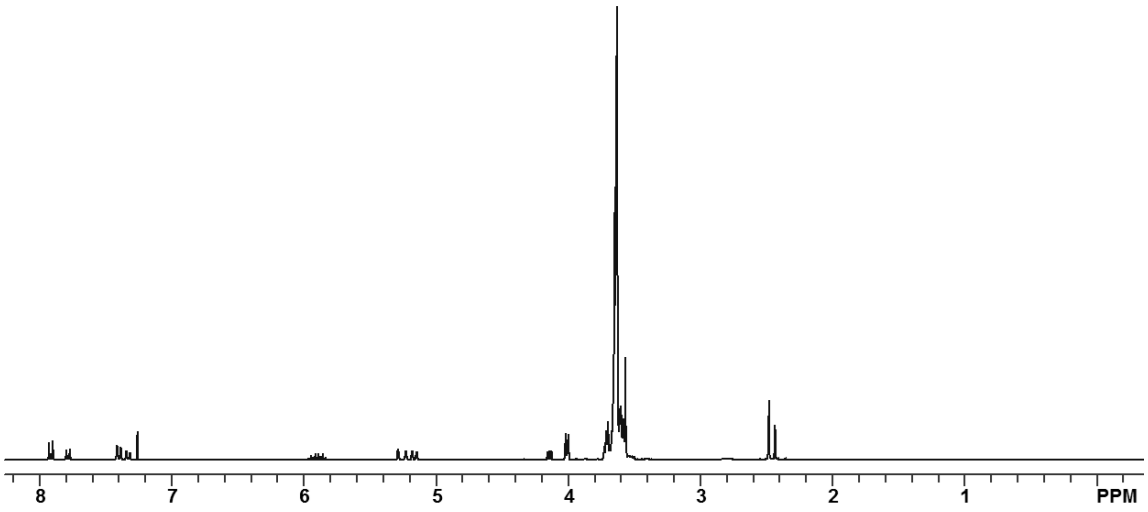

^{1}H NMR of tosylated allyloxy poly(ethylene oxide)$_{11}$ (**TsO-PEO$_{11}$-A**) [From Chapter V]

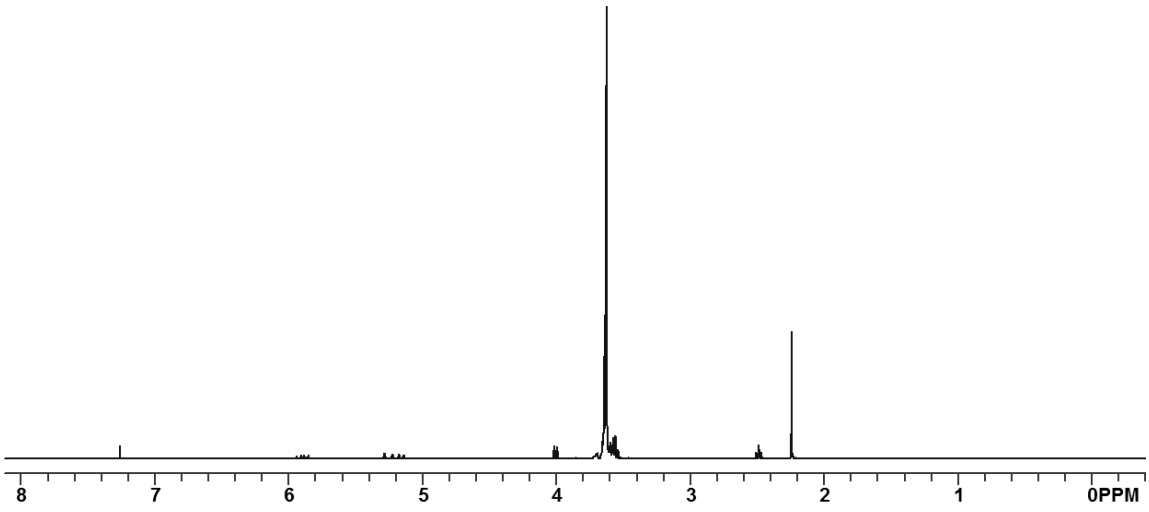

^{1}H NMR of dimethylethanolamino allyl poly(ethylene oxide)$_{11}$ (**DMEA-PEO$_{11}$-A**) [From Chapter V]

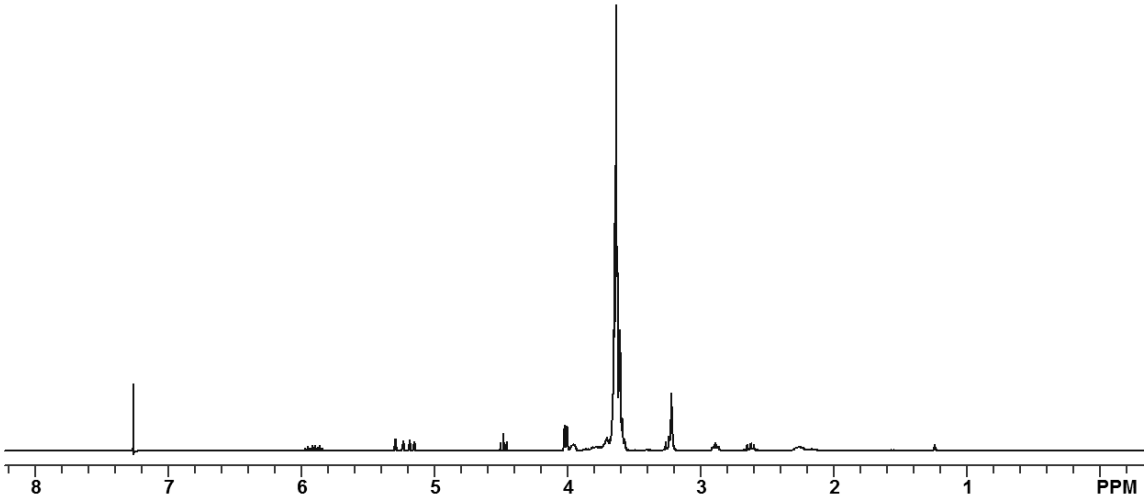

^{1}H NMR of allyl-ether-poly(ethylene oxide)$_{11}$-sulfobetaine (**A-PEO$_{11}$-SB**) [From Chapter V]

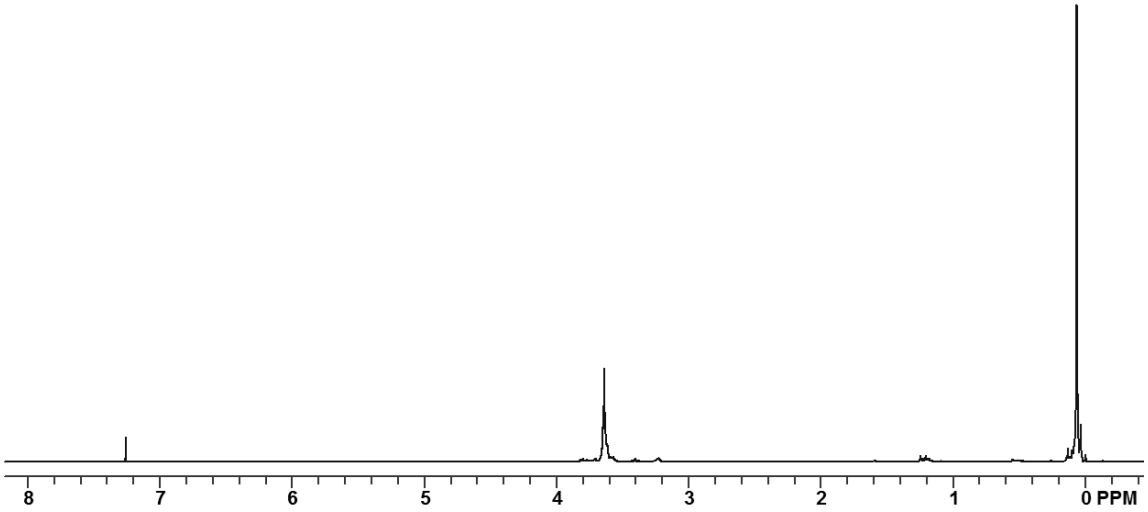

^{1}H NMR of triethoxysilylethyl-oligodimethylsiloxane$_{13}$-*block*-poly(ethylene oxide)$_{11}$-sulfobetaine (**TES-ODMS$_{13}$-PEO$_{11}$-SB**) [From Chapter V]

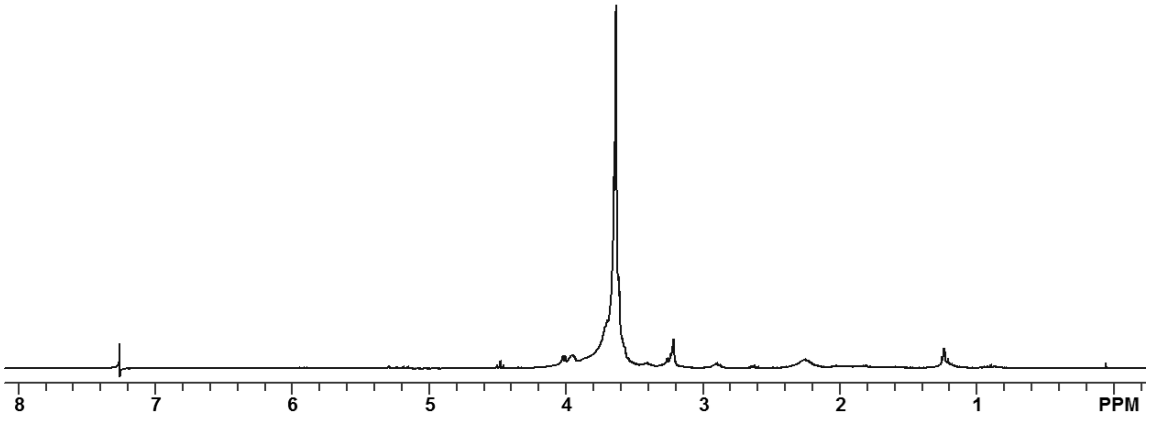

^{1}H NMR of triethoxysilylpropyl-poly(ethylene oxide)$_{11}$-sulfobetaine (**TES-PEO$_{11}$-SB**) [From Chapter V]